DESIGN AND ANALYSIS OF NON-ORTHOGONAL MULTIPLE ACCESS IN COMMUNICATION SYSTEMS

by

İsmail Coşandal

B.S., Electrical and Electronics Engineering, Boğaziçi University, 2018

Submitted to the Institute for Graduate Studies in
Science and Engineering in partial fulfillment of
the requirements for the degree of
Master of Science

Graduate Program in Electrical and Electronics Engineering
Boğaziçi University

2021

I dedicate this thesis to all the members of Boğaziçi University who have an uncompromising dedication to freedom and autonomy in academia.

ACKNOWLEDGEMENTS

I want to express my deepest appreciation and thanks to my advisor Prof. Mutlu Koca, without a doubt this thesis would not have been done without his support and guidance. I also want to thank Prof. Emin Anarım, Prof. Hikmet Sarı, Prof. Hakan Deliç and Prof. Ezio Biglieri whom I had a chance to work with and learned a lot from. Besides, I want to thank my project partner Yiğit Berkay Uslu for his great contribution to this thesis.

But most importantly, I want to thank my family. My wife Betül, my parents Mehmet Ali and Emine and my siblings Tuba, Maide and Ali. I owe them everything.

This work was supported by Scientific and Technical Research Council of Turkey (TUBITAK) under Contract 119N154. I also would like to thank TUBITAK which provided me with a graduate fellowship through the 2210/A program.

ABSTRACT

DESIGN AND ANALYSIS OF NON-ORTHOGONAL MULTIPLE ACCESS IN COMMUNICATION SYSTEMS

Non-Orthogonal Multiple Access (NOMA) has emerged as a promising technique to satisfy the high demand of users in future wireless networks. The NOMA literature is heavily based on Power-Domain NOMA (PD-NOMA), which inherently needs a power imbalance between superposed user signals. Another technique is based on using two sets of signal waveforms and is referred to as Waveform Domain NOMA (WD-NOMA). One of the forms of WD-NOMA is NOMA-2000 which does not need any power imbalance and avoids the outage floors typically encountered in PD-NOMA. In this thesis, we provide theoretical analyses of both PD-NOMA and NOMA-2000 using the performance metrics such as the outage probability and channel capacity. In NOMA literature on capacity calculations generally perfect successive interference cancelation (SIC) is assumed, which is not realistic due to the error floors in bit-error and outage performances. Therefore, we consider capacity under the imperfect SIC approach which basically is based on the assumption that if a user is in outage, its signal cannot be cancelled perfectly with SIC. The analysis is first presented for Rayleigh fading channels and then enhanced to generalized fading channels described by the κ-μ fading model. Our analysis not only shows that compared to PD-NOMA and Orthogonal Multiple Access (OMA), NOMA-2000 has superior performance but also indicates that NOMA-2000 can reach analytical lower/upper bounds in most cases. Overall, our analysis and results confirm that NOMA-2000 represents a very attractive multiple access technique for future wireless networks.

ÖZET

HABERLEŞME SİSTEMLERİNDE DİKGEN OLMAYAN ÇOKLU ERİŞİMİN TASARIM VE ANALİZİ

Dikgen-Olmayan Çoklu Erişim (DOÇE) gelecek nesil haberleşme ağlarındaki yüksek kullanıcı talebi için ümit vaadeden bir teknoloji olarak görülmektedir. DOÇE literatürü ağırlıklı olarak, kullanıcı sinyalleri arasında yüksek miktarda ayrım gerektiren Güç-Düzleminde DOÇE (GD-DOÇE) üzerinden oluşturulmuştur. Bir alternatif yöntem ise iki farklı dalga formu kullanan Dalga Formları Düzleminde DOÇE (DFD-DOÇE). Bir DFD-DOÇE formu olan NOMA-2000'de, kullanıcılar arasında güç farkı gereksinimine o kadar ihtiyaç duymaz ve GD-DOÇE'de karşılaşan hataların önüne geçebilir. Bu tezde, kesinti olasılığı ve kanal kapasitesini temel alan teorik analizleri sunmaktayız. DOÇE literatüründe kapasite hesapları genellikle kusursuz Ardışık Girişim Giderici (AGG) varsayımı altında yapılmakta, fakat sabit hatadan ötürü gerçekçi bir yaklaşım değil. Bu sebepten, biz kapasiteyi mükemmel olmayan AGG varsayımı altında hesaplamaktayız, bu varsayıma göre bir kullanıcı kesintiye uğruyorsa, o kullanıcın sinyali AGG ile giderilemez. Çalışmalarımız ilk olarak Rayleigh sönümlemeli kanallar için sunulmuş, daha sonra κ-μ sönümlemeli kanallar olarak ifade edilebilen daha genelleşmiş sönümlemeli kanallar için ifade edilmiştir. Analizlerimiz göstermektedir ki, NOMA-2000 GD-DOÇE ve Dikgen Çoklu Erişim (DÇE)'den daha iyi bir performansa sahip olmakla kalmayıp aynı zamanda teorik alt/üst limitlere de çoğu zaman ulaşabilmektedir. Sonuç alarak, çalışmalarımız NOMA-2000'in gelecek nesil haberleşme ağlarında kullanılabilecek çoklu erişim sistemi olmaya çok uygun olduğunu yansıtmaktadır.

TABLE OF CONTENTS

ACKNOWLEDGEMENTS iv
ABSTRACT v
ÖZET vi
LIST OF FIGURES ix
LIST OF TABLES xiii
LIST OF SYMBOLS xiv
LIST OF ACRONYMS/ABBREVIATIONS xvii
1. INTRODUCTION 1
2. Non-Orthogonal Multiple Access Techniques 6
2.1. Single Carrier NOMA 6
2.2. Multi Carrier NOMA 8
2.2.1. PD-NOMA 10
2.2.2. NOMA-2000 14
2.2.3. No-interference and OMA bounds 16
3. Design and Analysis of Non-Orthogonal Multiple Access over Rayleigh Fading Channels 19
3.1. Outage Probability 19
3.1.1. PD-NOMA 19
3.1.2. NOMA-2000 24
3.1.3. No-interference and OMA Bounds 27
3.2. Capacity 28
3.2.1. PD-NOMA 28
3.2.2. NOMA-2000 31
3.2.3. No-interference and OMA Bounds 33
3.3. Capacity under Imperfect SIC 34
3.3.1. PD-NOMA 34
3.3.2. NOMA-2000 37
3.4. Numerical Results 39

3.4.1. Outage Probability 39
3.4.2. Capacity 44
3.4.3. Capacity with Imperfect SIC 44
3.4.4. Analysis 53
4. Design and Analysis of Non-Orthogonal Multiple Access over Generalized Fading Channels 55
4.1. Mixture of Gamma Distribution Approach 55
4.2. Outage Probability 56
4.2.1. PD-NOMA 60
4.2.2. NOMA-2000 62
4.2.3. No-interference and OMA Bounds 63
4.3. Capacity 64
4.3.1. PD-NOMA 64
4.3.2. NOMA-2000 65
4.3.3. No-interference and OMA Bounds 65
4.4. Capacity under Imperfect SIC 66
4.4.1. PD-NOMA 66
4.4.2. NOMA-2000 68
4.4.3. No-interference and OMA Bounds 69
4.5. Numerical Results 69
4.5.1. Outage Probability 69
4.5.2. Capacity 74
4.5.3. Analysis 82
5. Conclusion 83
REFERENCES 85

LIST OF FIGURES

Figure 1.1. Resource allocation on a) PD-NOMA and b) NOMA-2000. 2

Figure 2.1. Transmitting and decoding scheme of uplink OMA and NOMA. . 7

Figure 2.2. Channel gains of both user groups which are divided and corresponding threshold τ values a) OF=25%, b) OF=50%, c) OF=75% d) OF=100% 8

Figure 2.3. Channel gains of users on U_1 and interference powers on their subcarrier for PD-NOMA, N=128 Subcarriers, a) OF=100% and $\epsilon = 1.0$, b) OF=100% and $\epsilon = 0.5$, c) OF=50% and $\epsilon = 1.0$. 12

Figure 2.4. ML Detection Regions for the Superposed NOMA Signal. 13

Figure 2.5. Decoding scheme of NOMA-2000. 16

Figure 2.6. Channel gains of users on U_1 and interference powers on their subcarrier for NOMA-2000, N=128 Subcarriers, a) OF=100% and $\epsilon = 1.0$, b) OF=100% and $\epsilon = 0.5$, c) OF=50% and $\epsilon = 1.0$. 17

Figure 3.1. Integral regions for equation (4.30). 35

Figure 3.2. Outage performance of the single carrier case. 40

Figure 3.3. Outage probability comparisons between PD-NOMA and NOMA-2000 when target rate is 1.2 bits/s/Hz a) $\epsilon = 0.5$, b) $\epsilon = 1.0$. . . . 41

Figure 3.4. Outage probability comparisons between PD-NOMA and NOMA-2000 when target rate is 1.5 bits/s/Hz a) $\epsilon = 0.5$, b) $\epsilon = 1.0$. . . . 42

Figure 3.5. Outage probability comparisons between PD-NOMA and NOMA-2000 when target rates is 1.8 bits/s/Hz a) $\epsilon = 0.5$, b) $\epsilon = 1.0$. . . . 43

Figure 3.6. Capacity comparisons between PD-NOMA and NOMA-2000 when a) $\epsilon = 0.5$ and OF= 100%, b) $\epsilon = 1.0$ and OF= 100%. 45

Figure 3.7. Capacity comparisons between PD-NOMA and NOMA-2000 when target rate is 1.2 bits/s/Hz a) $\epsilon = 0.5$, and b) there is no power imbalance ($\epsilon = 1.0$). 46

Figure 3.8. Capacity comparisons between PD-NOMA and NOMA-2000 when target rate is 1.5 bits/s/Hz and a) $\epsilon = 0.5$, and b) there is no power imbalance ($\epsilon = 1.0$). 47

Figure 3.9. Capacity comparisons between PD-NOMA and NOMA-2000 when target rate is 1.8 bits/s/Hz and a) $\epsilon = 0.5$, and b) there is no power imbalance ($\epsilon = 1.0$). 48

Figure 3.10. Capacity comparisons between PD-NOMA and NOMA-2000 when target rate is 1.5 bits/s/Hz a) in 10 dB and b) in 15 dB. 49

Figure 3.11. Capacity comparisons between PD-NOMA and NOMA-2000 when target rate is 1.8 bits/s/Hz a) in 10 dB and b) in 15 dB. 50

Figure 3.12. Capacity comparisons between PD-NOMA and NOMA-2000 when ϵ values are selected to maximize capacity and target rates are a)$\hat{R} = 1.2$ bits/s/Hz and b) $\hat{R} = 1.5$ bits/s/Hz. 51

Figure 3.13. Capacity comparisons between PD-NOMA and NOMA-2000 when ϵ values are selected to maximize capacity and target rates are a)$\hat{R} = 1.8$ bits/s/Hz and b) $\hat{R} = 2.0$ bits/s/Hz. 52

Figure 4.1. Agreement with the MGD Approximation and the exact PDFs of generalized fading channel models. 60

Figure 4.2. The outage probability of Rician shadowed fading ($K = 2, m = 2$) when target rate= 1.8 bits/s/Hz, a) $\epsilon = 0.5$ and b) $\epsilon = 1.0$. 70

Figure 4.3. The outage probability of $\kappa-\mu$ shadowed fading ($\kappa = 3, \mu = 2, m = 2$) when target rate= 1.8 bits/s/Hz, a) $\epsilon = 0.5$ and b) $\epsilon = 1.0$. . . . 71

Figure 4.4. The outage probability of generalized fading channel models when target rate= 1.8 bits/s/Hz and $\epsilon = 0.5$ for a) PD-NOMA and b) for NOMA-2000. 72

Figure 4.5. The outage probability of generalized fading channel models when target rate= 1.8 bits/s/Hz and there is no power imbalance ($\epsilon = 1.0$) for a) PD-NOMA and b) for NOMA-2000. 73

Figure 4.6. Capacity of Rician shadowed fading ($K = 2, m = 2$) when target rate= 1.8 bits/s/Hz, a) $\epsilon = 0.5$ and b) $\epsilon = 1.0$. 74

Figure 4.7. Capacity of $\kappa - \mu$ shadowed fading ($\kappa = 3, \mu = 2, m = 2$) when target rate= 1.8 bits/s/Hz, a) $\epsilon = 0.5$ and b) $\epsilon = 1.0$. 75

Figure 4.8. Capacity under perfect SIC assumption comparisons between PD-NOMA and NOMA-2000 when a)$\epsilon = 0.5$, b) $\epsilon = 1.0$. 76

Figure 4.9. Capacity comparisons under imperfect SIC between PD-NOMA and NOMA-2000 when target rate is 1.8 bits/s/Hz and a)$\epsilon = 0.5$, b) $\epsilon = 1.0$. 77

Figure 4.10. Capacity comparisons between PD-NOMA and NOMA-2000 for Nakagami-m fading ($m = 3$) when ϵ values are selected to maximize capacity and target rates are a) $\hat{R} = 1.5$ bits/s/Hz, and b) $\hat{R} = 1.8$ bits/s/Hz. 78

Figure 4.11. Capacity comparisons between PD-NOMA and NOMA-2000 for Rician shadowed fading($K = 2, m = 2$) when ϵ values are selected to maximize capacity and target rates are a) $\hat{R} = 1.5$ bits/s/Hz, and b) $\hat{R} = 1.8$ bits/s/Hz. 79

Figure 4.12. Capacity comparisons between PD-NOMA and NOMA-2000 for $\kappa - \mu$ shadowed fading($\kappa = 3, \mu = 2, m = 2$) when ϵ values are selected to maximize capacity and target rates are a) $\hat{R} = 1.5$ bits/s/Hz, and b) $\hat{R} = 1.8$ bits/s/Hz. 80

Figure 4.13. Capacity comparisons between PD-NOMA and NOMA-2000 when ϵ values are selected to maximize capacity and target rates is $\hat{R} =$ 1.8 bits/s/Hz for a) $\kappa-\mu$ fading($\kappa = 2, \mu = 2$) and b) Rician fading ($K = 2$). 81

LIST OF TABLES

Table 3.1. Table of indefinite integrals in Chapter 3. 32

Table 4.1. Mixture of Gamma Distribution representations of some fading models. 57

Table 4.2. List of integrals involving Gamma function or the PDF of Gamma distribution. 58

LIST OF SYMBOLS

a	Information bit of user 1
a_n	Information bit of n-th user in U_1
$\hat{a}$	Decoded signal of user 1
$\hat{a_n}$	Decoded signal of n-th user in U_1
b	Information bit of user 1
b_m	Information bit of m-th user in U_2
C_1	Normalization coefficient for U_1
C_2	Normalization coefficient for U_2
$Ei(\cdot)$	Exponential integral function
E_n^{WD}	Coverage event of n-th user for NOMA-2000
E_n^{PD}	Coverage event of n-th user for PD-NOMA
$f_X(x)$	PDF of random variable X
$F_X(x)$	CDF of random variable X
g_i	Channel gain of i-th user
h_i	Channel coefficients of i-th user
$I_{U_1,n}$	Interference affects the n-th user of U_1
$I_{U_2,m}$	Interference affects the m-th user of U_2
$\Im$	Imaginary part
K	Total number of users
L	Number of elements on MGD
l_i	Distance between i-th user and the Base Station
M	Number of exceed users
N	Number of subcarriers
$\mathcal{N}\ (\mu, \sigma^2)$	Gaussian distribution with mean of μ and variance of σ^2.
P_i	Power of i-th user
$P_{I_U}^{(i)}$	Interference power effects the user group U in the iteration i.
$Pr_{U,\text{out}}^{PD}$	Outage probability of user group U for PD-NOMA
Pr_{out}^{PD}	Outage probability for PD-NOMA

$Pr^{WD}_{U,\text{out}}$	Outage probability of user group U for NOMA-2000
Pr^{WD}_{out}	Outage probability for NOMA-2000
$Pr^{NI}_{U,\text{out}}$	No-interference bound for outage probability of user group U
Pr^{NI}_{out}	No-interference bound for outage probability
$Pr^{OMA}_{U,\text{out}}$	OMA bound for outage probability of user group U
Pr^{OMA}_{out}	OMA bound for outage probability
r	Received signal for single carrier case
r_n	Received signal on n-th subcarrier
$\hat{R}$	Target rate
R^{PD}_k	Rate of k-th user for PD-NOMA
R^{WD}_k	Rate of k-th user for NOMA-2000
R^{PD}_U	Average rate of user group U for PD-NOMA
R^{PD}	Average rate for PD-NOMA
R^{WD}_U	Average rate of user group U for NOMA-2000
R^{WD}	Average rate for NOMA-2000
$R^{NI}_{U,}$	No-interference bound for the average rate of User Group U
R^{NI}	No-interference bound for the average rate
R^{OMA}_U	OMA bound for the average rate of User Group U
R^{OMA}	OMA bound for the average rate
$\Re$	Real part
S_i	SNR value of user i
$S^{(n)}_{U_1}$	SNR value of n-th user in U_1
$S^{(m)}_{U_2}$	SNR value of m-th user in U_2
t_i	Transmitted signal of i-th user
T_l	Scale parameter of l-th element for MGD model
t_l	Shape parameter of l-th element for MGD model
U_1	User group 1
$\tilde{U}_1$	User group includes to users share their subcarriers
$\hat{U}_1$	User group includes to users do not share their subcarriers
U_2	User group 2
w_l	Weight coefficient of l-th element for MGD model

z	Additive white noise
z_n	Additive white noise on n-th subcarrier
β_i	Threshold value of the outage condition for user group i
ϵ	Power imbalance coefficient
μ_W	Mean value of channel gains of U_1 makes interference on U_2
μ_Z	Mean value of channel gains of U_2 makes interference on U_1
τ	A threshold value between channel gains of both user groups
ϕ	Target SINR

LIST OF ACRONYMS/ABBREVIATIONS

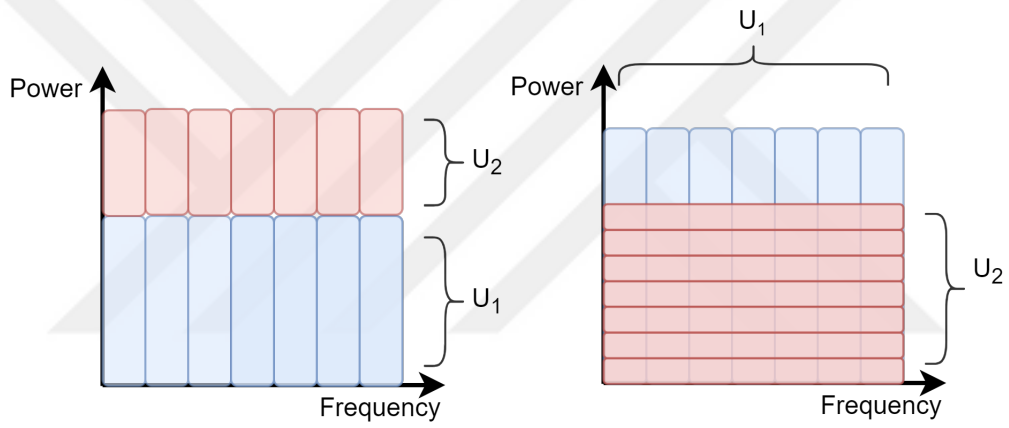
ABER	Average Bit Error Rate
ASER	Average Symbol Error Rate
AWGN	Additive White Gaussian Noise
BER	Bit Error Rate
BPSK	Binary Phase-Shift Keying
CDF	Cumulative Distribution Function
dB	Decibel
GD	Gamma Distribution
OFDMA	Orthogonal Frequency-Division Multiple Access
OMA	Orthogonal Multiple Access
MC-CDMA	Multiple-Carrier Code-Division Multiple Access
MGD	Mixture of Gamma Distribution
ML	Maximum Likelihood
NOMA	Non-Orthogonal Multiple Access
PDF	Probability Density Function
PD-NOMA	Power Domain Non-Orthogonal Multiple Access
QoS	Quality-of-Service
QPSK	Quadrature Phase-Shift Keying
SIC	Successive Interference Cancellation
SINR	Signal to Noise Plus Interference Ratio
SNR	Signal to Noise Ratio
WD-NOMA	Waveform Domain Non-Orthogonal Multiple Access
WH	Walsh-Hadamard

1. INTRODUCTION

Non-Orthogonal Multiple Access (NOMA), seen as a key enabling technology to realize the data rate requirements envisioned for the next generation networks, relies on allocating multiple user signals on each resource block at the transmitter side which are decoded by using successive interference cancellation at the receiver. A variety of techniques such as the use of different codebooks, waveforms, modulation types or power levels have been used to differentiate these superimposed user signals from each other as summarized in [1, 2]. Among these approaches, power-domain NOMA (PD-NOMA) has attracted the most attention in the literature where multiple Orthogonal Frequency Domain Multiple Access (OFDMA) users are assigned to the same frequency block and at the receiver, the received messages are decoded in an order depending on the channel gains by applying Successive Interference Cancellation (SIC) [3]. Notice that despite its ease of implementation and potential to achieve improved data rates, PD-NOMA encounters two essential drawbacks in practice: First, because the power differentiation among different users means either a trade-off with the provided quality of services (QoS) for the users with the weak signal or alternatively the need to employ elaborate resource block and/or power allocation algorithms. Second, because superimposed user signals are detected with a single-shot SIC receiver, it may cause error floors or a significant error degradation can be observed unless there is significant power difference among different user signals.

An attractive alternative to PD-NOMA, another NOMA technique where different user groups use different waveforms, namely waveform-domain NOMA (WD-NOMA), is proposed as discussed in [4]. One of them was proposed in [5–7] to alleviate the drawbacks of PD-NOMA, is called NOMA with orthogonal multiple waveforms or NOMA-2000 because it is based on a NOMA concept first introduced in 2000 (see [8] and [9]). For multi-carrier systems envisioned for 5G and beyond 5G wireless communications standards, it can be described as follows: The first group of user signals are assigned to orthogonal frequency-division multiple access (OFDMA) subcarriers as

in the conventional multi-carrier Orthogonal Multiple Access (OMA) schemes. Then unlike PD-NOMA where the second group of user signals are also assigned to the same subcarriers with one more user signal per subcarrier principle, in NOMA-2000 signals of second group of users are transmitted with multi-carrier code-division multiple access (MC-CDMA) waveforms where each user signal is spread over all subcarriers with an orthogonal spreading code. Notice that this spreading introduces an inherent power imbalance between the first group and the second group of user signals which is something that has to be imposed explicitly in PD-NOMA. Resource allocation schemes of both NOMA are summarized in Figure 1.1.



(a) (b)

Figure 1.1. Resource allocation on a) PD-NOMA and b) NOMA-2000.

At the receiver side, NOMA-2000 architecture lends itself to the use of iterative SIC making it possible to significantly reduce and in some cases virtually eliminate the bit error rate (BER) degradation generally observed in PD-NOMA and increase its coverage performance. Notice that the advantage of NOMA-2000 over PD-NOMA in terms of average BER performance has been shown in [5] for ideal Gaussian channels and in [7, 10] over fading channels where both static and dynamic channel assignment strategies are considered.

Then in [11], analytical expressions for the outage probability performances of NOMA-2000 and PD-NOMA are obtained for Rayleigh fading channels where both analytical and also simulation results show that NOMA-2000 has better outage performance than PD-NOMA in all channel and overload conditions. It is also worth

noting that in that work, the remaining interference power after the first iteration was modeled and calculations were made under this assumption.

As a result of being the most popular NOMA technique, there are plenty of works investigating PD-NOMA performance using different metrics and scenarios. Shannon's capacity is one of the metrics, and in [12] the use of NOMA instead of OMA is proven to increase the capacity region in terms of this metric. In [13], power allocation algorithms are proposed for the average rate, weighted sum rate and minimum rate. In [14–17], more sophisticated resource allocation schemes including user pairing, subcarrier and power allocation are analyzed. All of these works have defined the capacity under the assumption of perfect SIC. On the other hand, in [18–23] the residual interference caused after imperfect SIC has been taken into account for capacity. In these works, this interference power is expressed as proportional to a static variable in the range of 0 to 1. While, 0 indicates perfect SIC, 1 means that the interference power is not removed at all.

The outage probability performance of PD-NOMA has been studied in works such as [24–27] but all with the simplifying assumption of independence of outage events corresponding to different users. Unfortunately, the inherent signal superposition in NOMA makes this assumption invalid, causing relatively big mismatches between the analytical derivations and the simulated performances. For this reason, in works, this dependence is taken into consideration where exact derivations for the single-user case are obtained in [28] and outage probability expressions for multi-carrier PD-NOMA and NOMA-2000 are obtained in [11]. While in [11] analytical calculations of the outage performance in the first iteration have been performed, in this thesis we extend this work for further iterations.

In [29], it is shown that Rician fading, Nakagami-m fading and Rayleigh fading can be expressed with the parameters of the $\kappa - \mu$ fading. Furthermore, in [30] statistical characteristics of the $\kappa - \mu$ shadowed fading are discussed, and it is implied that $\kappa - \mu$ fading and Rician shadowed fading are specific cases of $\kappa - \mu$ shadowed fading.

Moreover, in [31], fluctuating Beckmann fading is proposed by implying that it is a more generalized version of $\kappa-\mu$ shadowed fading. Rician fading, Nakagami-m fading, Rayleigh fading and $\kappa-\mu$ fading can be expressed as a mixture of Gamma distribution (MGD) in [32, 33]. In [34], $\kappa-\mu$ shadowed fading with integer parameters are expressed as an MGD. In [33], the MGD approximation has been used for the analytical calculations of a wireless channel. In [32], these analyses are adopted to NOMA systems. There exist alternative formulations for real-valued parameters, however these formulations include infinite sum in [35, 36]. In [37], the outage probability, capacity and bit error rate are calculated without MGD approximation.

As illustrated by the aforementioned references, the literature is rich in the analysis and optimization of PD-NOMA performance in terms of capacity and the outage probability. On the other hand, as interest in NOMA-2000 is relatively recent, studies on its performance are not many. Particularly, the capacity analysis of NOMA-2000 is not investigated at all. To partially close this gap in the literature, we investigate uplink NOMA-2000 and PD-NOMA systems in which users experience Rayleigh fading and more generalized fading channels. During all analysis, we assume the use of a simple user grouping strategy in order to satisfy the power imbalance between user groups. In this regard, the outage probability calculations are derived by taking into account the interference remained after SIC and the dependency between outage events for both user groups. Second, we define the capacity of NOMA-2000 and PD-NOMA with generally accepted SNR/SINR definitions. Furthermore, we define new SINRs for both NOMA schemes with the interference caused by imperfect SIC. This interference is related to the outage performance of the system and we provide analytical calculations for the capacity with these new SINR definitions. Finally, we extend all derivations to generalized fading channels which are useful in describing $\kappa-\mu$ shadowed fading, $\kappa-\mu$ fading, Rician fading, Rician shadowed fading, Nakagami-m fading channel models. The overall contribution of this thesis is the comparison of NOMA-2000 and PD-NOMA performances in terms of common performance metrics outage probability and capacity over various channel scenarios. We demonstrate with both analytical derivations and simulation results that NOMA-2000 forms an attractive alternative to

conventional PD-NOMA in almost all the considered performance metrics.

The rest of this thesis is organized as follows: In chapter 2 the system model has been introduced. In Chapter 3 analyses have been derived for the Rayleigh fading channel model. In Chapter 4, previous derivations have been extended to more generalized fading channel models. Finally, the thesis has been concluded in Chapter 5.

2. Non-Orthogonal Multiple Access Techniques

In this chapter, basic principles of uplink NOMA are introduced with a simple 2-user case. Then, the system model is expanded to the multi-carrier case. Finally, a user grouping strategy that satisfies the fundamental requirement for multi-carrier NOMA is discussed.

2.1. Single Carrier NOMA

We consider an uplink system model where two users share the same resources to send their signals. Transmitted signals for user 1 and user 2, respectively, are

$$\mathrm{t}_1 = \sqrt{P_1}a, \quad \mathrm{t}_2 = \sqrt{P_2}b, \tag{2.1}$$

where a and b are information bits, P_t transmitted power of users, ϵ is the power imbalance coefficient $0 \leq \epsilon \leq 1$. In the BS, the signal is received as

$$r = \sqrt{P_1}h_1 a + \sqrt{P_2}h_2 b + z, \tag{2.2}$$

where z is the additive white Gaussian noise (AWGN) with zero mean and variance σ^2, $\mathcal{N}\ (0, \sigma^2)$, and h_i is the channel coefficient for user $i = 1, 2$. Each channel coefficient can be expressed as $h_i = g_i/l_i$, where l_i is the large-scale path loss and g_i is the small-scale channel fading coefficient, which we assume to have a Rayleigh distribution. The random variable $V \triangleq |g_i|^2$, called "channel gain," has the exponential probability density function (PDF)

$$f_V(v) = \frac{1}{2\mu^2} e^{-\frac{v}{2\mu^2}}, \quad v \geq 0. \tag{2.3}$$

In conventional communication systems, user powers are determined so as to compensate for the effect of path loss (see [38]). Specifically, as shown in [24], the power assignment to user 1 and user 2 can be done respectively, so as to generate a

power imbalance for NOMA as

$$P_1 = P_t l_1^2, \qquad P_2 = \epsilon P_t l_2^2, \tag{2.4}$$

where P_t is the target received power and $\epsilon \in (0, 1)$ is a system parameter that determines the amount of power imbalance. This enables our analysis to depend primarily on the small scale fading coefficients.

Now, we assume that channel gain of user 1 is higher than user 2, in other words, $|g_1|^2 > |g_2|^2$. BS detects the signal of the user 1, $\hat{a}$, under the interference of the user 2, and it is extracted from the received signal. This procedure is called SIC. After SIC, the remaining signal can be expressed as

$$\hat{r} = \sqrt{P_1} h_1 (a - \hat{a}) + \sqrt{P_2} h_2 b + z. \tag{2.5}$$

Notice that, when the signal of the first user is decoded correctly, user 2 detects its signal from the remaining signal, $\hat{r} = \sqrt{P_2} h_2 b + z$. The decoding scheme and its difference from OMA are summarized in Figure 2.1 in [39].

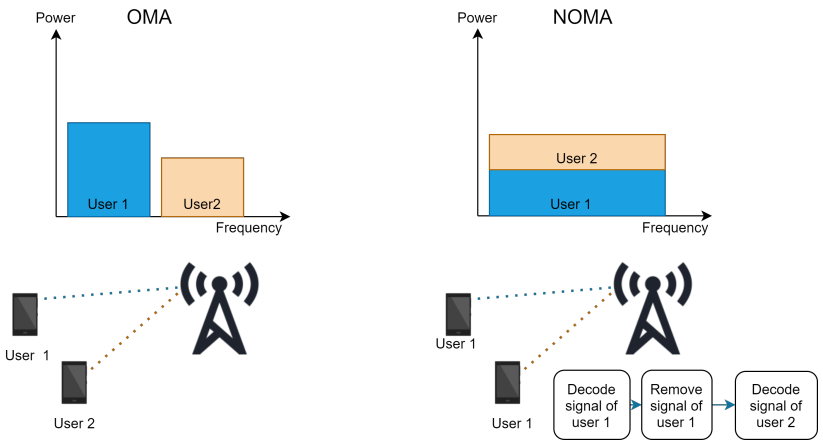


Figure 2.1. Transmitting and decoding scheme of uplink OMA and NOMA.

Then, we can express the signal to noise ratio (SNR) and the signal to noise plus interference ratio (SINR) for user 1 and user 2, respectively, as

$$S_1 = \frac{P_t |g_1|^2}{\epsilon P_t |g_2|^2 + \sigma^2}, \qquad S_2 = \frac{\epsilon P_t |g_2|^2}{\sigma^2}. \tag{2.6}$$

2.2. Multi Carrier NOMA

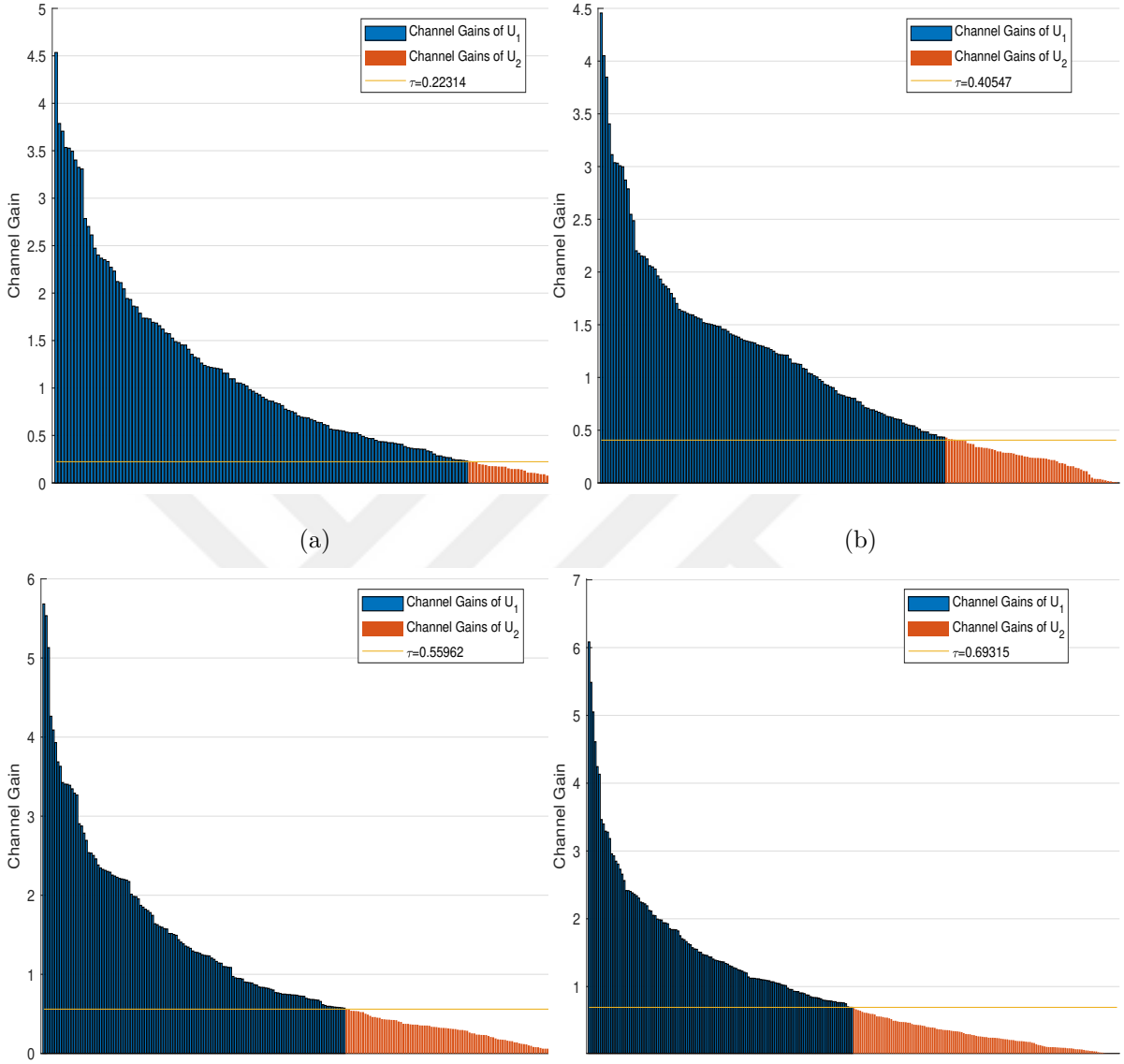


Figure 2.2. Channel gains of both user groups which are divided and corresponding threshold τ values a) OF=25%, b) OF=50%, c) OF=75% d) OF=100% .

In this section we present the basic principles and system models of the uplink NOMA systems under investigation. We investigate a multicarrier system with N subcarriers and $K > N$ users. We define $M = K - N$ as the number of excess users and the overloading factor (OF) as the ratio $\frac{M}{N}$ of the excess users to the total number of subcarriers. Notice that we can partition the users into two groups, say U_1 and U_2.

In order to satisfy the fundamental assumption of the NOMA, users from U_1 should have higher channel gains than users from U_2. To achieve that, the users with the N highest channel gains are assigned to the group U_1, while the remaining M users are assigned to the group U_2. The strategy can be summarized as follows: If $|g_n|^2 > |g_m|^2$, then User $n \in U_1$ and User $m \in U_2$.

In order to calculate performance metrics, we first need to define the PDFs of user groups separately. First, we define random variables X and Y correspond to channel gains of users in U_1 and U_2, respectively. Then, we assume a threshold τ which is smaller than the channel gains of all users in U_1, but greater than the channel gains of users in U_2. The value of τ can be calculated as

$$\frac{M}{N}\int_0^{\tau} \frac{1}{2\mu^2} e^{-\frac{v}{2\mu^2}} dv = \int_{\tau}^{\infty} \frac{1}{2\mu^2} e^{-\frac{v}{2\mu^2}}, \quad \tau = 2\mu^2 \ln(1+\frac{M}{N}). \tag{2.7}$$

Finally, we can express the PDFs of random variables X and Y by using the PDFs in (2.3) as

$$f_X(x) = \begin{cases} \frac{C_1}{2\mu^2} e^{-\frac{x}{2\mu^2}} dx, & x \geq \tau, \\ 0, & x < \tau, \end{cases}, \tag{2.8}$$

$$f_Y(y) = \begin{cases} \frac{C_2}{2\mu^2} e^{-\frac{y}{2\mu^2}}, & y < \tau, \\ 0, & y, \geq \tau, \end{cases} \tag{2.9}$$

respectively, where C_1 and C_2 are normalization constants which makes $\int f_X(x)dx = \int f_Y(y)dy = 1$. Explicitly, they can be calculated, respectively, as

$$\int_{\tau}^{\infty} C_1 f_V(v)dv = 1, \quad C_1 = \frac{1}{1-F_V(\tau)} = \frac{1}{\exp(-\frac{\tau}{2\mu^2})} = \frac{K}{M}, \tag{2.10}$$

$$\int_0^{\tau} C_2 f_V(v)dv = 1, \quad C_2 = \frac{1}{F_V(\tau)} = \frac{1}{1-\exp(-\frac{\tau}{2\mu^2})} = \frac{K}{N}. \tag{2.11}$$

Notice that X and Y are jointly independent and

$$\int_0^{\tau}\int_{\tau}^{\infty} f_{X,Y}(x,y)dxdy = \int_0^{\tau}\int_{\tau}^{\infty} f_X(x)f_Y(y)dxdy = 1. \tag{2.12}$$

In Figure 2.2, some examples are illustrated on realizations for different overloading factors. With these realizations, we can verify the assumption that channel gains of all users from U_1 are higher than the threshold value τ. Finally, power assignment scheme in (2.4) can be modified as

$$P_i = \begin{cases} P_{\mathrm{t}}\, l_i^2, & i \in U_1, \\ \epsilon P_{\mathrm{t}}\, l_i^2, & i \in U_2, \end{cases} \tag{2.13}$$

for multi-carrier NOMA.

2.2.1. PD-NOMA

We first consider the uplink PD-NOMA signal model. In PD-NOMA each subcarrier is either assigned to a single user from U_1, or to two users, one from U_1 and the other from U_2. To distinguish between these two cases, we also partition U_1 into two subgroups $\hat{U}_1$ and $\tilde{U}_1$, where $\hat{U}_1$ includes the users not sharing the subcarrier.

If users $n \in U_1$ and $N+n \in U_2$ are assigned to subcarrier n, the superimposed signal r_n received on subcarrier n can be written, for user n in $\hat{U}_1$ and user $N+n$ in U_2, as

$$r_n = \sqrt{P_n}h_n a_n + \sqrt{P_{N+n}}h_{N+n}b_n + z_n, \tag{2.14}$$

where P_n and P_{n+N} are the powers of the two users on subcarrier n, h_n and h_{n+N} are their channel coefficients, a_n and b_n are the information symbols transmitted by these two users, and z_n is an additive white Gaussian noise (AWGN) term with variance σ^2.

The BS decodes users' signals with their power order by treating interfering signals as noises. After the first signal is decoded, the interference affecting the first-user

signal is subtracted from the superimposed signal before the detection for the second-user signal starts in the SIC operation. In the Figure 2.3, the channel gains of U_1 and the interference powers caused by U_2 are illustrated for different overloading factors and ϵ values. It can be observed that for high ϵ values, some subcarriers may suffer from relatively higher interference. The consequences of this situation will be discussed in the subsequent chapters.

The corresponding SINR for the first group of users (strong signal users) and the SNR for the second group of users (weak signal users) can be written, respectively, at each subcarrier as

$$S_{U_1}^{(n)} = \frac{P_n|h_n|^2}{P_{N+n}|h_{N+n}|^2 + \sigma^2}, \quad S_{U_2}^{(n)} = \frac{P_{N+n}|h_{N+n}|^2}{\sigma^2}, \qquad n \in \hat{U}_1. \tag{2.15}$$

On the other hand, if user k in $\tilde{U}_1$ is the single user in a subcarrier, the received signal r_k can be expressed as

$$r_k = \sqrt{P_k} h_k a_k + z_k, \tag{2.16}$$

and the corresponding SNR is

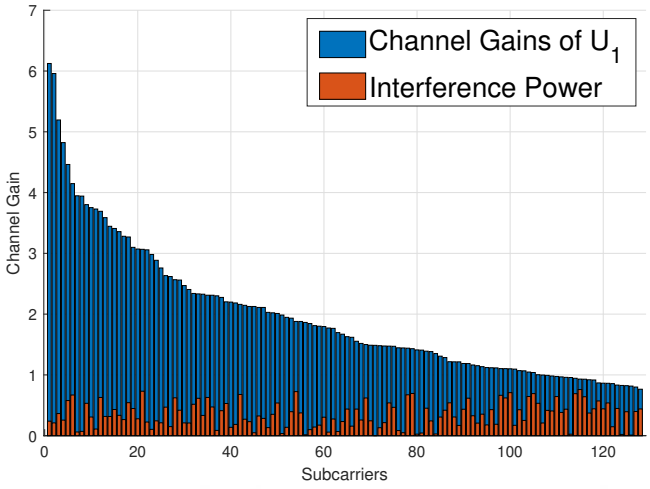
$$S_{\tilde{U}_1}^{(k)} = \frac{P_k|h_k|^2}{\sigma^2}, \qquad k \in \tilde{U}_1. \tag{2.17}$$

Lemma 2.1. *A single shot SIC procedure is the optimum decoding way equivalent to Maximum Likelihood detection for PD-NOMA, thus any iteration cannot increase the system performance.*

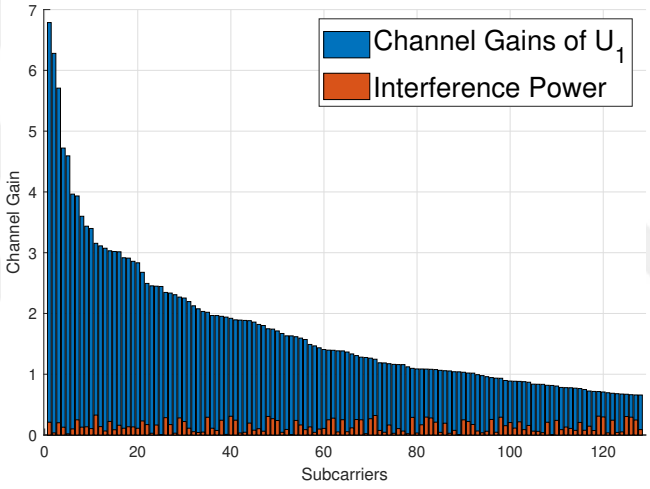
Proof. We consider the simplest case where $h_i = 1$ for $i = 1, 2$ and $P_t = 1$. Then we can express the received signal in (2.5) as

$$r = a + \epsilon b + z. \tag{2.18}$$

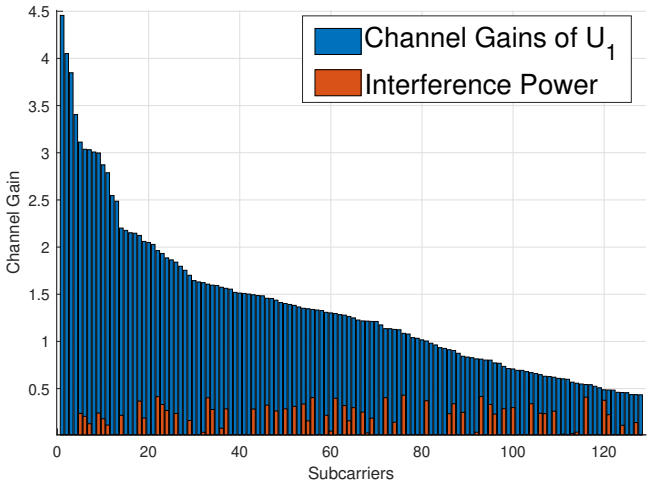
Now, we assume that a and b are binary phase-shift keying (BPSK) modulated signals for user 1 and user 2, respectively.



(a)



(b)



(c)

Figure 2.3. Channel gains of users on U_1 and interference powers on their subcarrier for PD-NOMA, N=128 Subcarriers, a) OF=100% and $\epsilon = 1.0$, b) OF=100% and $\epsilon = 0.5$, c) OF=50% and $\epsilon = 1.0$.

Then, an Maximum Likelihood (ML) detector should minimize the metric:

$$\arg\min ||r - a - \epsilon b||_2, \tag{2.19}$$

over all combinations of $a = \pm 1$ and $b = \pm 1$.

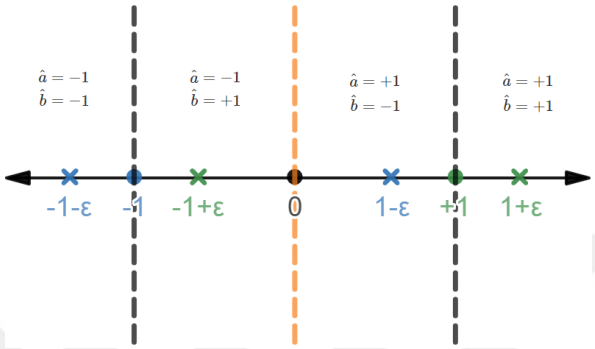


Figure 2.4. ML Detection Regions for the Superposed NOMA Signal.

We can visualize the detection regions in Figure 2.4. In this figure, dashed lines divide the detection regions, circles and crosses represent the modulation points for the first and second user, and $\hat{a}$ and $\hat{b}$ represent detected symbols of user 1 and user 2, respectively. To express mathematically, detection should be done for information bits a and b, respectively, as

$$\hat{a} = \begin{cases} +1 & r > 0, \\ -1 & r < 0, \end{cases} \tag{2.20}$$

$$\hat{b} = \begin{cases} +1 & r > 1, \quad \text{OR} \quad -1 < r < 0, \\ -1 & r < -1, \quad \text{OR} \quad 0 < r < +1. \end{cases} \tag{2.21}$$

Now, we can perform the single-shot SIC detection. For the $\hat{a}$, we can rewrite the same detection method can be written as

$$\hat{a} = \begin{cases} +1 & r > 0, \\ -1 & r < 0. \end{cases} \tag{2.22}$$

For $\hat{b}$, detection is done after cancellation. In other words, $\hat{b}$ is detected with the signal

$r - \hat{a}$ as

$$\hat{b} = \begin{cases} +1 & r - \hat{a} > 0, \\ -1 & r - \hat{a} < 0. \end{cases} \tag{2.23}$$

If (2.22) is plugged into (2.23), $\hat{b}$ detection rule can be obtained as,

$$\hat{b} = \begin{cases} +1 & (r > 1 \quad \text{OR} \quad -1 < r < 0) \implies r - \hat{a} > 0, \\ -1 & (r < -1 \quad \text{OR} \quad 0 < r < +1) \implies r - \hat{a} < 0, \end{cases} \tag{2.24}$$

which is equivalent to (2.21). This shows that SIC detection is the optimum detection method. This proof can be easily extended to other modulation types, or multiple users and multi-carriers. □

2.2.2. NOMA-2000

Following [5–7, 40], the uplink system model for NOMA-2000 can be described as follows. In NOMA-2000 two sets of orthogonal signal waveforms are utilized: while OFDMA forms the first signal set, and MC-CDMA is used as the second signal set. The first N users operate in OFDMA mode with one subcarrier assigned to each of them, while the additional M users are assigned to one MC-CDMA waveform by spreading their signals using a length-N Walsh-Hadamard (WH) code. As with PD-NOMA, we assume that users are grouped according to the method described in [7]. The corresponding signal on subcarrier n ($n = 1, 2, \ldots, N$) can written as

$$r_n = \sqrt{P_n} h_n a_n + I_{U_1,n} + z_n. \tag{2.25}$$

Here I_n denotes the interference on subcarrier n, given by

$$I_{U_1,n} = \frac{1}{\sqrt{N}} \sum_{i=1}^{M} \sqrt{P_{N+i}} (w_{i,n} h_{N+i}) b_i, \tag{2.26}$$

where $w_{m,n}$ is the n-th chip of the WH sequence associated with user m. The factor $1/\sqrt{N}$ is included for energy normalization. Because of the spreading, MC-CDMA

users interfere less with OFDMA users, and the OFDMA user signals can be decoded under this interference. After that, the decoded signal $\hat{a}_n$, $n \in U_1$, is subtracted from the superimposed signal. By using the multi-user MC-CDMA detection method in [41], the signal of the m-th MC-CDMA user can be decoded from the signal

$$\hat{r}_m = \sqrt{P_{N+m}} h_{N+m} b_m + I_{U_2,m} + u_m, \tag{2.27}$$

where u_m is an AWGN term with the same statistics as z_n. $I_{U_2,m}$ is the interference caused by the spreading of the OFDMA signals, and can be expressed as

$$I_{U_2,m} = \frac{1}{\sqrt{N}} \sum_{j=1}^{N} \sqrt{P_j} (w_{j,m} h_j)(a_j - \hat{a}_j). \tag{2.28}$$

Interference cancellation is done iteratively. The detected OFDMA symbols at each iteration are used to synthesize and cancel their interference on MC-CDMA symbols, and new decisions are made on these symbols. This operation is repeated until convergence occurs.

The peak interference power may cause a full closure of the eye diagram and the occurrence of a BER floor. To prevent that, a decoding method namely soft decision interference cancellation is used in [8, 10, 11]. Assuming that both user groups use quadrative phase-shift keying (QPSK), soft decisions at the first iteration use

$$\hat{a}_n = \mathbf{\Phi}\left(\Re(r_n)\right) + i\mathbf{\Phi}\left(\Im(r_n)\right), \tag{2.29}$$

$$\hat{b}_m = \mathbf{\Phi}\left(\Re(\hat{r}_m)\right) + i\mathbf{\Phi}\left(\Im(\hat{r}_m)\right), \tag{2.30}$$

respectively, where $\mathbf{\Phi}(\cdot)$ denotes an approximation to the hyperbolic tangent function, defined as

$$\mathbf{\Phi}(x) \triangleq \begin{cases} -1, & x \leq -\lambda, \\ x/\lambda, & -\lambda < x < \lambda, \\ +1, & x \geq \lambda, \end{cases} \tag{2.31}$$

where λ is a parameter that can be optimized to achieve the best performance. This detection method is easily adapted for other modulation types and further iterations. The decoding scheme for NOMA-2000 is illustrated in Figure 2.5.

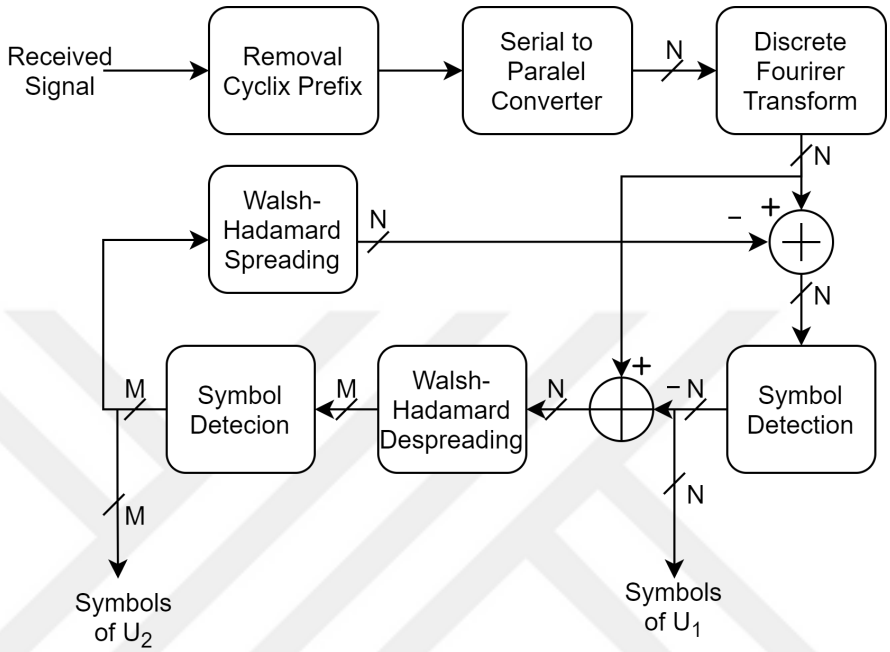


Figure 2.5. Decoding scheme of NOMA-2000.

In Figure 2.6, the channel gains of U_1 and the interference powers caused by U_2 are illustrated for different overloading factors and ϵ values. It can be observed that the interference power on each subcarrier is equal. The interference power is caused by spreading and depends on the overloading factor and ϵ value. The final SINR value of the n-th OFDMA user and the SNR value of the m-th MC-CDMA user can be written, respectively, as

$$\mathrm{S}_n^{WD} = \frac{P_n|h_n|^2}{\frac{1}{N}\sum_{i=1}^{M} P_{i+N}|h_{i+N}|^2 + \sigma^2}, \quad \mathrm{S}_m^{WD} = \frac{P_m|h_m|^2}{\sigma^2}. \tag{2.32}$$

2.2.3. No-interference and OMA bounds

In order to show the system performance, all performance metrics are also compared with an ideal case when each user uses its subcarrier solely, thus is not affected by any interference.

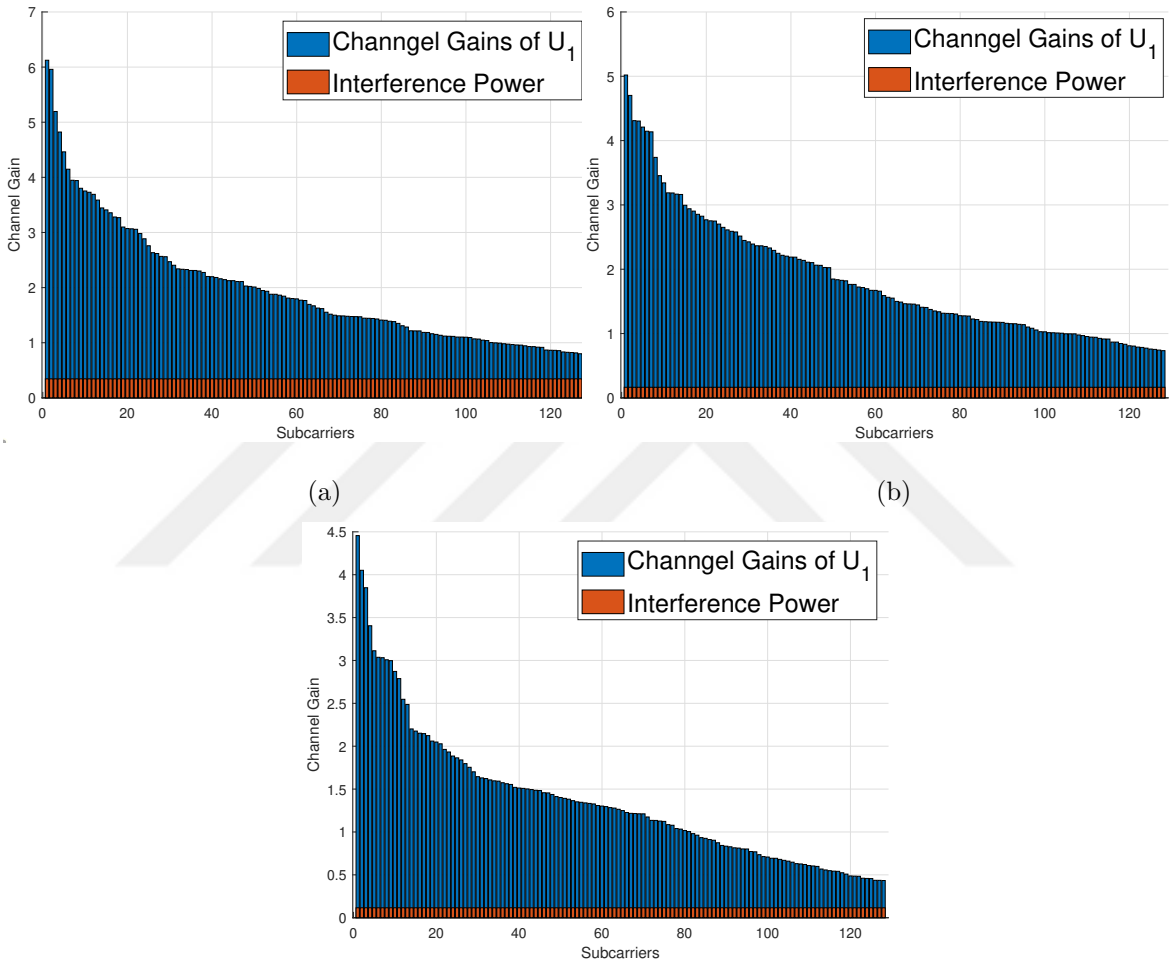


Figure 2.6. Channel gains of users on U_1 and interference powers on their subcarrier for NOMA-2000, N=128 Subcarriers, a) OF=100% and $\epsilon = 1.0$, b) OF=100% and $\epsilon = 0.5$, c) OF=50% and $\epsilon = 1.0$.

We can call this case as *no-interference* case and express SNR values of users as

$$\mathrm{S}_k^{NI} = \frac{P_m |h_m|^2}{\sigma^2}, \qquad k \in \{1, ..., M+N\}. \tag{2.33}$$

Notice that since in OMA users do not share their frequency resources, their bandwidhts are normalized with the factor $\frac{N}{M+N}$.

3. Design and Analysis of Non-Orthogonal Multiple Access over Rayleigh Fading Channels

In this chapter, we provide analytical expressions for the system models discussed in Chapter 2. We first define the outage probabilities and provide analytical calculations. Then, we provide analytical expressions for Shannon's capacity by using the SNR/SINR definitions provided in the previous chapter. Notice that these SNR/SINR definitions assume perfect SIC for U_2 in any case. In order to reach a more realistic capacity definition, we finally investigate capacity under imperfect SIC, and we use the outage events as a condition for SIC.

3.1. Outage Probability

In this section, we define the outage events and derive the outage probabilities for NOMA users. We start with the simplest case of a single carrier and two users, next we extend our calculations to multicarrier NOMA. For PD-NOMA, the coverage events for both users are defined, and the outage probabilities are derived by using the dependency between these two events. For NOMA-2000, we calculate the interference powers for each iteration are calculated separately in the deviation of the outage probabilities.

3.1.1. PD-NOMA

Based on the system model of Chapter 2 in which user $n \in \hat{U}_1$ and user $N+n \in U_2$ share the same subcarrier, E_n^{PD} and E_{N+n}^{PD} are defined as the coverage events where user n has an SINR level higher than the target SINR and user $N+n$ has an SNR level higher than a target SNR after SIC, respectively. The outage of user n is defined when E_n^{PD} does not occur. On the other hand, user $N+n$ is in outage if neither E_n^{PD} nor E_{N+n}^{PD} occurs, in which case the BS cannot decode the signal of user $N+n$ because it fails to decode the signal of user n.

The corresponding events can be written, respectively, as

$$\begin{aligned} E_n^{PD} &= \left\{ \frac{P_n|h_n|^2}{P_{N+n}|h_{N+n}|^2+\sigma^2} \geq \phi \right\} \\ &= \left\{ |g_n|^2 \geq \phi \frac{P_{N+n} l_n^2}{P_n l_{N+n}^2} |g_{N+n}|^2 + \beta_1 \right\} \\ &= \left\{ |g_n|^2 \geq \alpha |g_{N+n}|^2 + \beta_1 \right\}, \end{aligned} \tag{3.1}$$

$$\begin{aligned} E_{N+n}^{PD} &= \left\{ \frac{P_{N+n}|h_{N+n}|^2}{\sigma^2} \geq \phi \right\} \\ &= \left\{ P_{N+n}|h_{N+n}|^2 \geq \phi\sigma^2 \right\} = \left\{ |g_{N+n}|^2 \geq \beta_2 \right\}, \end{aligned} \tag{3.2}$$

$$E_n^{PD} \cap E_{N+n}^{PD} = \left\{ |g_n|^2 \geq \alpha |g_{N+n}|^2 + \beta_1, |g_{N+n}|^2 \geq \beta_2 \right\}, \tag{3.3}$$

where $\beta_1 \triangleq \frac{\phi}{P_t}\sigma^2$, $\beta_2 \triangleq \frac{\phi}{\epsilon P_t}\sigma^2$, $\alpha \triangleq \phi\epsilon$, $\phi \triangleq (2^{\hat{R}}-1)$ and $\hat{R}$ is the target rate. Then the outage probabilities of users n and $N+n$ can be formulated, respectively, as

$$Pr_{n,\text{out}} = 1 - Pr(E_n^{PD}), \tag{3.4}$$

$$Pr_{N+n,\text{out}} = 1 - Pr(E_n^{PD} \cap E_{N+n}^{PD}). \tag{3.5}$$

In some works (e.g., [24–27]), the events E_n^{PD} and E_{N+n}^{PD} are assumed to be independent, which leads to $Pr_{\text{out,N+n}} = 1 - Pr(E_n^{PD})Pr(E_{N+n}^{PD})$. However, it can be seen that the random variable $|g_{N+n}|^2$ is common to both events, and therefore these are generally not independent. Starting with the simplest case where $N = 1$ and $K = 2$, outage probabilities of the events E_1^{PD} E_2^{PD} and $E_1^{PD} \cap E_2^{PD}$ can be computed, respectively, in closed form, using equations (3.1), (3.3), (3.4) and (3.5), as

$$Pr(E_1^{PD}) = 2\int_0^\infty \int_{\alpha x_2+\beta_1}^\infty f_{V_1}(v_1) f_{V_2}(v_2) dv_1 dv_2$$

$$= \frac{2}{\alpha+1}\exp(-\beta_1/2\mu^2), \tag{3.6}$$

$$Pr(E_2^{PD}) = \int_{\beta_2}^{\infty} 2f_V(v)(1-F_V(v))dv = \exp(-\beta_2/\mu^2), \tag{3.7}$$

$$\begin{aligned} Pr(E_1^{PD} \cap E_2^{PD}) &= 2\int_{\beta_2}^{\infty}\int_{\alpha v_2+\beta_1}^{\infty} f_{V_1}(v_1)f_{V_2}(v_2)dv_1dv_2 \\ &= \frac{2}{\alpha+1}\exp\left\{-\frac{(\alpha+1)\beta_2}{2\mu^2}\right\}\exp(-\beta_1/2\mu^2). \end{aligned} \tag{3.8}$$

Notice that the independence assumption is only valid when $\alpha = 1$, which makes $Pr(E_1^{PD} \cap E_2^{PD}) = Pr(E_2^{PD})Pr(E_1^{PD})$.

Next, we consider the general case of N subcarriers and K users. The outage probability of users who share their subcarriers with an excess user, denoted $Pr_{\hat{U}_1,\text{out}}^{PD}$, can be found as

$$\begin{aligned} Pr_{\hat{U}_1,\text{out}}^{PD} &= 1 - Pr\left(|g_n|^2 > \alpha|g_m|^2 + \beta_1 | |g_n|^2 > \tau, |g_m|^2 < \tau\right) \\ &= 1 - Pr\left(x > \alpha y + \beta_1\right) \\ &= 1 - \int_0^{\tau}\int_{\alpha y+\beta_1}^{\infty} f_X(x)f_Y(y)dxdy \\ &= 1 - \int_0^{max(0,\frac{\tau-\beta_1}{\alpha})}\int_{\tau}^{\infty} f_X(x)f_Y(y)dxdy \\ &\quad - \int_{max(0,\frac{\tau-\beta_1}{\alpha})}^{\tau}\int_{\alpha y+\beta_1}^{\infty} f_X(x)f_Y(y)dxdy \\ &= 1 - \int_0^{max(0,\frac{\tau-\beta_1}{\alpha})} f_Y(y)dy - \int_{max(0,\frac{\tau-\beta_1}{\alpha})}^{\tau}\int_{\alpha y+\beta_1}^{\infty} f_X(x)f_Y(y)dxdy \\ &= 1 - \left(-C_2 e^{-\frac{y}{2\mu^2}}\right)\Bigg|_0^{max(\frac{\tau-\beta_1}{\alpha},0)} - \left(C_1\int_{max(\frac{\tau-\beta_1}{\alpha},0)}^{\tau} -e^{\frac{x}{2\mu^2}} f_Y(y)dy\right)\Bigg|_{\alpha y+\beta_1}^{\infty} \\ &= 1 - C_2\left(1 - e^{-\frac{max(0,\frac{\tau-\beta_1}{\alpha})}{2\mu^2}}\right) - C_1 e^{-\frac{\beta_1}{2\mu^2}}\int_{max(0,\frac{\tau-\beta_1}{\alpha})}^{\tau}\frac{C_2}{2\mu^2}e^{-\frac{(\alpha+1)y}{2\mu^2}}dy \end{aligned}$$

$$
\begin{aligned}
&= 1 - C_2\left(1 - e^{-\frac{max(0,\frac{\tau-\beta_1}{\alpha})}{2\mu^2}}\right) - \frac{C_1C_2}{\alpha+1}e^{-\frac{\beta_1}{2\mu^2}}\left(-e^{-\frac{(\alpha+1)y}{2\mu^2}}\right)\Bigg|_{max(0,\frac{\tau-\beta_1}{\alpha})}^{\tau} \\
&= 1 - C_2\left(1 - e^{-\frac{max(0,\frac{\tau-\beta_1}{\alpha})}{2\mu^2}}\right) \\
&- \frac{C_1C_2}{\alpha+1}e^{-\frac{\beta_1}{2\mu^2}}\left(e^{-\frac{(\alpha+1)max(0,\frac{\tau-\beta_1}{\alpha})}{2\mu^2}} - e^{-\frac{(\alpha+1)\tau}{2\mu^2}}\right) \\
&= \begin{cases} 1 - \frac{C_2C_1}{\alpha+1}e^{-\frac{\beta_1}{2\mu^2}}\left(1 - e^{-\frac{(\alpha+1)\tau}{2\mu^2}}\right), & \beta_1 \geq \tau, \\ 1 - C_2\left(1 - e^{-\frac{\tau-\beta_1}{2\mu^2\alpha}}\right) - \frac{C_2C_1}{\alpha+1}e^{-\frac{\beta_1}{2\mu^2}}\left(e^{-\frac{(\alpha+1)(\tau-\beta_1)}{2\mu^2\alpha}} - e^{-\frac{(\alpha+1)\tau}{2\mu^2}}\right), & \beta_1 < \tau. \end{cases} \qquad (3.9)
\end{aligned}
$$

The integral is divided into two parts because when the secondary users have channel gain lower than $\frac{\tau-\beta_1}{\alpha}$, the primary users on the same subcarrier are always in coverage. In order to exclude the negative borders of the integral, ρ is defined as $\rho = 1$ when $\beta_1 < \tau$, otherwise 0. Additionally, the outage probability for the users who are the sole dwellers of their respective subcarriers, denoted $Pr^{PD}_{\tilde{U}_1,\text{out}}$, can be derived as

$$
\begin{aligned}
Pr^{PD}_{\tilde{U}_1,\text{out}} &= 1 - Pr\left(\left\{|g_k|^2 \geq \beta_1\right\}\right) = 1 - \int_{\max(\tau,\beta_1)}^{\infty} f_X(x)dx \\
&= 1 - \exp\left(-\frac{\max(\tau,\beta_1)}{2\mu^2}\right). \qquad (3.10)
\end{aligned}
$$

The outage probability of U_1 can be found as

$$
Pr^{PD}_{U_1,\text{out}} = \frac{M}{N}\left(Pr^{PD}_{\hat{U}_1,\text{out}}\right) + \frac{N-M}{N}\left(Pr^{PD}_{\tilde{U}_1,\text{out}}\right), \qquad (3.11)
$$

and for U_2 as

$$
\begin{aligned}
Pr^{PD}_{U_2,out} &= 1 - Pr\left(|g_m|^2 > \beta_2, |g_n|^2 > \alpha|g_m|^2 + \beta_1 | |g_n|^2 > \tau, |g_m|^2 < \tau\right)\right) \\
&= 1 - Pr(y > \beta_2, x > \alpha y + \beta_1) \\
&= 1 - \int_{min(\beta_2,\tau)}^{\tau}\int_{\alpha y+\beta_1}^{\infty} f_X(x)f_Y(y)dxdy. \qquad (3.12)
\end{aligned}
$$

Notice that when $\beta_2 > \tau$, it means that no users from U_2 can reach the threshold to satisfy the minimum rate condition, thus its outage probability will be 1. the other case, the integrals can be calculated as

$$
\begin{aligned}
Pr^{PD}_{U_2,out|\beta_2\leq\tau} &= 1-\int_{\beta_2}^{\tau}\int_{\alpha y+\beta_1}^{\infty} f_X(x)f_Y(y)dxdy \\
&= 1-\int_{\beta_2}^{max(\beta_2,\frac{\tau-\beta_1}{\alpha})}\int_{\tau}^{\infty} f_X(x)f_Y(y)dxdy \\
&- \int_{max(\beta_2,\frac{\tau-\beta_1}{\alpha})}^{\tau}\int_{\alpha y+\beta_1}^{\infty} f_X(x)f_Y(y)dxdy \\
&= 1-\int_{\beta_2}^{max(\beta_2,\frac{\tau-\beta_1}{\alpha})} f_Y(y)dy - \int_{max(\beta_2,\frac{\tau-\beta_1}{\alpha})}^{\tau}\int_{\alpha y+\beta_1}^{\infty} f_X(x)f_Y(y)dxdy \\
&= 1-\left(-C_2 e^{-\frac{y}{2\mu^2}}\right)\Bigg|_{0}^{max(\frac{\tau-\beta_1}{\alpha},\beta_2)} \\
&- \left(C_1\int_{max(\frac{\tau-\beta_1}{\alpha},\beta_2)}^{\tau} -e^{\frac{x}{2\mu^2}} f_Y(y)dy\right)\Bigg|_{\alpha y+\beta_1}^{\infty} \\
&= 1-C_2\left(e^{-\frac{\beta_2}{2\mu^2}} - e^{-\frac{max(\beta_2,\frac{\tau-\beta_1}{\alpha})}{2\mu^2}}\right) \\
&- C_1 e^{-\frac{\beta_1}{2\mu^2}}\int_{max(\beta_2,\frac{\tau-\beta_1}{\alpha})}^{\tau}\frac{C_2}{2\mu^2}e^{-\frac{(\alpha+1)y}{2\mu^2}}dy \\
&= 1-C_2\left(e^{-\frac{\beta_2}{2\mu^2}} - e^{-\frac{max(\beta_2,\frac{\tau-\beta_1}{\alpha})}{2\mu^2}}\right) \\
&- \frac{C_1C_2}{\alpha+1}e^{-\frac{\beta_1}{2\mu^2}}\left(-e^{-\frac{(\alpha+1)y}{2\mu^2}}\right)\Bigg|_{max(\beta_2,\frac{\tau-\beta_1}{\alpha})}^{\tau} \\
&= 1-C_2\left(e^{-\frac{\beta_2}{2\mu^2}} - e^{-\frac{max(\beta_2,\frac{\tau-\beta_1}{\alpha})}{2\mu^2}}\right) \\
&- \frac{C_1C_2}{\alpha+1}e^{-\frac{\beta_1}{2\mu^2}}\left(e^{-\frac{(\alpha+1)max(\beta_2,\frac{\tau-\beta_1}{\alpha})}{2\mu^2}} - e^{-\frac{(\alpha+1)\tau}{2\mu^2}}\right). \qquad (3.13)
\end{aligned}
$$

Finally, we can express the outage probability for U_2 as

$$Pr_{U_2,out}^{PD} = \begin{cases} 1, & \beta_2 > \tau, \\ 1 - \frac{C_1 C_2}{\alpha+1} e^{-\frac{\beta_1}{2\mu^2}} \left(e^{-\frac{(\alpha+1)\beta_2}{2\mu^2}} - e^{-\frac{(\alpha+1)\tau}{2\mu^2}} \right), & \tau \geq \beta_2 > \dfrac{\tau - \beta_1}{\alpha}, \\ 1 - C_2 \left(e^{-\frac{\beta_2}{2\mu^2}} - e^{-\frac{\tau-\beta_1}{2\mu^2\alpha}} \right) & \\ -\frac{C_1 C_2}{\alpha+1} e^{-\frac{\beta_1}{2\mu^2}} \left(e^{-\frac{(\alpha+1)(\tau-\beta_1)}{2\mu^2\alpha}} - e^{-\frac{(\alpha+1)\tau}{2\mu^2}} \right), & \beta_2 \leq \dfrac{\tau - \beta_1}{\alpha}. \end{cases} \tag{3.14}$$

Then, PD-NOMA outage probability can be expressed as

$$Pr_{\text{out}}^{PD} = \frac{N Pr_{U_1,\text{out}}^{PD} + M Pr_{U_2,\text{out}}^{PD}}{M+N}. \tag{3.15}$$

3.1.2. NOMA-2000

As discussed in Chapter 2, SIC is performed iteratively in NOMA-2000. Therefore, we can assume that if a user is in coverage, its signal can be decoded correctly and it does not cause an interference for other user groups. Then, we can calculate interference power of each user group iteratively, until it convergences.

For the first iteration, the interference power for U_1, $P_{I_{U_1}}^{(1)}$, that is equal to summation of received powers per subcarrier, that is given as

$$P_{I_{U_1}}^{(1)} = \frac{\epsilon P_t}{N} \sum_{n=1}^{N} |g_{N+n}|^2. \tag{3.16}$$

Then, we can calculate SINR for U_1 in the first iteration as

$$S_{U_1,n}^{(1),WD} = \frac{P_t |g_n|^2}{P_{I_{U_1}}^{(1)} + \sigma^2}. \tag{3.17}$$

The BS, on the other hand, performs SIC before decoding signal of U_2. Then, the interference power and the SINR are calculated, respectively, by taking the received

powers of U_1 in outage into account, as

$$P_{U_2}^{(1)} = \frac{P_t}{N} \sum_{n \in R_{U_1,n}^{(1)} < \hat{R}} |g_n|^2, \tag{3.18}$$

$$S_{U_2,N+n}^{(1),WD} = \frac{P_t |g_{N+n}|^2}{P_{I_{U_2}}^{(1)} + \sigma^2}. \tag{3.19}$$

Notice that $n \in R_{U_1,n}^{(1)} < \hat{R}$ represents the indices of users who cannot satisfy the minimum rate condition and $P_{U_2}^{(1)}$ represent the interference power caused by these U_2 users.

Now, we can define the coverage events in each iteration separately. For user $n \in U_1$ it is denoted as $E_{U_1,n}^{(i),WD}$ and for user $m \in U_2$ it is denoted as $E_{U_2,m}^{(i),WD}$. Now, the outage probabilities for the n-th user in U_1 and for the m-th user in U_2 in iteration i can be defined, respectively, as

$$Pr_{out}^{(i)FD}(U_1, n) = 1 - Pr(E_{U_1,n}^{(i),WD}) = 1 - Pr\left(|g_n|^2 > \frac{\phi}{P_t} P_{I_{U_1}}^{(i)} + \beta_1\right), \tag{3.20}$$

$$Pr_{out}^{(i)FD}(U_2, m) = 1 - Pr(E_{U_2,m}^{(i),WD}) = 1 - Pr\left(|g_{N+m}|^2 > \frac{\phi}{\epsilon P_t} P_{I_{U_2}}^{(i)} + \beta_2\right). \tag{3.21}$$

In order to make analytical derivations, we first define a new random variable $Z \triangleq N^{-1} \sum_{k=1}^{M} Y_k$ modeling the interference on each subcarrier caused by the signals from U_2. Invoking the central limit theorem, we approximate Z with a Gaussian random variable. The following relations hold between the channel gains of the MC-CDMA users and the interference:

$$E[Z] = \frac{M}{N} E[Y], \tag{3.22}$$

$$\begin{aligned} E[Z^2] &= \frac{1}{N^2} \left(E\left[\sum_{k=1}^{M} Y_k^2 + \sum_{k=1}^{M} \sum_{j \neq k} Y_k Y_j \right] \right) \\ &= \frac{M}{N^2} E[Y^2] + \frac{M^2 - M}{N^2} E[Y]^2, \end{aligned} \tag{3.23}$$

$$\mathrm{Var}(Z) \;=\; \frac{M}{N^2}E[Y^2] - \frac{M}{N^2}E[Y]^2, \tag{3.24}$$

where $E[Y] = 2\,C_2\mu^2 - C_2 e^{-\frac{\tau}{2\mu^2}}(\tau + 2\mu^2)$, and $E[Y^2] = 8\,C_2\mu^4 - C_2 e^{-\frac{\tau}{2\mu^2}}(\tau^2 + 4\tau\mu^2 + 8\mu^4)$. Moreover, following [42], we approximate the probability distribution of $\dfrac{Z-\mu_Z}{\sigma_Z}$ as a normal random variable, i.e., $\dfrac{Z-\mu_Z}{\sigma_Z} \sim \mathcal{N}(0,1)$. We hasten to observe that, since Z is a finite sum of non-negative random variables, this approximation becomes less and less valid when the tails of the distribution are involved in the calculations.

Notice that, for normalized channel gains ($2\mu^2 = 1$) making $\mu_Z \gg \sigma_Z^2$. As a result, $Pr\{\mu_Z(1-\delta) \le Z \le \mu_Z(1+\delta)\} \approx 1$ for small δ values. Then, outage probability for U_1 users in first iteration can be derived as

$$\begin{aligned} Pr^{(1),WD}_{U_1,\mathrm{out}} &= 1 - Pr(X > \frac{\phi}{P_t}P^{(1)}_{I_{U_1}} + \beta_1) \\ &= 1 - Pr(\phi\epsilon Z + \beta_1) \approx 1 - Pr(X > \phi\epsilon\mu_Z + \beta_1) \\ &= 1 - \int_{\max(\phi\epsilon\mu_Z+\beta_1,\tau)}^{\infty} f_X(x)dx = 1 - C_1 e^{-\dfrac{\max(\phi\epsilon\mu_Z+\beta_1,\tau)}{2\mu^2}}. \end{aligned} \tag{3.25}$$

Signals of U_2 can decoded under the interference caused by the imperfect SIC of users in U_1 thanks to spreading. Similarly, we can model the interference in first iteration, $P^{(1)}_{I_{U_2}}$, with a new random variable $P_t W \triangleq P^{(1)}_{I_{U_2}}$. Then, the outage probability of U_2 in the first iteration is equal to

$$Pr^{(1),WD}_{U_2,\mathrm{out}} = \begin{cases} C_2 - C_2 \exp\left(-\frac{\beta_2+\mu_W\Phi}{\epsilon 2\mu^2}\right), & \beta_2 \ge \tau, \\ 1, & \beta_2 < \tau. \end{cases} \tag{3.26}$$

where μ_W is the mean value of the interference caused by OFDMA users in outage in first iteration, which can be calculated as

$$\begin{aligned} \mu^{(i)}_W &= \int_{\tau}^{\max(\beta_1+\phi\epsilon\mu_z,\tau)} x f_X(x)dx \\ &= e^{\frac{\tau}{2\mu^2}}(2\mu^2+\tau) - e^{\frac{\max(\beta_1+\phi\epsilon\mu_z,\tau)}{2\mu^2}}(2\mu^2 + \max(\beta_1+\phi\epsilon\mu_z,\tau)). \end{aligned} \tag{3.27}$$

For the next iterations, interference power and outage probabilities can be calculated by taking account of received power of previous iterations. In other words, values of $\mu_Z, \mu_W, Pr_{U_1,\text{out}}^{(i),WD}$ and $Pr_{\text{out}}^{(i),WD}$ can be calculated for i-th iteration, respectively, as

$$\begin{aligned}\mu_Z^{(i)} &= \int_0^{\min(\frac{\phi}{\epsilon}\mu_W^{(i-1)}+\beta_1,\tau)} y f_Y(y)dx \qquad (3.28)\\ &= C_2\mu^2 - C_2 \exp\left(-\frac{\min(\frac{\phi}{\epsilon}\mu_W^{(i-1)}+\beta_1,\tau)}{2\mu^2}\right)(\min(\frac{\phi}{\epsilon}\mu_W^{(i-1)}+\beta_1,\tau)+2\mu^2),\end{aligned}$$

$$\begin{aligned}\mu_W^{(i)} &= \int_\tau^{\max(\phi\epsilon\mu_Z^{(i)}+\beta_1,\tau)} x f_X(x)dx\\ &= \exp\left(\frac{\tau}{2\mu^2}\right)(2\mu^2+\tau) - \exp\left(\frac{\max(\beta_1+\phi\epsilon\mu_Z^{(i)},\tau)}{2\mu^2}\right)\\ &\quad \left(2\mu^2+\max(\beta_1+\phi\epsilon\mu_Z^{(i)},\tau)\right), \qquad (3.29)\end{aligned}$$

$$Pr_{U_1,\text{out}}^{(i),WD} = 1 - C_1 e^{-\frac{\max(\phi\epsilon\mu_Z^{(i)}+\beta_1,\tau)}{2\mu^2}}, \qquad (3.30)$$

$$Pr_{U_2,\text{out}}^{(i),WD} = C_2 - C_2 \exp\left(-\min(\frac{\tau}{2\mu^2}, \frac{\beta_2+\mu_W^{(i)}\Phi)}{\epsilon 2\mu^2}\right). \qquad (3.31)$$

Finally, the average outage probability can be written as

$$Pr_{\text{out}}^{(i),WD} = \frac{NPr_{U_1,\text{out}}^{(i),WD} + MPr_{U_2,\text{out}}^{(i),WD}}{M+N}. \qquad (3.32)$$

3.1.3. No-interference and OMA Bounds

In order to show the performance of NOMA-2000 a theoretical lower bound Pr_{out}^{NI} is also derived by using (2.33). This lower bound indicates the outage performance when there is no interference or decoding dependency. It is calculated as

$$Pr_{\text{out}}^{NI} = \frac{N}{K}\int_\tau^{\max(\beta_1,\tau)} f_Y(y)dy + \frac{M}{K}\int_0^{\min(\beta_2,\tau)} f_X(x)dx \qquad (3.33)$$

$$= \frac{N}{K}C_1\left(e^{-\frac{\tau}{2\mu^2}} - e^{-\frac{\max(\beta_1,\tau)}{2\mu^2}}\right) + \frac{M}{K}C_2\left(1 - e^{-\frac{\min(\beta_2,\tau)}{2\mu^2}}\right).$$

Furthermore, an OMA bound can be calculated similarly. Because bandwidth is normalized with the factor of $\frac{N}{K}$, the threshold values β_1 and β_2 turn into $\hat{\beta}_1 \triangleq \sigma^2\left(2^{\hat{R}\frac{K}{N}} - 1\right)$ and $\hat{\beta}_2 \triangleq \frac{\sigma^2}{\epsilon}\left(2^{\hat{R}\frac{K}{N}} - 1\right)$, respectively. Then, the OMA bound can be expressed as

$$Pr_{\text{out}}^{OMA} = \frac{N}{K}\int_{\tau}^{\max(\hat{\beta}_1,\tau)} f_Y(y)dy + \frac{M}{K}\int_{0}^{\min(\hat{\beta}_2,\tau)} f_X(x)dx \tag{3.34}$$

$$= \frac{N}{K}C_1\left(e^{-\frac{\tau}{2\mu^2}} - e^{-\frac{\max(\hat{\beta}_1,\tau)}{2\mu^2}}\right) + \frac{M}{K}C_2\left(1 - e^{-\frac{\min(\hat{\beta}_2,\tau)}{2\mu^2}}\right).$$

3.2. Capacity

In this section, we derive the capacity expressions for the PD-NOMA and NOMA-2000 by using the SNR/SINR values in Chapter 2. However, these definitions assume perfect SIC for U_2. Therefore, we also derive the capacity expressions under imperfect SIC assumption in the next section.

3.2.1. PD-NOMA

In this part, we first obtain the individual user rates and then we use them to obtain the average sum rate for PD-NOMA. Following [13], the data rate of the k-th user measured in bits/s/Hz is defined as

$$R_k^{PD} \triangleq \log_2(1 + S_k^{PD}), \qquad k \in U_1 \cup U_2, \tag{3.35}$$

where S_k^{PD} denotes the SINR or SNR depending on whether user k belongs to U_1 or U_2, given in equation (2.32).

To calculate the average sum rate, the average rate of each user is estimated first and then the average rate of each user group is evaluated. Starting with the users in group U_2, the average rate can be written as

$$R_{U_2}^{PD} = \int_0^{\tau} \log_2\left(1 + \frac{\epsilon P_t}{\sigma^2} y\right) f_Y(y) dx. \tag{3.36}$$

Using integration by parts with the variables $u \triangleq \log_2(1+ax)$ and $\frac{dv}{dx} \triangleq C_2 b e^{-bx}$ for $a \triangleq \frac{\epsilon P_t}{\sigma^2}$ and $b \triangleq \frac{1}{2\mu^2}$, equation (3.36) can be rewritten as $R_{U_2} = uv\Big|_0^{\tau} - \int_0^{\tau} v du$ which can be expressed as

$$R_{U_2}^{PD} = -C_2 \log_2(1+a\tau)e^{-b\tau} + \frac{C_2 e^{\frac{b}{a}}}{\ln(2)}\left(\mathrm{E_i}\left(-b\tau - \frac{b}{a}\right) - \mathrm{E_i}\left(-\frac{b}{a}\right)\right), \tag{3.37}$$

where $\mathrm{E_i}$ is the exponential integral function which can be expressed as $\mathrm{E_i}(x) = \int_{-\infty}^{x} \frac{e^t}{t} dt$.

Now, we can perform similar steps for users on $\hat{U}_1$ and $\tilde{U}_1$. Starting from $\hat{U}_1$, the average rate can be expressed as

$$R_{\hat{U}_1}^{PD} = \int_0^{\tau}\int_{\tau}^{\infty} log_2(1 + \frac{P_t x}{\sigma^2 + \epsilon P_t y})\frac{C_1}{2\mu^2} exp(-\frac{x}{2\mu^2})\frac{C_2}{2\mu^2} exp(-\frac{y}{2\mu^2}) dx dy. \tag{3.38}$$

By using slack variables $a_1 = \frac{C_1}{2\mu^2}, a_2 = \frac{P_t}{\sigma^2 + \epsilon P_t Y}, a_3 = \frac{1}{2\mu^2}$, the outer integral can be computed as

$$\begin{aligned}
R_{\hat{U}_1}^{PD} &= \int_0^{\tau} \frac{C_2}{2\mu^2}\exp(-\frac{y}{2\mu^2})\left[\int_{\tau}^{\infty} a_1 \log_2(1+a_2 x)\exp(-a_3 x) dx\right] dy \\
&= \int_0^{\tau} \frac{C_2}{2\mu^2}\exp(-\frac{y}{2\mu^2})\left[\frac{a_1}{a_3 \ln(2)}\exp(\frac{a_3}{a_2}) Ei(-\frac{a_3}{a_2} - a_3 x)\right. \\
&- \left.\frac{a_1}{a_3 \ln(2)}\exp(-a_3 x)\log(1+a_2 x)\Big|_{\tau}^{\infty}\right] dy \\
&= \int_0^{\tau} \frac{C_2}{2\mu^2}\exp(-\frac{y}{2\mu^2})\left[-\frac{a_1}{a_3 \ln(2)}\exp(\frac{a_3}{a_2}) Ei(-\frac{a_3}{a_2} - a_3 \tau)\right. \\
&+ \left.\frac{a_1}{a_3 \ln(2)}\exp(-a_3\tau)\log(1+a_2\tau)\right] dy,
\end{aligned} \tag{3.39}$$

which is equal to

$$R_{\hat{U}_1}^{PD} = \int_0^{\tau} \frac{C_1 C_2}{2\mu^2} exp(-\frac{\tau}{2\mu^2}) log_2(1+\frac{P_t\tau}{\sigma^2+\epsilon P_t Y}) exp(-\frac{y}{2\mu^2}) dy \tag{3.40}$$

$$- \int_0^{\tau} \frac{C_1 C_2}{2\mu^2 \ln(2)} \exp(\frac{\sigma^2}{2\mu^2}) Ei(-\frac{\tau}{2\mu^2} - \frac{\sigma^2}{2\mu^2} - \frac{\epsilon y}{2\mu^2}) \exp(-\frac{(1-\epsilon)y}{2\mu^2}) dy.$$

By using indefinite integrals in Table 3.1, equation (3.41) can be expressed as

$$R_{\hat{U}_1}^{PD} = \frac{C_1 C_2}{\ln(2) 2\mu^2} \exp(-\frac{\tau}{2\mu^2}) \left(\mathcal{I}_4^{(-\frac{1}{2\mu^2}, P_t\tau, \sigma^2, \epsilon P_t)}(\tau) - \mathcal{I}_4^{(-\frac{1}{2\mu^2}, P_t\tau, \sigma^2, \epsilon P_t)}(0) \right) \tag{3.41}$$

$$- \frac{C_1 C_2}{\ln(2) 2\mu^2} \exp\left(-\frac{\sigma^2}{2\mu^2}\right) \left(\mathcal{I}_1^{(-\frac{(1-\epsilon)}{2\mu^2}, -\frac{\tau}{2\mu^2} - \frac{\sigma^2}{2\mu^2}, -\frac{\epsilon}{2\mu^2})}(\tau) - \mathcal{I}_1^{(-\frac{(1-\epsilon)}{2\mu^2}, -\frac{\tau}{2\mu^2} - \frac{\sigma^2}{2\mu^2}, -\frac{\epsilon}{2\mu^2})}(0) \right).$$

On the other hand, $R_{\tilde{U}_1}^{PD}$ correspond to rate of users who use their subcarriers solely and it can be expressed as

$$R_{\tilde{U}_1}^{PD} = \int_{\tau}^{\infty} \log_2\left(1 + \frac{\epsilon P_t}{\sigma^2} y\right) f_Y(y) dx. \tag{3.42}$$

The integral is similar to the integral in equation (3.36) with different limits. Using integration by parts with the variables $u \triangleq \log_2(1+ax)$ and $\frac{dv}{dx} \triangleq C_1 b e^{-bx}$ for $a \triangleq \frac{P_t}{\sigma^2}$ and $b \triangleq \frac{1}{2\mu^2}$, it can be rewritten as $R_{\tilde{U}_1}^{PD} = uv\Big|_{\tau}^{\infty} - \int_{\tau}^{\infty} v du$ which equivalent to

$$R_{\tilde{U}_1}^{PD} = C_1 \log_2(1+a\tau) e^{-b\tau} - \frac{C_1 e^{\frac{b}{a}}}{\ln(2)} \mathrm{E_i}\left(-b\tau - \frac{b}{a}\right). \tag{3.43}$$

Finally, the average rate of U_1 and all users on PD-NOMA can be expressed as

$$R_{U_1}^{PD} = \frac{M}{N} R_{\hat{U}_1}^{PD} + \frac{N-M}{N} R_{\tilde{U}_1}^{PD}, \tag{3.44}$$

$$R^{PD} = \frac{M}{K} R_{U_2}^{PD} + \frac{N}{K} R_{U_1}^{PD}. \tag{3.45}$$

3.2.2. NOMA-2000

In this part, we will repeat the previous calculations done for PD-NOMA for NOMA-2000. The data rate of the k-th user measured in bits/s/Hz is defined as

$$R_k^{WD} \triangleq \log_2(1 + S_k^{WD}), \qquad k \in U_1 \cup U_2, \tag{3.46}$$

where S_k^{WD} denotes the SINR or SNR depending on whether user k belongs to U_1 or U_2, given in equation (2.32). To calculate the average sum rate, the average rate of each user is estimated first and then the average rate of each user group is evaluated. Starting with the users in group U_2, the average rate can be written as

$$R_{U_2}^{WD} = \int_0^{\tau} \log_2\left(1 + \frac{\epsilon P_t}{\sigma^2} y\right) f_Y(y) dx. \tag{3.47}$$

Using integration by parts with the variables $u \triangleq \log_2(1 + ax)$ and $\frac{dv}{dx} \triangleq C_2 b e^{-bx}$ for $a \triangleq \frac{\epsilon P_t}{\sigma^2}$ and $b \triangleq \frac{1}{2\mu^2}$, equation (3.47) can be rewritten as $R_{U_2} = uv\Big|_0^{\tau} - \int_0^{\tau} v du$ which can then be expressed as

$$R_{U_2}^{WD} = -C_2 \log_2(1 + a\tau) e^{-b\tau} + \frac{C_2 e^{\frac{b}{a}}}{\ln(2)} \left(\mathrm{E_i}\left(-b\tau - \frac{b}{a}\right) - \mathrm{E_i}\left(-\frac{b}{a}\right)\right). \tag{3.48}$$

For the users in group U_1, the average rate can be expressed by the double integral

$$R_{U_1}^{WD} = \int_{\tau}^{\infty} \int_0^{\infty} \log_2\left(1 + \frac{P_t x}{\sigma^2 + \epsilon P_t z}\right) f_Z(z) f_X(x) dz dx. \tag{3.49}$$

Notice that, for normalized channel gains ($2\mu^2 = 1$) making $\mu_Z \gg \sigma_Z^2$. As a result, $Pr\{\mu_Z(1-\delta) \leq Z \leq \mu_Z(1+\delta)\} \approx 1$ for small δ values. Then, we can make the following approximation

$$R_{U_1}^{WD} \approx \int_{\tau}^{\infty} \log_2\left(1 + \frac{P_t x}{\sigma^2 + \epsilon P_t E[Z]}\right) f_x(x) dx. \tag{3.50}$$

Table 3.1. Table of indefinite integrals in Chapter 3.

$\mathcal{I}_0^{(k_1,k_2)}(y)$	$\int \ln(1+k_1 y)\exp(-k_2 y)dy$	$\frac{e^{k_2/k_1}Ei\left(-\frac{k_1k_2y+k_2}{k_1}\right)}{k_2} - \frac{e^{-k_2y}\ln(1+k_1y)}{k_2} + \text{constant}$
$\mathcal{I}_1^{(k_1,k_2,k_3)}(y)$	$\int \exp(-k_1 y)Ei(-k_2-k_3y)dy$	$\frac{e^{k_1k_2/k_3}Ei\left(-k_1k_2/k_3-k_2-(k_1+k_3)y\right)}{k_1} - \frac{e^{-k_1y}Ei(-k_2-k_3x)}{k_1} + \text{constant}$
$\hat{\mathcal{I}}_1^{(k_1,k_2)}(y)$	$\int Ei(-k_1-k_2y)dy$	$\frac{(k_1+k_2y)Ei(-k_1-k_2y)}{k_2} + \frac{\exp(-k_1-k_2y)}{k_2} + \text{constant}$
$\mathcal{I}_2^{(k_1,k_2)}(y)$	$\int \exp(-k_1y)Ei(-k_2)dy$	$-\frac{\exp(-k_1y)Ei(-k_2)}{k_1} + \text{constant}$
$\mathcal{I}_3^{(k_1,k_2,k_3,k_4)}(y)$	$\int \ln\left(1+\frac{k_1y}{k_2+k_4y}\right)\exp(-k_3y)dy$	$e^{k_2k_3/(k_1+k_3)}\frac{Ei(-k_2k_3/(k_1+k_3)-k_3y)}{k_3} - \exp(-k_3y)\frac{\ln\left(1+\frac{k_1y}{k_2+dy}\right)}{k_3}$ $- \exp(-k_2k_3/k_3)\frac{Ei\left(-yk_3-k_2k_3/k_3\right)}{k_3} + \text{constant}$
$\mathcal{I}_4^{(k_1,k_2,k_3,k_4)}(y)$	$\int \exp(-k_1y)\ln\left(1+\frac{k_2}{k_3+k_4y}\right)dy$	$-\frac{e^{k_1k_3/k_4}Ei(-k_1y-\frac{k_1k_3}{k_4})}{k_1} + \frac{e^{\frac{k_1k_2+k_1k_3}{k_4}}Ei(-k_1x-\frac{k_1k_2}{k_4}-\frac{k_1k_3}{k_4})}{k_1}$ $-\frac{e^{-k_1x}\log(1+\frac{k_2}{k_3+k_4x})}{k_1} + \text{constant}$

Then using the same steps as above with $u \triangleq \log_2(1+\bar{a}x)$, $\frac{dv}{dx} \triangleq C_1 b e^{-bx}$ and $\bar{a} \triangleq \frac{P_t}{\sigma^2+\epsilon P_t \mu_Z}$, $R_{U_1}^{WD}$ can be approximated as $R_{U_1}^{WD} \approx uv\Big|_{\tau}^{\infty} - \int_{\tau}^{\infty} v du$ which can be evaluated as

$$R_{U_1}^{WD} \approx C_1 \log_2(1+\bar{a}\tau)e^{-b\tau} - \frac{C_1 e^{\frac{b}{\bar{a}}}}{\ln(2)} \mathrm{E_i}\left(-b\tau - \frac{b}{\bar{a}}\right). \tag{3.51}$$

Finally, using the average user rates obtained as given above, the average sum rate can be computed as

$$R^{WD} = \frac{N R_{U_1}^{WD} + M R_{U_2}^{WD}}{M+N}. \tag{3.52}$$

3.2.3. No-interference and OMA Bounds

Similar to outage probability, we can define the *no-interference* and *OMA* bounds for capacity. Note that, the SNR definitions for both cases are identical. However, the entire bandwidth is shared for K users in OMA, the relation between capacities of OMA and no-interference bounds is $R^{OMA} = \frac{N}{K} R^{NI}$. Finally, the analytical calculations can be expressed, respectively, as

$$\begin{aligned} R_{U_1}^{NI} &= \int_{\tau}^{\infty} \log_2\left(1+\frac{x}{\sigma^2}\right) f_X(x) dx \\ &= C_1 \log_2\left(1+\frac{P_t\tau}{\sigma^2}\right) e^{-\frac{\tau}{2\mu^2}} - \frac{C_1 e^{\frac{\sigma^2}{P_t 2\mu^2}}}{\ln(2)} \mathrm{E_i}\left(-\frac{\tau}{2\mu^2} - \frac{\sigma^2}{P_t 2\mu^2}\right), \end{aligned} \tag{3.53}$$

$$\begin{aligned} R_{U_2}^{NI} &= \int_{0}^{\tau} \log_2\left(1+\frac{y}{\sigma^2}\right) f_Y(y) dy \\ &= -C_2 \log_2\left(1+\frac{\epsilon P_t\tau}{\sigma^2}\right) e^{-\frac{\tau}{2\mu^2}} \\ &+ \frac{C_2 e^{\frac{\sigma^2}{P_t 2\mu^2}}}{\ln(2)} \left(\mathrm{E_i}\left(-\frac{\tau}{2\mu^2} - \frac{\sigma^2}{P_t 2\mu^2}\right) - \mathrm{E_i}\left(-\frac{\sigma^2}{P_t 2\mu^2}\right)\right), \end{aligned} \tag{3.54}$$

$$R^{NI} = \frac{N R_{U_1}^{NI} + M R_{U_2}^{NI}}{M+N}. \tag{3.55}$$

3.3. Capacity under Imperfect SIC

In previous sections, we have calculated analytical expressions of outage probabilities and capacity for both NOMA schemes. During these calculations, it is assumed that BS can perform perfect SIC to decode signals of U_2, and U_1 experiences full interference. However, in NOMA-2000 an iterative SIC scheme has been proposed which means BS can also use SIC in order to decode the signal of U_1. Furthermore, if U_1 experiences high interference, SIC cannot be performed perfectly for signals of U_2. In this section, we investigate the capacities of PD-NOMA and NOMA-2000 under the imperfect SIC. During these calculations, we assume that if a user is in outage, its signal cannot be decoded and BS cannot perform SIC to signal of this user.

3.3.1. PD-NOMA

For PD-NOMA, the capacity under imperfect SIC assumption is defined as follows:

- Because BS decodes signal of U_1 without any SIC, its capacity does not change under this assumption.
- When a user from U_1 in outage, we assume that its signal cannot be decoded, thus, SIC cannot be performed for that user.
- Therefore, capacity of U_2 depends on the outage probability of U_1. We assume that if a user from U_1 is in coverage, the BS decodes signal of another user from U_2 on the same subcarrier under the interference of its signal.

The capacity expressions can be redefined, respectively, as

$$R_{U_1,n} = \log_2\left(1+\frac{P_t|g_n|^2}{\epsilon P_t|g_{n+N}|^2+\sigma^2}\right), \tag{3.56}$$

$$R_{U_2,n} = \begin{cases} \log_2\left(1+\dfrac{\epsilon P_t|g_{n+N}|^2}{\sigma^2}\right), & |g_n|^2 \geq \alpha|g_{n+N}|^2+\beta, \\ \log_2\left(1+\dfrac{\epsilon P_t|g_{n+N}|^2}{P_t|g_n|^2+\sigma^2}\right), & |g_n|^2 < \alpha|g_{n+N}|^2+\beta. \end{cases} \tag{3.57}$$

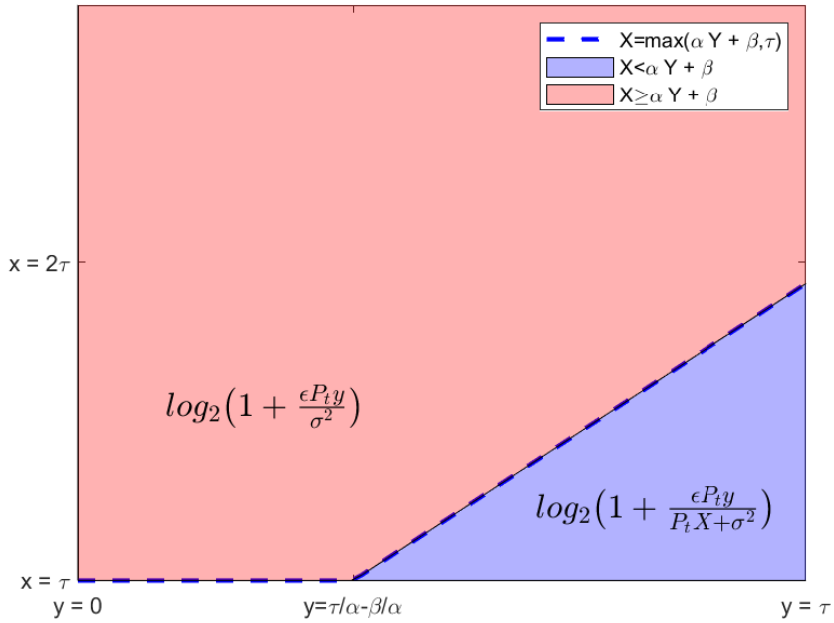


Figure 3.1. Integral regions for equation (4.30).

Because the capacity definition does not change for U_1, we only calculate the capacity for U_2 in this section. By using equation (4.30), the average value can be expressed as

$$R_{U_2}^{PD} = \int_0^{\tau} \int_{\max(\alpha y+\beta_1,\tau)}^{\infty} \log_2\left(1+\frac{\epsilon P_t Y}{\sigma^2}\right) \frac{C_1}{2\mu^2} e^{-\frac{x}{2\mu^2}} \frac{C_2}{2\mu^2} e^{-\frac{y}{2\mu^2}} dxdy$$

$$+ \int_0^{\tau} \int_{\tau}^{\max(\alpha y+\beta,\tau)} \log_2\left(1+\frac{\epsilon P_t y}{P_t x+\sigma^2}\right) \frac{C_1}{2\mu^2} e^{-\frac{x}{2\mu^2}} \frac{C_2}{2\mu^2} e^{-\frac{y}{2\mu^2}} dxdy. \qquad (3.58)$$

In Figure 3.1, the rate conditions according to X and Y are illustrated. The red area corresponds to the rate that U_2 can perform perfect SIC because U_1 is in coverage, the first integral in the (3.58), which can be calculated as

$$\int_0^{\tau} \int_{\max(\alpha y+\beta_1,\tau)}^{\infty} \log_2\left(1+\frac{\epsilon P_t Y}{\sigma^2}\right) \frac{C_1}{2\mu^2} \exp\left(-\frac{x}{2\mu^2}\right) \frac{C_2}{2\mu^2} \exp\left(-\frac{y}{2\mu^2}\right) dxdy$$

$$= \int_0^{\tau} \log_2\left(1+\frac{\epsilon P_t Y}{\sigma^2}\right) \left[1 - F_X(\max(\alpha y+\beta_1,\tau))\right] \frac{C_2}{2\mu^2} \exp\left(-\frac{y}{2\mu^2}\right) dy$$

$$= \int_0^{\tau} \log_2\left(1+\frac{\epsilon P_t Y}{\sigma^2}\right) C_1 \exp\left(\frac{-\max(\alpha y+\beta,\tau)}{2\mu^2}\right) \frac{C_2}{2\mu^2} \exp\left(-\frac{y}{2\mu^2}\right) dy$$

$$= \int_0^{\max(\frac{\tau-\beta}{\alpha},0)} \frac{C_1C_2}{2\mu^2} \log_2\left(1+\frac{\epsilon P_t Y}{\sigma^2}\right) e^{-\frac{\tau}{2\mu^2}} \exp\left(-\frac{y}{2\mu^2}\right) dy$$

$$+ \int_{\max(\frac{\tau-\beta}{\alpha},0)}^{\tau} \frac{C_1C_2}{2\mu^2} \log_2\left(1+\frac{\epsilon P_t Y}{\sigma^2}\right) e^{-\frac{\beta_1}{2\mu^2}} \exp\left(-\frac{(\alpha+1)y}{2\mu^2}\right) dy$$

$$= \frac{C_1C_2}{2\mu^2\ln(2)}\Bigg(\exp\left(-\frac{\tau}{2\mu^2}\right)(I_0^{(\frac{\epsilon P_t}{\sigma^2},\frac{1}{2\mu^2})}(\frac{\tau-\beta}{\alpha}) - I_0^{(\frac{\epsilon P_t}{\sigma^2},\frac{1}{2\mu^2})}(0)$$

$$+ \exp\left(-\frac{\beta_1}{2\mu^2}\right)(I_0^{(\frac{\epsilon P_t}{\sigma^2},\frac{\alpha+1}{2\mu^2})}(\tau) - I_0^{(\frac{\epsilon P_t}{\sigma^2},\frac{\alpha+1}{2\mu^2})}(\frac{\tau-\beta}{\alpha})\Bigg). \tag{3.59}$$

On the other hand, the blue area corresponds to the rate that U_2 cannot SIC because U_1 is in coverage, the second integral in equation (3.58), which can be calculated as

$$\int_0^{\tau}\int_{\tau}^{\max(\alpha y+\beta,\tau)} \log_2\left(1+\frac{\epsilon P_t y}{P_t x+\sigma^2}\right) \frac{C_1}{2\mu^2} e^{-\frac{x}{2\mu^2}} \frac{C_2}{2\mu^2} e^{-\frac{y}{2\mu^2}} dxdy$$

$$= \frac{C_1C_2}{2\mu^2\ln(2)} \int_{\max(\frac{\tau-\beta}{\alpha},0)}^{\tau} \exp(-\frac{y}{2\mu^2})\Bigg[e^{\frac{\sigma^2}{2\mu^2P_t}} \exp(\frac{\epsilon y}{2\mu^2}) Ei(-\frac{\sigma^2}{2\mu^2P_t} - \frac{\epsilon}{2\mu^2}y - \frac{x}{2\mu^2})$$

$$- e^{\frac{\sigma^2}{2\mu^2P_t}} Ei(-\frac{\sigma^2}{2\mu^2P_t} - \frac{x}{2\mu^2}) - \exp(-\frac{x}{2\mu^2}) \ln\left(1+\frac{\epsilon P_t y}{\sigma^2+P_t x}\right)\Bigg]_{\tau}^{\alpha y+\beta} dy$$

$$= \frac{C_1C_2}{2\mu^2\ln(2)}\Bigg[\exp\left(\frac{\sigma^2}{2\mu^2P_t}\right) \underbrace{\int_{\max(\frac{\tau-\beta}{\alpha},0)}^{\tau} e^{-\frac{(1-\epsilon)}{2\mu^2}} Ei(-\frac{\sigma^2}{2\mu^2P_t} - \frac{\beta_1}{2\mu^2} - \frac{(\alpha+\epsilon)}{2\mu^2}y) dy}_{\text{I}}$$

$$- \exp\left(\frac{\sigma^2}{2\mu^2P_t}\right) \underbrace{\int_{\max(\frac{\tau-\beta}{\alpha},0)}^{\tau} \exp(-\frac{(1-\epsilon)}{2\mu^2}y) Ei(-\frac{\sigma^2}{2\mu^2P_t} - \frac{\tau}{2\mu^2} - \frac{\epsilon}{2\mu^2}y) dy}_{\text{II}}$$

$$- \exp\left(\frac{\sigma^2}{2\mu^2P_t}\right) \underbrace{\int_{\max(\frac{\tau-\beta}{\alpha},0)}^{\tau} \exp(-\frac{y}{2\mu^2}) Ei(-\frac{\sigma^2}{2\mu^2P_t} - \frac{\beta_1}{2\mu^2} - \frac{\alpha}{2\mu^2}y) dy}_{\text{III}}$$

$$+\exp\left(\frac{\sigma^2}{2\mu^2 P_t}\right)\underbrace{\int_{\max(\frac{\tau-\beta}{\alpha},0)}^{\tau}\exp(-\frac{y}{2\mu^2})Ei(-\frac{\sigma^2}{2\mu^2 P_t}-\frac{\tau}{2\mu^2})dy}_{\text{IV}}$$

$$+\exp\left(-\frac{\beta_1}{2\mu^2}\right)\underbrace{\int_{\max(\frac{\tau-\beta}{\alpha},0)}^{\tau}e^{-\frac{(\alpha+1)}{2\mu^2}}\ln\left(1+\frac{\epsilon P_t y}{\sigma^2+P_t\beta+\alpha P_t y}\right)dy}_{\text{V}}$$

$$-\exp\left(-\frac{\tau}{2\mu^2}\right)\underbrace{\int_{\max(\frac{\tau-\beta}{\alpha},0)}^{\tau}\exp(-\frac{y}{2\mu^2})\ln\left(1+\frac{\epsilon P_t y}{\sigma^2+P_t\tau}\right)dy}_{\text{VI}}\Bigg]. \tag{3.60}$$

By using indefinite integral definitions in Table 3.1, we can conclude our analysis by calculating all terms in equation (3.60), respectively, as

$$\text{I} = \begin{cases}\mathcal{I}_1^{(\frac{1-\epsilon}{2\mu^2},\frac{\sigma^2}{2\mu^2 P_t}+\frac{\beta_1}{2\mu^2},\frac{\alpha+\epsilon}{2\mu^2})}(\tau)-\mathcal{I}_1^{(\frac{1-\epsilon}{2\mu^2},\frac{\sigma^2}{2\mu^2 P_t}+\frac{\beta_1}{2\mu^2},\frac{\alpha+\epsilon}{2\mu^2})}\max\left(\frac{\tau-\beta}{\alpha},0\right) & \epsilon\neq 1\\ \hat{\mathcal{I}}_1^{(\frac{\sigma^2}{2\mu^2 P_t}+\frac{\beta_1}{2\mu^2},\frac{\alpha+1}{2\mu^2})}(\tau)-\hat{\mathcal{I}}_1^{(\frac{\sigma^2}{2\mu^2 P_t}+\frac{\beta_1}{2\mu^2},\frac{\alpha+1}{2\mu^2})}\max\left(\frac{\tau-\beta}{\alpha},0\right) & \epsilon=1\end{cases}, \tag{3.61}$$

$$\text{II} = \begin{cases}\mathcal{I}_1^{(\frac{1-\epsilon}{2\mu^2},\frac{\sigma^2}{2\mu^2 P_t}+\frac{\tau}{2\mu^2},\frac{\epsilon}{2\mu^2})}(\tau)-\mathcal{I}_1^{(\frac{1-\epsilon}{2\mu^2},\frac{\sigma^2}{2\mu^2 P_t}+\frac{\tau}{2\mu^2},\frac{\epsilon}{2\mu^2})}\max\left(\frac{\tau-\beta}{\alpha},0\right) & \epsilon\neq 1\\ \hat{\mathcal{I}}_1^{(\frac{\sigma^2}{2\mu^2 P_t}+\frac{\tau}{2\mu^2},\frac{1}{2\mu^2})}(\tau)-\hat{\mathcal{I}}_1^{(\frac{\sigma^2}{2\mu^2 P_t}+\frac{\tau}{2\mu^2},\frac{1}{2\mu^2})}\max\left(\frac{\tau-\beta}{\alpha},0\right) & \epsilon=1\end{cases}, \tag{3.62}$$

$$\text{III} = \mathcal{I}_1^{(\frac{1-\epsilon}{2\mu^2},\frac{1}{2\mu^2},\frac{\sigma^2}{2\mu^2 P_t}+\frac{\beta_1}{2\mu^2},\frac{\alpha}{2\mu^2})}(\tau)-\mathcal{I}_1^{(\frac{1-\epsilon}{2\mu^2},\frac{1}{2\mu^2},\frac{\sigma^2}{2\mu^2 P_t}+\frac{\beta_1}{2\mu^2},\frac{\alpha}{2\mu^2})}\max\left(\frac{\tau-\beta}{\alpha},0\right), \tag{3.63}$$

$$\text{IV} = \mathcal{I}_2^{(\frac{1-\epsilon}{2\mu^2},\frac{1}{2\mu^2},\frac{\sigma^2}{2\mu^2 P_t}+\frac{\tau}{2\mu^2})}(\tau)-\mathcal{I}_2^{(\frac{1-\epsilon}{2\mu^2},\frac{1}{2\mu^2},\frac{\sigma^2}{2\mu^2 P_t}+\frac{\tau}{2\mu^2})}\max\left(\frac{\tau-\beta}{\alpha},0\right), \tag{3.64}$$

$$\text{V} = \mathcal{I}_3^{(\epsilon P_t,\sigma^2+P_t\beta,\frac{\alpha+1}{2\mu^2},\alpha P_t)}(\tau)-\mathcal{I}_3^{(\epsilon P_t,\sigma^2+P_t\beta,\frac{\alpha+1}{2\mu^2},\alpha P_t)}\max\left(\frac{\tau-\beta}{\alpha},0\right), \tag{3.65}$$

$$\text{VI} = \mathcal{I}_0^{(\tau,\frac{\epsilon P_t}{P_t\tau+\sigma^2},\frac{1}{2\mu^2})}(\tau)-\mathcal{I}_0^{(\tau,\frac{\epsilon P_t}{P_t\tau+\sigma^2},\frac{1}{2\mu^2})}\max\left(\frac{\tau-\beta}{\alpha},0\right). \tag{3.66}$$

3.3.2. NOMA-2000

In this part, we calculate the average capacities under the imperfect SIC assumption for both user groups. Previously, capacity has been defined and calculated with

the SINR/SNR definition in Chapter 2 which is based on the assumption that BS can perform SIC perfectly when decoding signals of U_1 and U_2. However, in the previous section, we have calculated the interference values caused by imperfect SIC in each iteration, and have calculated outage probability by using them. In this section, we also provide the average capacity of NOMA-2000 under the imperfect SIC assumption by using the calculated interference values. To calculate the average sum rate, the average rate of each user is estimated first and then the average rate of each user group is evaluated.

Starting with the users in group U_1, the average rate can be written as

$$\begin{aligned} R_{U_1} &= \int_{\tau}^{\infty} \log_2\left(1+\frac{P_t x}{P_{I_{U_1}}+\sigma^2}\right) f_X(x)dx \\ &\approx \int_{\tau}^{\infty} \log_2\left(1+\frac{P_t x}{\epsilon P_t \mu_Z^{(last)}+\sigma^2}\right) f_X(x)dx, \end{aligned} \tag{3.67}$$

where $u \triangleq \log_2(1+ax)$, $\frac{dv}{dx} \triangleq C_1 b e^{-bx}$ and $a \triangleq \frac{P_t}{\sigma^2+\epsilon P_t \mu_Z^{(last)}}$, R_{U_1} can be approximated as $R_{U_1} \approx uv\Big|_{\tau}^{\infty} - \int_{\tau}^{\infty} v du$ which can be evaluated as

$$R_{U_1}^{WD} \approx C_1 \log_2(1+\bar{a}\tau)e^{-b\tau} - \frac{C_1 \exp\left(\frac{b}{\bar{a}}\right)}{\ln(2)} \mathrm{E_i}\left(-b\tau-\frac{b}{\bar{a}}\right). \tag{3.68}$$

For users in group U_2, the average rate can be expressed

$$R_{U_2}^{WD} = \int_{0}^{\tau} \log_2\left(1+\frac{\epsilon P_t y}{P_{I_{U_2}}+\sigma^2}\right) f_Y(y)dy \tag{3.69}$$

$$\approx \int_{\tau}^{\infty} \log_2\left(1+\frac{\epsilon P_t y}{P_t \mu_W^{(last)}+\sigma^2}\right) f_Y(y)dy. \tag{3.70}$$

Then using the same steps as above with $u \triangleq \log_2(1+\bar{a}x)$, $\frac{dv}{dx} = C_2 b e^{-bx}, \bar{a} \triangleq \frac{\epsilon P_t}{\sigma^2+P_t\mu_W^{(last)}}$ and $b = \frac{1}{2\mu^2}$, R_{U_2} can be approximated as $R_{U_2} \approx uv\Big|_{\tau}^{\infty} - \int_{\tau}^{\infty} v du$ which

can be evaluated as

$$\begin{aligned} R_{U_2}^{WD} &= -C_2 \log_2(1+a\tau)e^{-b\tau} \\ &+ \frac{C_2 e^{\frac{b}{a}}}{\ln(2)} \left(\mathrm{E_i}\left(-b\tau - \frac{b}{a}\right) - \mathrm{E_i}\left(-\frac{b}{a}\right)\right). \end{aligned} \tag{3.71}$$

Finally, using the average user rates obtained as given above, the average rate can be computed as

$$R^{WD} = \frac{N R_{U_1}^{WD} + M R_{U_2}^{WD}}{M+N}. \tag{3.72}$$

3.4. Numerical Results

In this part, we validate our analysis and compare the two NOMA schemes using computer simulations. For all simulations, the overload factor and number of subcarriers (N) were selected as 100% and 1024, respectively, unless otherwise was mentioned. During simulations, 10^6 realizations were performed and average values are illustrated. In the outage probability simulations for NOMA-2000, the maximum number of iteration was chosen as 6. In addition, for all simulations, normalized channel gains were used, i.e., we set ($2\mu^2 = 1$). In all simulations, we use OMA bounds as a benchmark and no-interference bounds as theoretical limits for NOMA schemes.

3.4.1. Outage Probability

Figure 3.2 shows the outage probabilities for the single-carrier case. Simulations are repeated for different target rates. It is seen that the simulation results for all users and situations validate equations (3.6) and (3.8). On the other hand, we show that there is a significant difference between simulation results and the analytical results in [24] for a target rate 2.0 bit/s/Hz. This difference disappears when the target rate is 1.6 bit/s/Hz, because this value makes the value of α become close to 1, thus making events E_1 and E_2 approximately independent.

In Figure 3.3, Figure 3.4 and Figure 3.5 it can be seen in all these figures that the analytical derivations and the simulation results are in tight agreement for both NOMA systems. Additionally, we can observe that the outage probability of PD-NOMA reaches an error floor at SNR> 15 dB in most cases. This effect is due to the fact that some subcarriers experience relatively higher interference, which limits the performance as the power imbalance coefficient or target rate increases. On the other hand, in NOMA-2000 the interference is spread through all subcarriers, causing the outage probabilities to decrease dramatically as SNR increases. Moreover, with iterative decoding signals for both user groups may be canceled. Thus, we observe that NOMA-2000 reaches the no-interference bound in high SNR. It means that both users can perform SIC perfectly in that region.

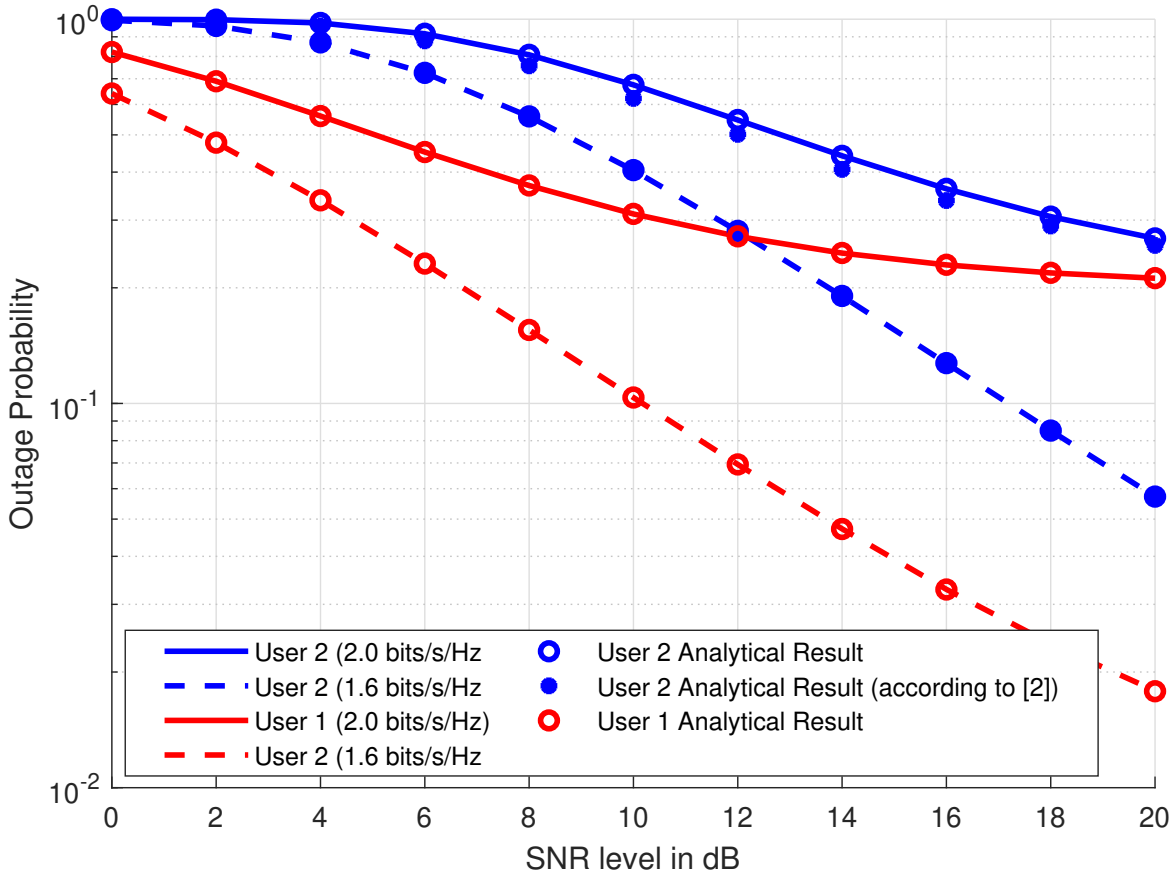
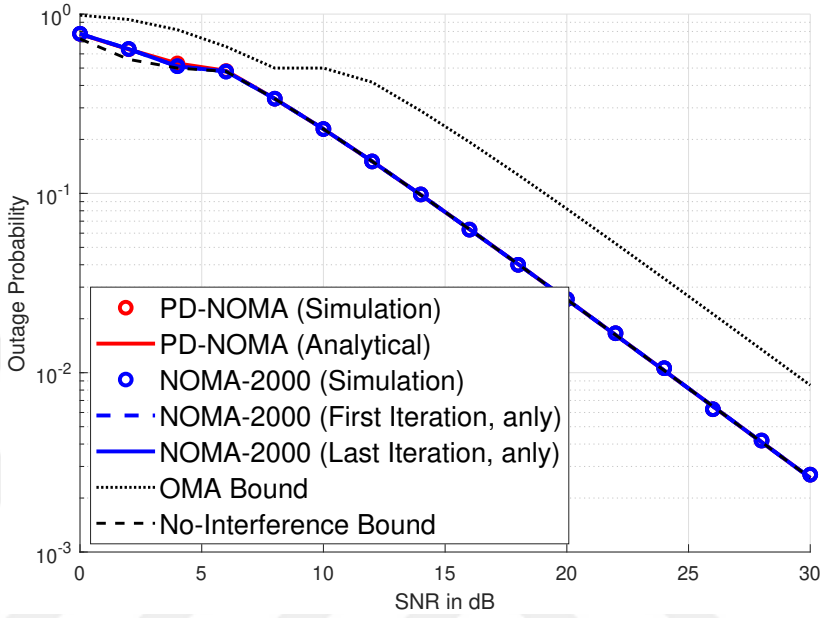
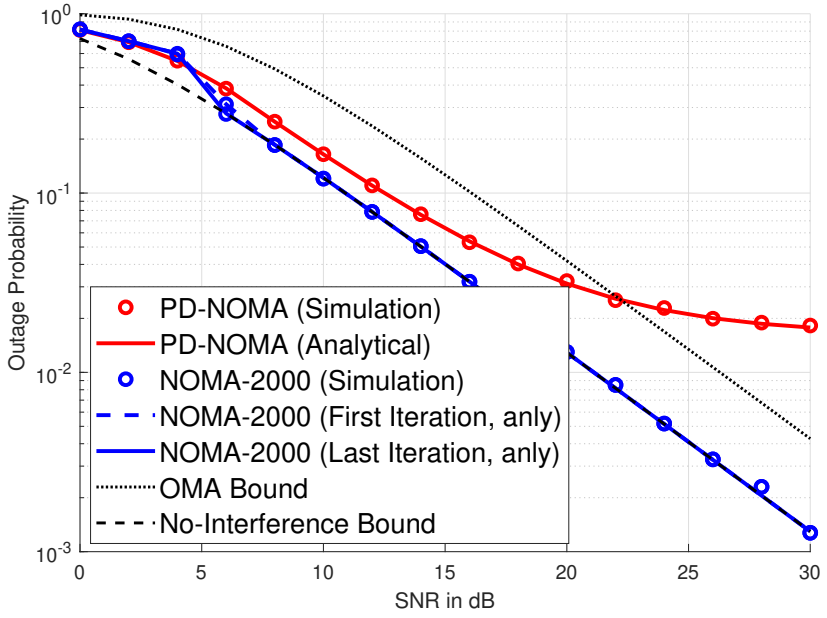


Figure 3.2. Outage performance of the single carrier case.

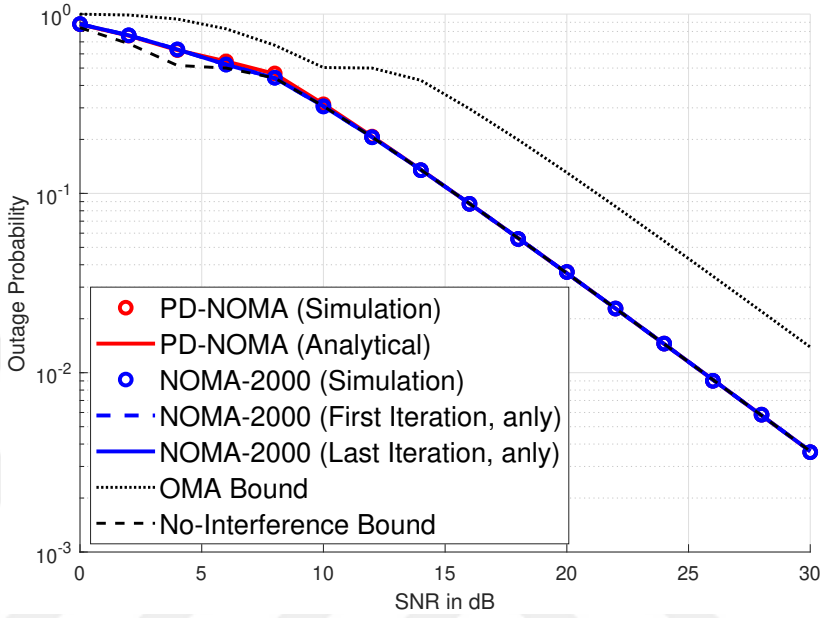


(a)

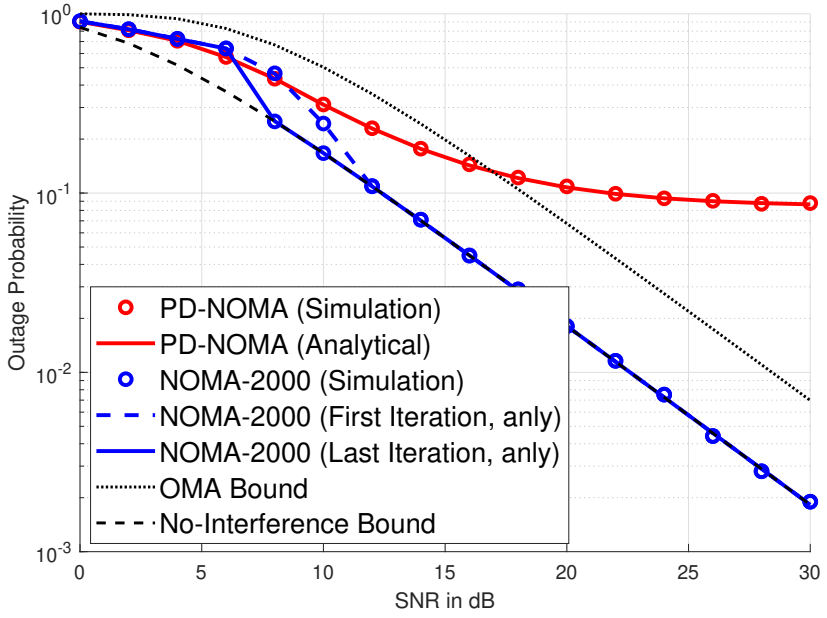


(b)

Figure 3.3. Outage probability comparisons between PD-NOMA and NOMA-2000 when target rate is 1.2 bits/s/Hz a) $\epsilon = 0.5$, b) $\epsilon = 1.0$.

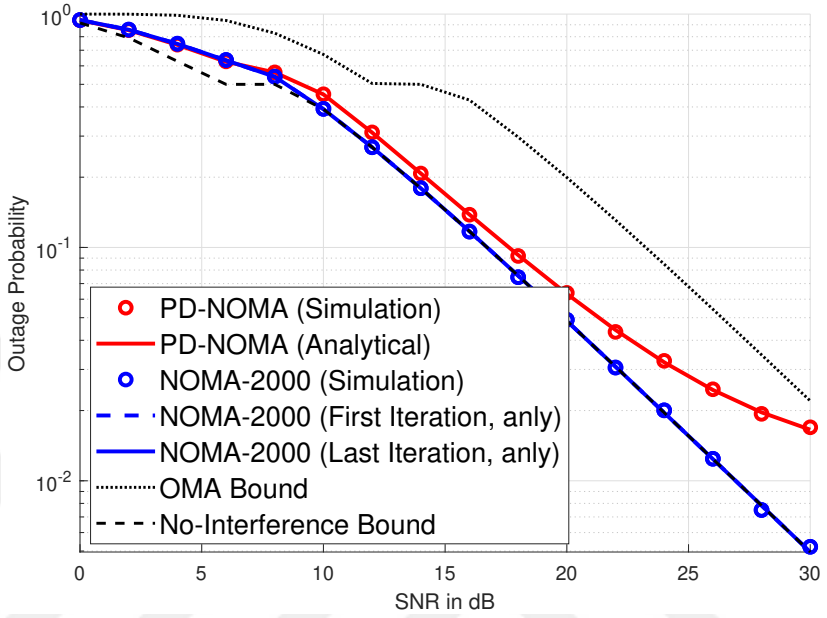


(a)

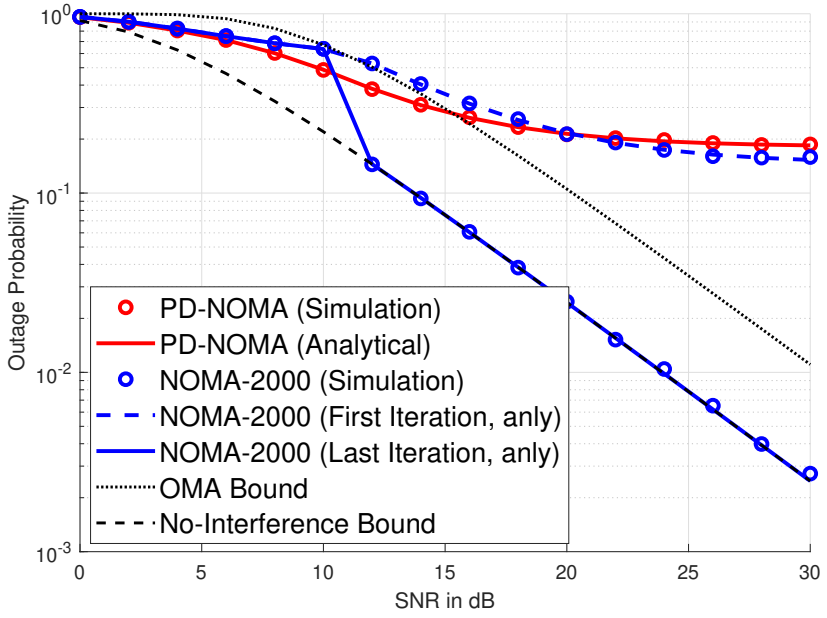


(b)

Figure 3.4. Outage probability comparisons between PD-NOMA and NOMA-2000 when target rate is 1.5 bits/s/Hz a) $\epsilon = 0.5$, b) $\epsilon = 1.0$.



(a)



(b)

Figure 3.5. Outage probability comparisons between PD-NOMA and NOMA-2000 when target rates is 1.8 bits/s/Hz a) $\epsilon = 0.5$, b) $\epsilon = 1.0$.

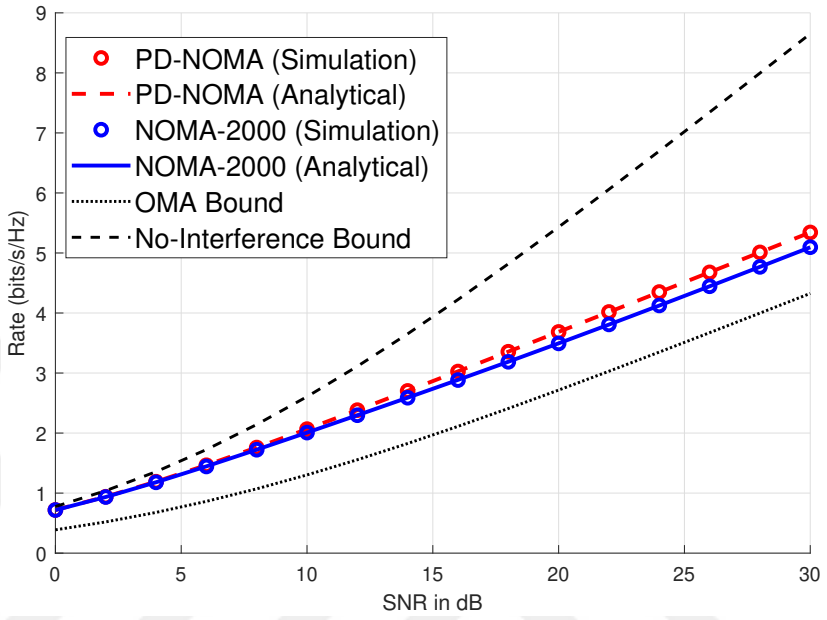
3.4.2. Capacity

In Figure 3.6, we provide a comparison for both NOMA schemes in terms of the achievable ergodic rates for all three power allocation strategies. Notice that these calculations are based on the SNR/SINR definitions in Chapter 2. In these definitions, it is assumed that signals of U_1 can be removed perfectly by SIC for both NOMA schemes. Unlike NOMA-2000, in PD-NOMA, the average capacity seems to increase monotonically with the interference power on the subcarrier even though in practice reliable communication is not possible at large interference values and thus these rates (despite being useful in serving as benchmarks) are never achievable. Moreover, for NOMA-2000 iterative SIC has been proposed, it means that BS can perform SIC to signals of U_2 after decode their signals. In the next subsections, we provide capacity results by considering all of these.

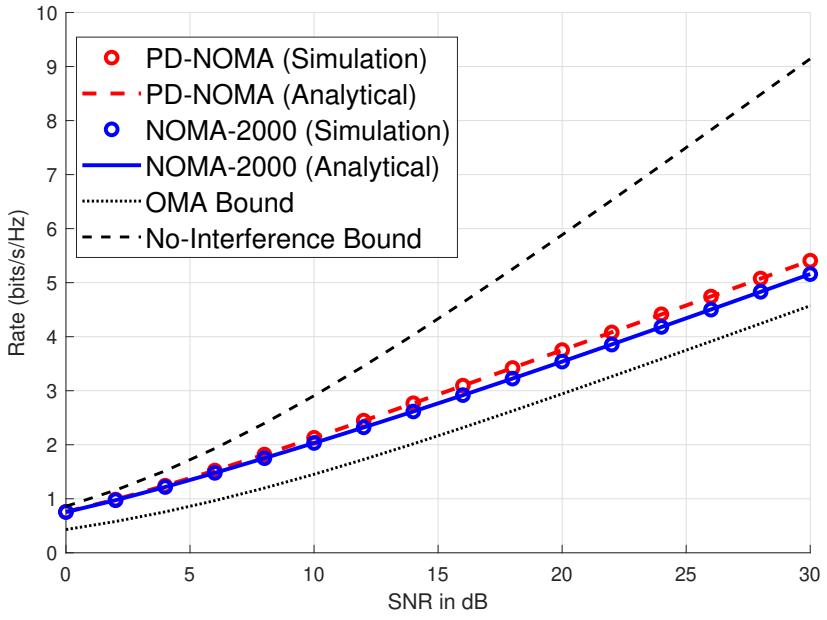
3.4.3. Capacity with Imperfect SIC

We provide a comparison of both NOMA schemes in terms of the achievable ergodic rates in Figure 3.7, Figure 3.8 and Figure 3.9 for different target rates and power imbalance factors with our assumption of imperfect SIC. When target rates are low, we can see that both NOMA schemes can reach to no-interference bound, because their outage performances also reach that bound. However, as target rates and power imbalance factors increase, more users stay in coverage for PD-NOMA. On the other hand, because NOMA-2000 can reach the no-interference bound even with high power imbalance factor for the outage probability, its rate also reaches that bound.

Furthermore, in Figures 3.10 and 3.11 the capacity performance for both NOMA schemes with different ϵ values in certain SNR values. As consistent with the results in Figure 3.7, Figures 3.8 and 3.9, we can observe that NOMA-2000 can work better with higher ϵ values in high SNR regions. Working with high ϵ values have two certain advantages: first, although the average results may not be affected dramatically, individual rates of users from U_2 are much better with ϵ values close to 1.

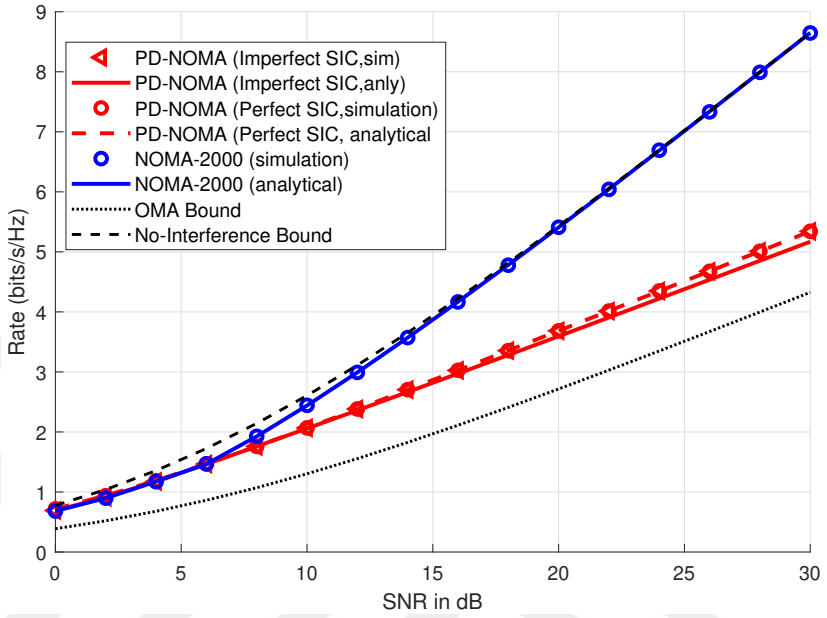


(a)

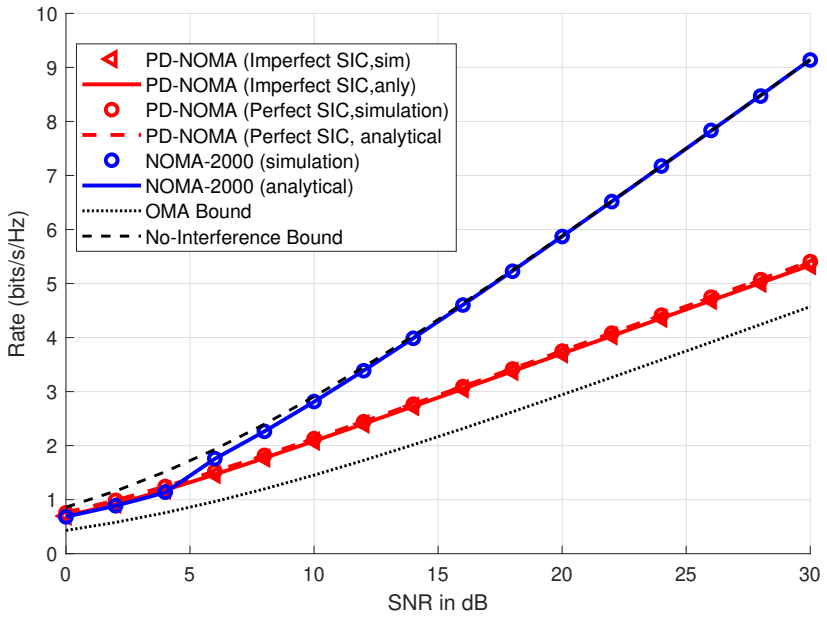


(b)

Figure 3.6. Capacity comparisons between PD-NOMA and NOMA-2000 when a) $\epsilon = 0.5$ and OF= 100%, b) $\epsilon = 1.0$ and OF= 100%.

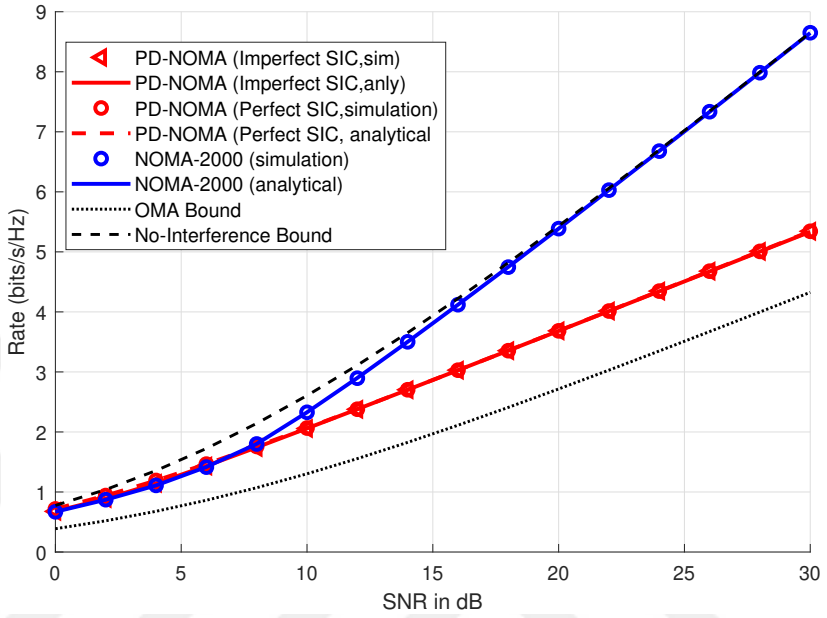


(a)

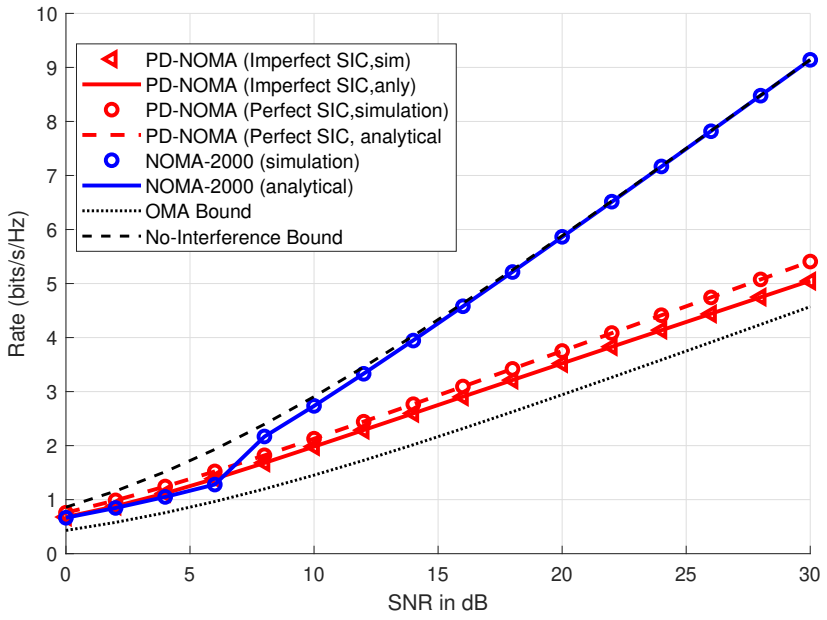


(b)

Figure 3.7. Capacity comparisons between PD-NOMA and NOMA-2000 when target rate is 1.2 bits/s/Hz a) $\epsilon = 0.5$, and b) there is no power imbalance ($\epsilon = 1.0$).

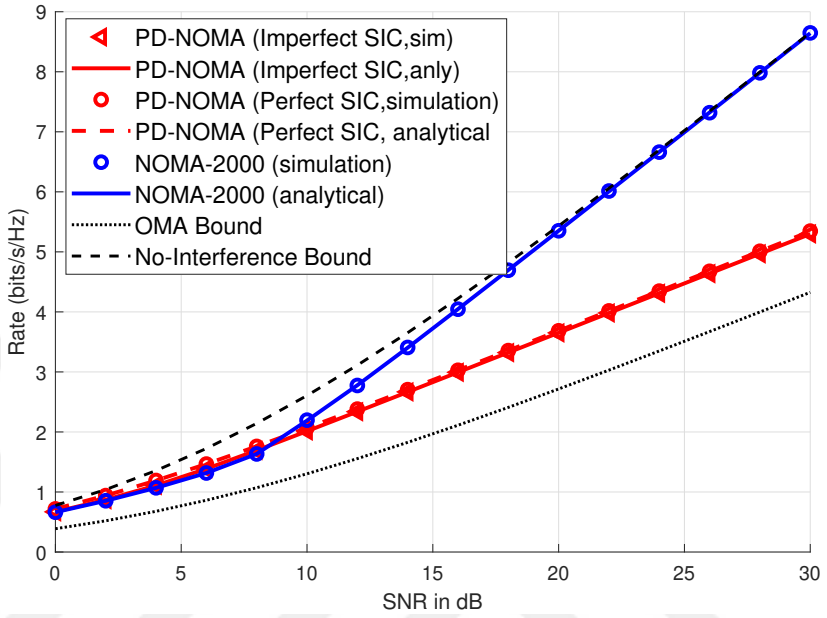


(a)

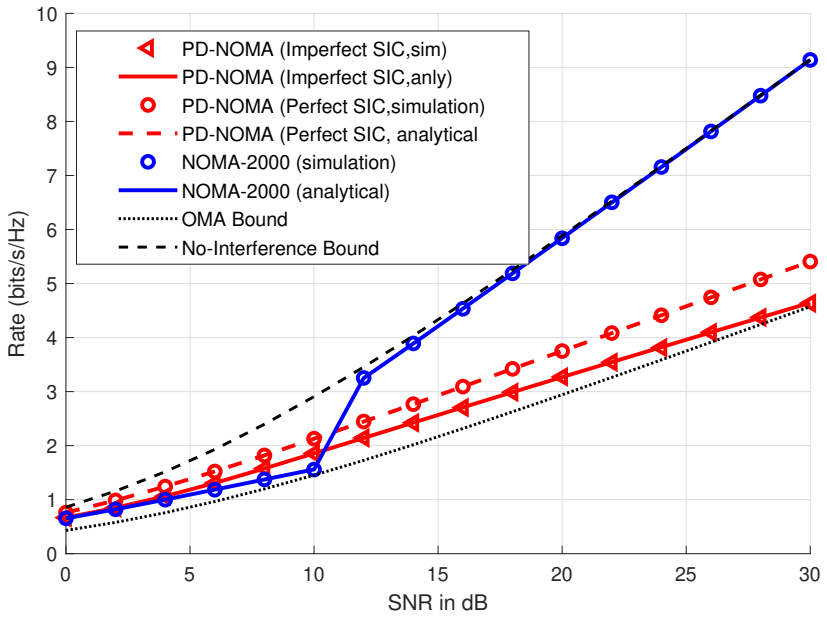


(b)

Figure 3.8. Capacity comparisons between PD-NOMA and NOMA-2000 when target rate is 1.5 bits/s/Hz and a) $\epsilon = 0.5$, and b) there is no power imbalance ($\epsilon = 1.0$).

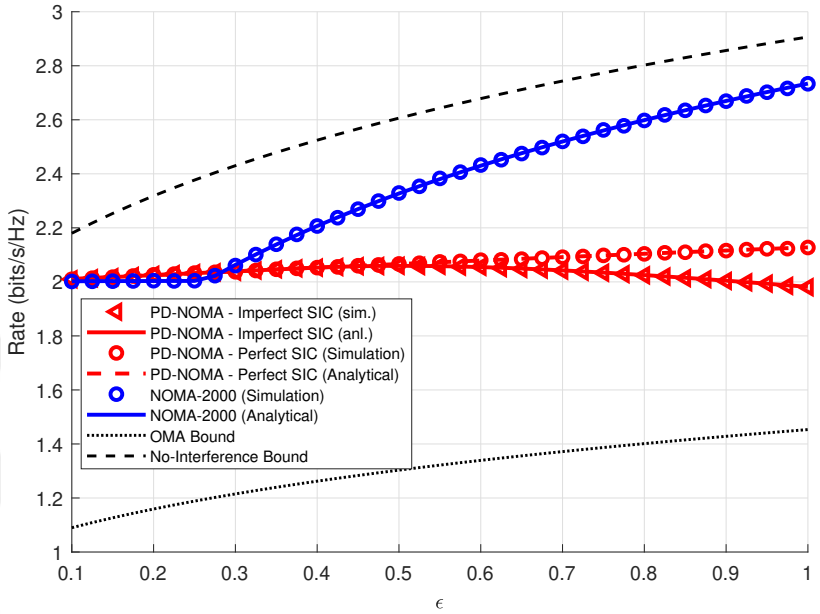


(a)

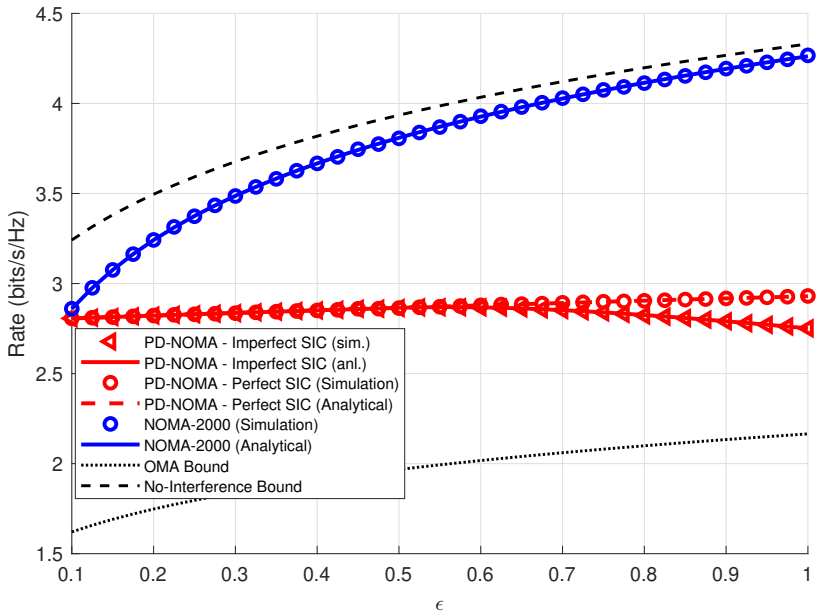


(b)

Figure 3.9. Capacity comparisons between PD-NOMA and NOMA-2000 when target rate is 1.8 bits/s/Hz and a) $\epsilon = 0.5$, and b) there is no power imbalance ($\epsilon = 1.0$).

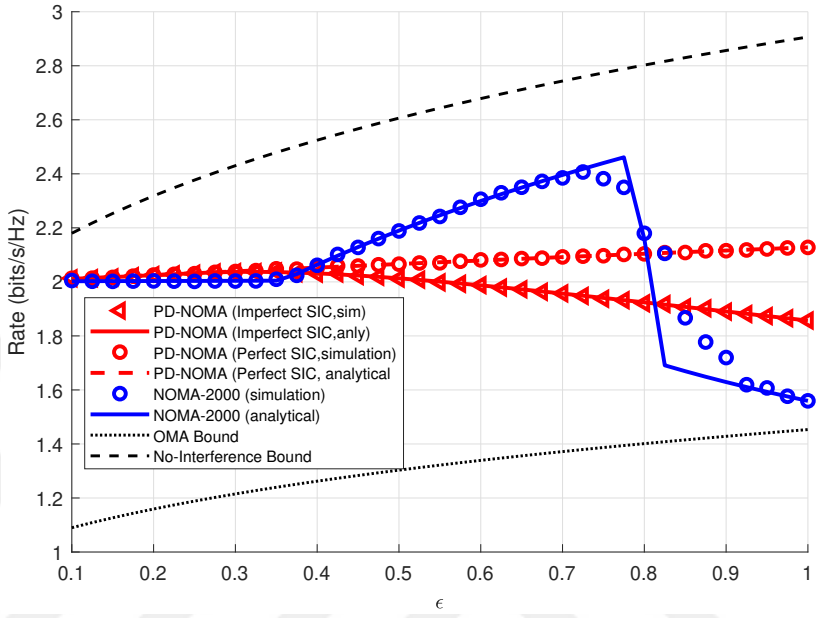


(a)

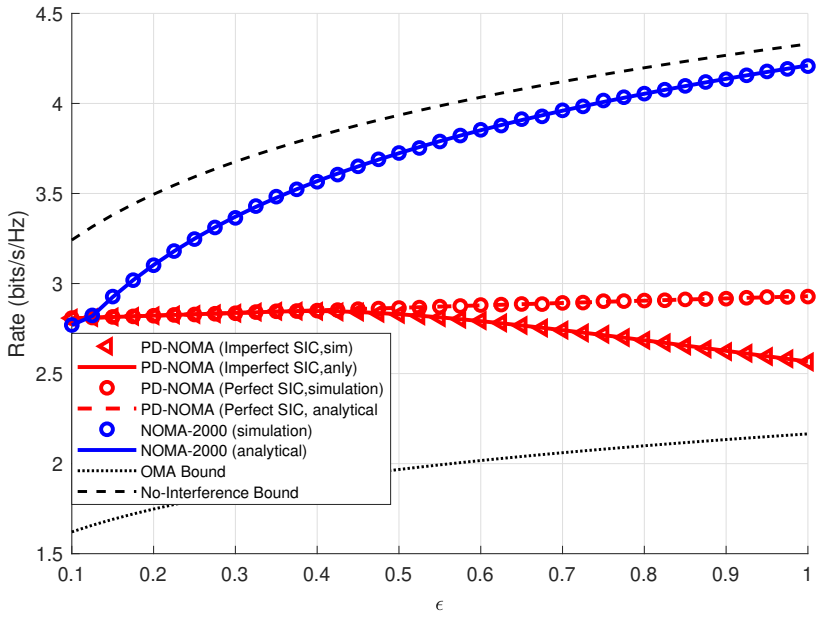


(b)

Figure 3.10. Capacity comparisons between PD-NOMA and NOMA-2000 when target rate is 1.5 bits/s/Hz a) in 10 dB and b) in 15 dB.

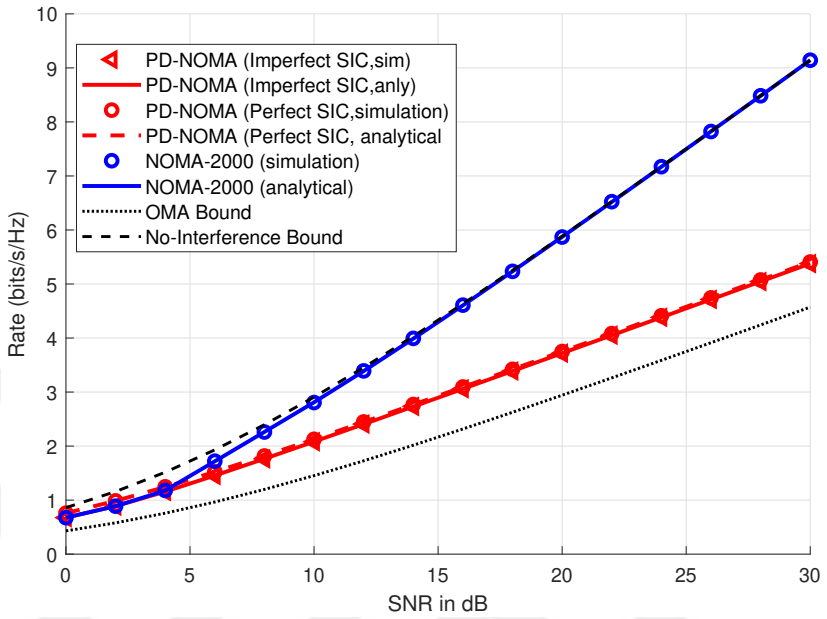


(a)

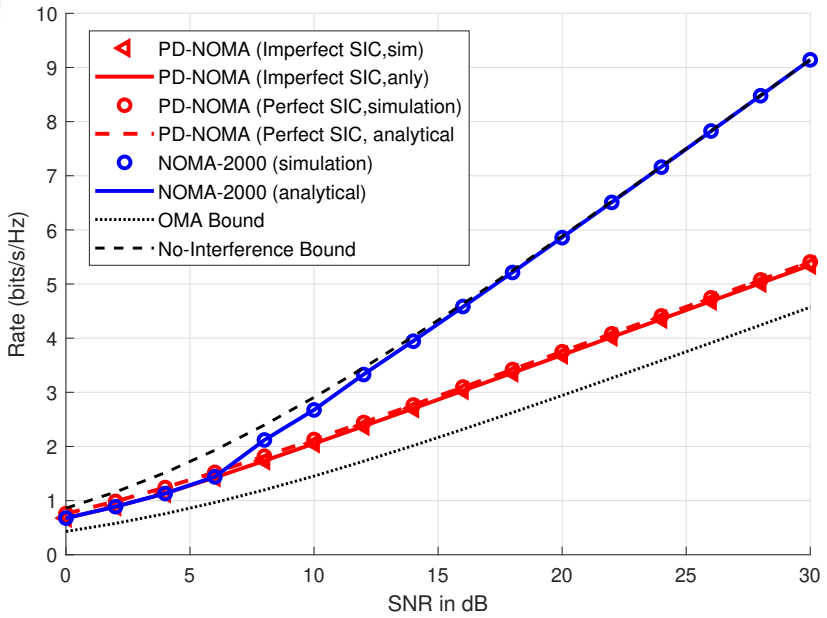


(b)

Figure 3.11. Capacity comparisons between PD-NOMA and NOMA-2000 when target rate is 1.8 bits/s/Hz a) in 10 dB and b) in 15 dB.

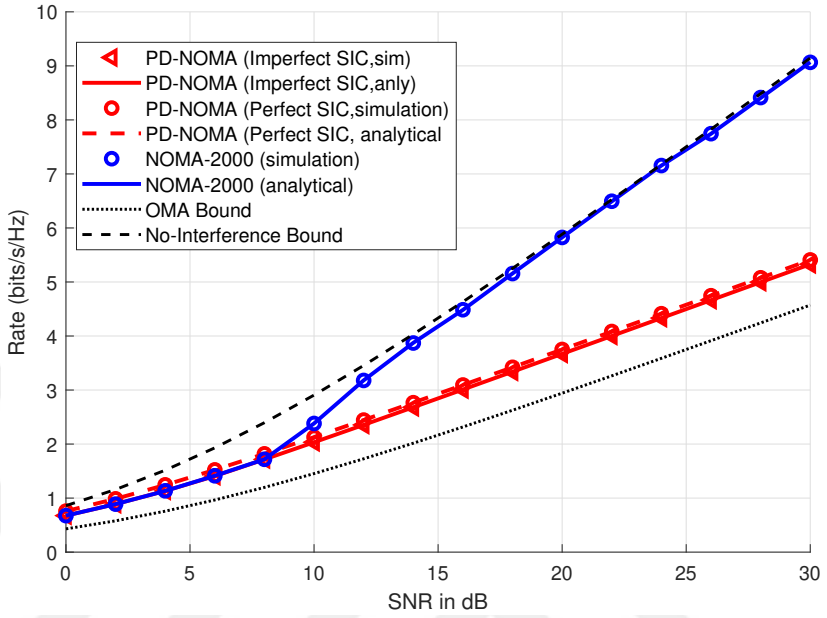


(a)

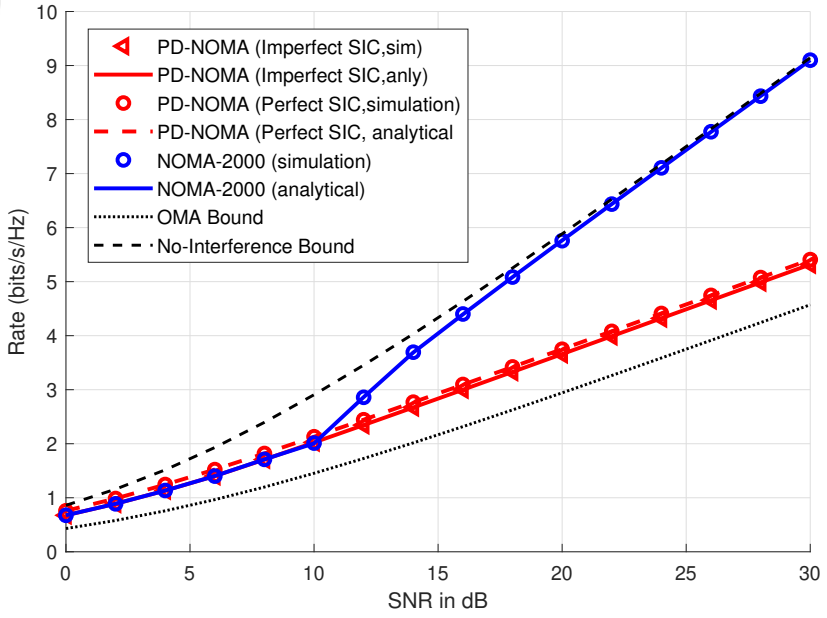


(b)

Figure 3.12. Capacity comparisons between PD-NOMA and NOMA-2000 when ϵ values are selected to maximize capacity and target rates are a)$\hat{R} = 1.2$ bits/s/Hz and b) $\hat{R} = 1.5$ bits/s/Hz.



(a)



(b)

Figure 3.13. Capacity comparisons between PD-NOMA and NOMA-2000 when ϵ values are selected to maximize capacity and target rates are a)$\hat{R} = 1.8$ bits/s/Hz and b) $\hat{R} = 2.0$ bits/s/Hz.

Second, it implies a system with low design complexity because it works well even there is no power imbalance between user groups. It is worth noting that in all mathematical calculations, our main assumption is that users from U_1 have higher channel gains than the value of τ. However, when $\epsilon\phi\mu_Z^{(i)} + \sigma^2\phi \approx \tau$ for any iteration i, this assumption causes a disagreement between the analytical derivations and simulation results.

Finally, in Figures 3.12 and 3.13, we compare both NOMA schemes with the ϵ values which maximize their capacities. Notice that while outage probability is dominated by U_2, the average capacity is dominated by U_1. Therefore, for PD-NOMA under the imperfect SIC, the ϵ value which guarantee that U_1 reaches the no-interference bound also maximize the capacity. This ϵ value is equal to $\max(0, \frac{\tau-\beta_1}{\tau\phi})$. On the other hand, NOMA-2000 can reach the no-interference bound with an ϵ value in all target rates as it reaches in coverage probability.

3.4.4. Analysis

In this chapter, the analytical derivations for PD-NOMA and NOMA-2000 are carried out assuming Rayleigh fading. As discussed in Chapter 2, we only assume a simple and random pairing scheme in order to satisfy the basic principle of NOMA for multi-carrier. Our numerical results have shown that NOMA-2000 can reach the theoretical bounds with this strategy but PD-NOMA may need more sophisticated pairing and power allocation method.

We have derived analytical expressions for the outage probability, the channel capacity under perfect SIC assumption, and the channel capacity under imperfect SIC assumption. In order to use as benchmarks, we also have derived an OMA and no-interference bounds. While OMA bound represents the state of the art performance of existing schemes, no-interference bound indicates the analytical lower/upper bounds a system with K users can reach.

For the outage probability, our simulations have shown that while PD-NOMA

experiences an error floor in high SNR, NOMA can remove all interference and reaches no-interference bounds. On the other hand, we have observed the superiority of PD-NOMA for the channel capacity under perfect SIC. However, assuming perfect SIC to decode signals of U_2 is not realistic, and this assumption also does not include performance gains of iterative decoding on NOMA-2000. Therefore, we have defined a new capacity under imperfect SIC. According to this assumption, the BS cannot perform SIC to the signal of a user if it is not in coverage. When we test this new definition with simulations, we have seen that in NOMA-2000 the BS can eliminate all interference thus can reach no-interference bound in high SNR.

In the next chapter, we will extend these works for $\kappa - \mu$ shadowed fading, $\kappa - \mu$ fading, Rician fading, Rician shadowed fading, Nakagami-m fading channel models. To achieve that, we will use the MGD approximations of these channel models. Finally, we will compare NOMA schemes for different channel models and scenarios.

4. Design and Analysis of Non-Orthogonal Multiple Access over Generalized Fading Channels

In this chapter, we extend the previous calculation to generalized fading channel models. We investigate $\kappa-\mu$ shadowed fading, $\kappa-\mu$ fading, Rician fading, Rician shadowed fading, Nakagami-m fading as well as Rayleigh fading channel models. During analysis of these fading models, we use their MGD approximations. In order to show the performance gains obtained by the NOMA schemes, analytical no- interference and OMA bounds are also derived as in the previous chapter.

4.1. Mixture of Gamma Distribution Approach

The common feature of the generalized fading channel model, that is considered in this chapter and that is applicable to a number of fading scenarios, is that the channel gains can be expressed or approximated by the Mixture of Gamma Distribution (MGD) with the PDF of

$$f_V(v) \approx \sum_{l=1}^{L} w_l f_l(v) = \sum_{l=1}^{L} \chi_l v^{t_l-1} \exp(-T_l v), \tag{4.1}$$

where $f_l(v) = \frac{T_l^{t_l}}{\Gamma(t_l)} v^{t_l-1} e^{-T_l v}$ is the PDF of a standard GD with shape parameter t_l and scale parameter T_l. Moreover, $w_l = \chi_l \Gamma(t_l) T_l^{-t_l}$ is the weighting coefficient which yields equation $\sum_{l=1}^{L} w_l = 1$ where $\chi_n = \theta_n (\sum_{m=1}^{N} \theta_m \Gamma(t_m) T^{-t_m})^{-1}$, $\Gamma(.)$ and $\Gamma(.,.)$ are *Gamma function* and *upper incomplete Gamma function*. Other parameters are summarized in Table 4.1 for fading models with standart deviation of λ. Because Rician fading and Rician shadowed fading are special cases of $\kappa-\mu$ fading and $\kappa-\mu$ shadowed fading for $\mu = 1$, respectively, their parameters are skipped in that table. Furthermore, during calculations we have encountered some integrals which include Gamma function or the PDF of Gamma function. In Table 4.2, these integrals are given.

The CDF of the MGD is equal to

$$F_\gamma(\gamma) \approx \sum_{l=1}^{L} \chi_l \tau_l^{-t_l} (\Gamma(t_l) - \Gamma(t_l, \tau_l \gamma)) = \sum_{l=1}^{L} w_l F_l(\gamma). \tag{4.2}$$

For integer valued parameters, the CDF of the MGD can be interpreted as $F_l(v) = 1 - \sum_{i=0}^{t_l-1} \frac{(T_l v)^i}{i!} \exp(-T_l v)$.

Notice that we have defined random variables X and Y as the channel gains of U_1 and U_2, respectively. We can express the PDFs of random variables X and Y, respectively, as

$$f_X(x) = \begin{cases} C_1 \sum_{l=1}^{L} f_l(x), & x \geq \tau, \\ 0 & x < \tau, \end{cases} \tag{4.3}$$

$$f_Y(y) = \begin{cases} C_2 \sum_{l=1}^{L} f_l(y), & y < \tau, \\ 0 & y \geq \tau. \end{cases} \tag{4.4}$$

where C_1 and C_2 are $\frac{K}{M}$ and $\frac{K}{N}$, respectively. Threshold value, τ, can be calculated by using lookup table of the Gamma function from $F_V(\tau) = \frac{M}{M+N}$.

In order to illustrate the consistency of the MGD model, the PDFs of the fading models which are considered in this thesis and their MGD approximations are illustrated in Figure 4.1. For Rician fading ($K = 2$) and $\kappa - \mu$ fading ($\kappa = 2, \mu = 2$), it is observed that the MGD approximation converges the original PDF when L=8 and L=12, respectively.

4.2. Outage Probability

In this section, we extend our outage probability derivations for Rayleigh fading channels in the previous chapter to the generalized fading channels.and our calculations in the outage probability for generalized fading channels.

Table 4.1. Mixture of Gamma Distribution representations of some fading models.

Fading		L	MGD parameters
Rayleigh fading		1	$\chi_1 = 1\ t_1 = 1\ T_n = 1$
Nakagami-m fading (m)		1	$\chi_1 = \dfrac{m^m}{\Gamma(m)}\ t_1 = m\ T_1 = m$
$\kappa - \mu$ fading (κ, μ)		$L \gg \mu$	$\theta_n = \dfrac{\mu(\kappa+1)}{\exp(\mu\kappa)\lambda^{\frac{\mu+1}{2}}} \dfrac{\left(\frac{\kappa(\kappa+1)}{\lambda}\right)^{\frac{2n+\mu-3}{2}}}{\Gamma(\mu+n-1)(n-1)!}, t_n = \mu+n-1, T_n = \dfrac{\mu(1+\kappa)}{\lambda}$
$\kappa - \mu$ shadowed fading (κ, μ, m)	$\mu > m$	μ	$t_l = \begin{cases} \mu - m - l + 1 & 0 \geq l \geq \mu - m \\ \mu - l + 1 & \mu - m < l \leq \mu \end{cases}$ $T_l = \begin{cases} \dfrac{\mu(1+\kappa)}{\lambda}, & 0 \geq l \leq \mu - m, \\ \dfrac{m\mu(1+\kappa)}{(\mu\kappa+m)\lambda}, & \mu - m < l \leq \mu, \end{cases}$ $\theta_l = \begin{cases} (-1)^m \binom{m+i-2}{i-1} [\frac{m}{\mu\kappa+m}]^{-m-i+1} [\frac{\mu\kappa}{\mu\kappa+m}]^{-m-i+1}, & 0 < i \leq \mu - m, \\ \binom{m+i-2}{i-1} [\frac{m}{\mu\kappa+m}]^{i-\mu+m-1} [\frac{\mu\kappa}{\mu\kappa+m}]^{-i+1}, & \mu - m < i \leq \mu, \end{cases}$
	$m \leq \mu$	$m - \mu + 1$	$\chi_l = \binom{m-\mu}{i-1} \left[\dfrac{m}{\mu\kappa+m}\right]^{i-1} \left[\dfrac{\mu\kappa}{\mu\kappa+m}\right]^{m-\mu-i-1} \dfrac{T_l^{t_l}}{\Gamma(t_l)}$, $t_l = m - i - 1$, $T_l = \dfrac{m\mu(1+\kappa)}{(\mu\kappa+m)\lambda}$.

Table 4.2. List of integrals involving Gamma function or the PDF of Gamma distribution.

$\mathcal{I}_{5,l}^{0\to\tau}(C,u)$	$\int_0^\tau C\log(1+uv)f_l(v)dv$	$(1-C)\log_2(1+u\tau)+\frac{C}{\ln(2)}e^{T_l/v}$ $\sum_{r=0}^{t_l-1}\sum_{r_1=0}^{r}\frac{1}{r!}\binom{r}{r_1}(-1)^{r-r_1}\Big(\Gamma(r_1,T_l/u)-\Gamma(r_1,T_l/u+T_l\tau)\Big)$
$\mathcal{I}_{5,l}^{\tau\to\infty}(C,u)$	$\int_\tau^\infty C\log(1+uv)f_l(v)dv$	$\log_2(1+u\tau)+\frac{C}{\ln(2)}e^{T_l/v}$ $\sum_{r=0}^{t_l-1}\sum_{r_1=0}^{r}\left(\frac{T_l}{u}\right)^{r-r_1}\frac{1}{r!}\binom{r}{r_1}(-1)^{r-r_1}\Gamma(r_1,T_l/u+T_l\tau)$
$\mathcal{I}_{6,l_1,l_2}^{(k_1,k_2,k_3)}$	$\int_{k_2}^{k_3}\int_{\alpha v_1+k_1}^{\infty}f_{l_1}(v)f_{l_2}(v)dv_{l_1}dv_{l_2}$	$\frac{T_{l_2}^{t_{l_2}}}{\Gamma(t_{l_2})}e^{-T_{l_1}k_1}\sum_{r=0}^{t_{l_1}-1}\frac{T_{l_1}^r}{r!}\sum_{r_1=0}^{r}\binom{r}{r_1}\beta_1^{r-r_1}\alpha^{r_1}(T_{l_1}\alpha+T_{l_2})^{-r_1-t_{l_2}}$ $\Big(\Gamma(r_1+t_{l_2},k_3(T_{l_1}\alpha+T_{l_2}))-\Gamma(r_1+t_{l_2},k_2(T_{l_1}\alpha+T_{l_2}))\Big).$
$\mathcal{I}_{7}^{k_1,k_2,k_3,k_4}(x)$	$\int\ln(k_1x+k_2)\frac{k_4^{k_3}}{\Gamma(k_3)}x^{k_3-1}e^{-k_4x}dx$	$(F_X(x)-1)\ln(k_1xk_2)-e^{k_1x+k_2}\sum_{r=0}^{t_l-1}\sum_{r_1=0}^{r}\frac{\binom{r}{r_1}}{r!}$ $(-k_1x-k_2)^{r-r_1}\Gamma\left(r_1,T_l(x+\frac{k_2}{k_1})\right)$
$\mathcal{I}_{8,l_1,l_2}^{k_1,k_2,k_3,k_4}(x)$	$\int\ln(k_1x+k_2)(F_{l_1}(k_3x+k_4)-1)$ $f_{l_2}(x)dx$	$-e^{-T_{l_1}k_4}\sum_{r=0}^{t_{l_1}-1}\sum_{r_1=0}^{r}T_{l_1}^r\frac{\binom{r}{r_1}}{r!}k_4^{r-r_1}k_3^{r_1}\frac{\Gamma(t_{l_2}+r_1)T_{l_2}^{t_{l_2}}}{\Gamma(t_{l_2})(T_{l_2}(k_3+1)^{t_2+r_1}})$ $\mathcal{I}_{7}^{k_1,k_2,t_{l_2}+r_1,\frac{t_{l_2}+r_1}{T_{l_2}(k_3+1)}}(x)$
$\mathcal{I}_{9,l}^{(k_1,k_2,k_3,k_4,k_5,k_6)}(x)$	$\int e^{k_1x+k_2}(-k_1x-k_2)^{k_5-k_6}$ $\Gamma(r_1,(k_1+k_3)x+k_2+k_4)f_l(x)dx$	$e^{k_2}(-1)^{k_5-k_6}\sum_{s=0}^{k_5-k_6}\binom{k_5-k_6}{s}k_2^{k_5-k_6-s}k_1^s\frac{T_l^{t_l}}{\Gamma(t_l)}\mathcal{I}_{10,l}^{(k_1,k_2,k_3,k_4,k_5,k_6)}(x)$

Table 4.2. List of integrals involving Gamma function or the PDF of Gamma distribution – continued from previous page

$\mathcal{I}_{10,l}^{(k_1,k_2,k_3,k_4,k_5,k_6)}(x)$	$\int x^{k_5+k_6-1}e^{-(T_l-k_1)x}$ $\Gamma(k_5,(k_1+k_3)x+k_2+k_4)dx$	$\frac{(T_l-k_1)^{t+s}}{\Gamma(t_l+s)}\left(\frac{\gamma(t_l,T_lx)}{\Gamma(x)}-1\right)\Gamma(k_5,k_1x+k_2)$ $-e^{\frac{T_lk_2}{k_1}}\sum_{s_1=0}^{t_l-1}\frac{\left(\frac{T_l}{k_1}\right)^{s_1}}{s_1!}\sum_{s_2=0}^{s_1}\binom{s_1}{s_2}(-k_2)^{s_1-s_2}$ $k_1\neq T_l$ $\mathcal{I}_{11}^{\left(k_5+s_2,\frac{T_l}{k_1}+1\right)}(k_1x+k_2)+\text{constant},$ $\frac{x^{t_l+k_6}}{t_l+k_6}\Gamma(k_5,(k_1+k_3)x+k_2+k_4)-\frac{(k_1+k_3)^{-(k_5+t_l)}}{k_5+t_l}$ $\sum_{v=0}^{k_5+t_l}\binom{k_5+t_l}{v}(-k_2-k_4)^{k_5+t_l-v}$ $k_1=T_l$ $\Gamma(v+k_5,(k_1+k_3)x+k_2+k_4)+\text{constant},$
$\mathcal{I}_{11}(k_1,k_2)$	$\int x^{k_1-1}e^{-k_2x}dx$	$\begin{cases}\frac{\gamma(k_1,k_2x)}{k_2^{k_1}}+\text{constant} & k_2\neq 0\\ \frac{x^{k_1}}{k_1}+\text{constant} & k_1\neq 0\&k_2=0\\ \ln x+\text{constant} & k_1=k_2=0\end{cases}$

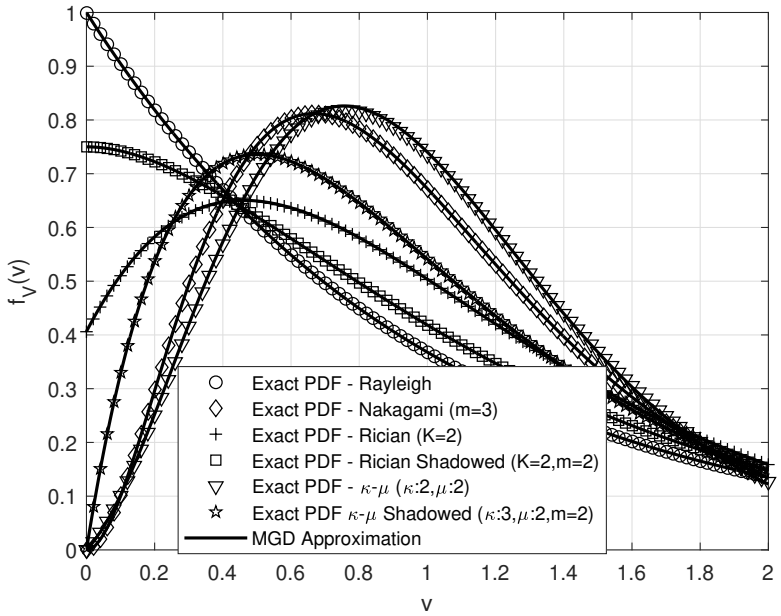


Figure 4.1. Agreement with the MGD Approximation and the exact PDFs of generalized fading channel models.

4.2.1. PD-NOMA

As discussed in the system model, $\hat{U}_1$ represents users who share the subcarrier with a user from U_2. Therefore, in order to calculate the outage probability, expectations with respect to X and Y should be taken as

$$\begin{aligned} Pr^{PD}_{\hat{U}_1,\text{out}} &= 1 - Pr\left(x > \alpha y + \beta_1\right) = 1 - \int_0^{\tau} \int_{\alpha y+\beta_1}^{\infty} f_X(x) f_Y(y) dx dy \\ &= 1 - \int_0^{\min(\tau,\max(0,\frac{\tau-\beta_1}{\alpha}))} f_Y(y) dy \\ &- \int_{\min(\tau,\max(0,\frac{\tau-\beta_1}{\alpha}))}^{\tau} \int_{\alpha y+\beta_1}^{\infty} f_X(x) f_Y(y) dx dy \\ &= 1 - F_Y(\min(\tau, \max(0, \frac{\tau-\beta_1}{\alpha}))) \\ &- C_1 C_2 \sum_{l_1=1}^{L} \sum_{l_2=1}^{L} w_{l_1} w_{l_2} \mathcal{I}_{6,l_1,l_2}(\beta_1, \min(\tau, \max(0, \frac{\tau-\beta_1}{\alpha})), \tau), \quad (4.5) \end{aligned}$$

where the integral of multiplication of the PDFs $\int_{\beta_2}^{\beta_3}\int_{\alpha v_1+\beta_1}^{\infty} f_{V_{l_1}}(v_{l_1})f_{V_{l_2}}(v_{l_2})dv_{l_1}dv_{l_2}$ is defined as $\mathcal{I}_{6,l_1,l_2}$ and given in Table 4.2. Users from $\tilde{U}_1$, on the other hand, use a subcarrier solely and their outage probability is calculated as

$$Pr^{PD}_{\tilde{U}_1,\text{out}} = \int_{\max(\beta_1,\tau)}^{\infty} f_X(x)dx = 1 - F_X(\max(\beta_1,\tau)). \tag{4.6}$$

Then, the outage probability for users in U_1 is computed as

$$Pr^{PD}_{U_1,\text{out}} = \frac{MPr^{PD}_{\tilde{U}_1,\text{out}}}{N} + \frac{(N-M)Pr^{PD}_{\tilde{U}_1,\text{out}}}{N}, \tag{4.7}$$

and for PD-NOMA as

$$Pr^{PD}_{\text{out}} = \frac{NPr^{PD}_{U_1,\text{out}}}{K} + \frac{MPr^{PD}_{U_2,\text{out}}}{K}. \tag{4.8}$$

Moreover, in order for a user from U_2 to be in coverage, the user from U_1 sharing the same subcarrier should also be in coverage. Notice that the outage probability of the U_1 is given in equation (4.5) that is also dependent on the channel gain of the user in U_2. The outage probability of U_2 can be calculated similarly as follows:

$$\begin{aligned}
Pr^{PD}_{U_2,out} &= 1 - Pr(y > \beta_2, x > \alpha y + \beta_1) \\
&= 1 - \int_{\min(\beta_2,\tau)}^{\tau}\int_{\alpha y+\beta_1}^{\infty} f_X(x)f_Y(y)dxdy \\
&= 1 - \mathrm{u}(\tau-\beta_2)\Bigg[F_Y(\min(\tau,\max(0,\frac{\tau-\beta_1}{\alpha}))) + F_Y(\beta_2) \qquad (4.9)\\
&- C_1C_2\sum_{l_1=1}^{L}\sum_{l_2=1}^{L} w_{l_1}w_{l_2}\mathcal{I}_{6,l_1,l_1}\left(\beta_1, \min\left(\left((\tau,\max(0,\frac{\tau-\beta_1}{\alpha}\right)\right),\tau\right)\Bigg].
\end{aligned}$$

4.2.2. NOMA-2000

We revisit the outage event and the outage probability definitions in equation (3.21), which were and note that the interference powers were defined, respectively, as

$$Pr_{out}^{(i)WD}(U_1,n) = 1 - Pr(E_{U_1,n}^{(i),WD}) = 1 - Pr\left(|g_n|^2 > \frac{\phi}{P_t}P_{I_{U_1}}^{(i)} + \beta_1\right), \quad (4.10)$$

$$Pr_{out}^{(i)WD}(U_2,m) = 1 - Pr(E_{U_2,m}^{(i),WD}) = 1 - Pr\left(|g_{N+m}|^2 > \frac{\phi}{\epsilon P_t}P_{I_{U_2}}^{(i)} + \beta_2\right) \quad (4.11)$$

and notice that we have defined interference powers as $P_tW^{(i)} \triangleq P_{I_{U_2}}^{(i)}$ and $\epsilon P_tZ^{(i)} \triangleq P_{I_{U_1}}^{(i)}$ for iteration i. Therefore, in order to calculate the outage probability we first calculate variables $W^{(i)}$ and $Z^{(i)}$ for each iteration. Starting from the first iteration, the variables can be defined, respectively, as

$$\begin{aligned}
\mu_Z^{(1)} &= \frac{M}{N}\int_0^{\tau} y f_Y(y)dy = \frac{M}{N}\sum_{l=0}^{L}\int_0^{\tau} y_l f_Y(y_l)dy_l \\
&= \frac{M}{N}\sum_{l=0}^{L}\int_0^{\tau} C_2 a_l y^{t_l} e^{-T_l y}dy = -\frac{M}{N}C_2\sum_{l=0}^{L} a_l T_l^{-t_l-1}\Gamma(t_l+1,T_l y)\Big|_0^{\tau} \\
&= \frac{M}{N}C_2\sum_{l=0}^{L} a_l T_l^{-t_l-1}\big(\Gamma(t_l+1) - \Gamma(t_l+1,T_l\tau)\big), \quad (4.12)
\end{aligned}$$

$$\begin{aligned}
\mu_W^{(1)} &= \int_{\tau}^{\max(\beta_1+\phi\epsilon\mu_z,\tau)} x f_X(x)dx = \sum_{l=0}^{L} Y_l f_X(x_l)dx_l, \\
&= C_1\sum_{l=L}^{N} w_l(\max(\beta_1+\phi\epsilon\mu_Z^{(1)},\tau)(F_V(\max(\beta_1+\phi\epsilon\mu_Z^{(1)},\tau)) - 1) - \tau(F_v(\tau)-1) \\
&+ \frac{1}{T_l}\sum_{s=0}^{t_l-1}\frac{1}{s!}\big(\Gamma(s+1,T_l\tau) - \Gamma(s+1,T_l\max(\beta_1+\phi\epsilon\mu_z,\tau)\big). \quad (4.13)
\end{aligned}$$

Similarly, for further iterations they can be expressed, respectively, as

$$\mu_Z^{(i)} = \frac{M}{N}\int_0^{\min(\frac{\phi}{\epsilon}\mu_W^{(i-1)}+\beta_1,\tau)} y f_Y(y)dx = \frac{M}{N}\int_0^{\min(\frac{\phi}{\epsilon}\mu_W^{(i-1)}+\beta_1,\tau)} y_l f_Y(y_l)dy_l$$

$$= \frac{M}{N}\sum_{l=1}^{L} C_2\chi_l T_l^{t_l-1}(\Gamma(t_l+1)-\Gamma(t_l+1,T_l\min(\frac{\phi}{\epsilon}\mu_W^{(i-1)}+\beta_1,\tau))), \quad (4.14)$$

$$\begin{aligned}\mu_W^{(i)} &= \int_{\tau}^{\max(\phi\epsilon\mu_Z^{(i)}+\beta_1,\tau)} x f_X(x)dx = \\ &= C_1\sum_{l=L}^{N} w_l\Big(\max(\beta_1+\phi\epsilon\mu_Z^{(i)},\tau)\big(F_V(\max(\beta_1+\phi\epsilon\mu_Z^{(1)},\tau))-1\big) \\ &- \tau(F_v(\tau)-1)+\frac{1}{T_l}\sum_{s=0}^{t_l-1}\frac{1}{s!}\Big(\Gamma(s+1,T_l\tau) \\ &- \Gamma(s+1,T_l\max(\beta_1+\phi\epsilon\mu_z,\tau))\Big). \end{aligned} \quad (4.15)$$

Finally, the outage probabilities for both user groups are defined, respectively, as

$$Pr_{U_1,\text{out}}^{(i),WD} = F_X(\max(\alpha\mu_Z+\beta_1,\tau)), \quad (4.16)$$

$$Pr_{U_2,\text{out}}^{(i),WD} = F_Y\left(min(\beta_2+\phi\frac{\mu_W}{\epsilon},\tau)\right). \quad (4.17)$$

4.2.3. No-interference and OMA Bounds

When there is no interference, an analytical lower bound can be derived as

$$\begin{aligned} Pr^{NI} &= \frac{N}{K}\int_{\tau}^{\max(\tau,\beta_1)} f_X(x)dx + \frac{N}{K}\int_{0}^{\min(\tau,\beta_2)} f_y(y)dy \\ &= F_V(\max(\tau,\beta_1)) - F_V(\tau) + F_V(\min(\tau,\beta_2)). \end{aligned} \quad (4.18)$$

For OMA bound, target rate should be normalized with the factor of $\frac{N}{K}$, and threshold values β_1 and β_2 turn into $\hat{\beta}_1 \triangleq \sigma^2\left(2^{\hat{R}\frac{K}{N}}-1\right)$ and $\hat{\beta}_2 \triangleq \frac{\sigma^2}{\epsilon}\left(2^{\hat{R}\frac{K}{N}}-1\right)$. Then, OMA bound can be expressed as

$$Pr^{OMA} = \frac{N}{K}\int_{\tau}^{\max(\tau,\hat{\beta}_1)} f_X(x)dx + \frac{N}{K}\int_{0}^{\min(\tau,\hat{\beta}_2)} f_y(y)dy$$

$$= F_V(\max(\tau, \hat{\beta}_1)) - F_V(\tau) + F_V(\min(\tau, \hat{\beta}_2)). \quad (4.19)$$

4.3. Capacity

In this section, we express the capacity expressions for both NOMA schemes by using the SNR/SINR definitions in equations (2.15) and (2.32).

4.3.1. PD-NOMA

The capacities of users for PD-NOMA can be defined by using SNR/SINR definitions in equation (2.15) as $R^{PD}_{U_1,n} = \log_2(1 + S^{PD}_n)$ and $R^{PD}_{U_2,m} = \log_2(1 + S^{PD}_m)$, respectively. Starting from U_2, the average capacity can be calculated by using equation in Table 4.2 as

$$R^{PD}_{U_2} = \int_0^{\tau} \log_2(1 + \frac{\epsilon P_t}{\sigma^2} y) f_Y(y) dy = \sum_{l=1}^{L} w_l \mathcal{I}^{0\to\tau}_{5,l}\left(C_2, \epsilon \frac{P_t}{\sigma^2}\right). \quad (4.20)$$

The average capacity for U_1, on the other hand, is much more complex because of dependency on the channel gains of U_2. Its analytical calculation can be expressed as

$$\begin{aligned}
R^{PD}_{\hat{U}_1} &= \int_0^{\tau}\int_{\tau}^{\infty} \log_2(1 + \frac{P_t X}{\epsilon P_t Y + \sigma^2}) f_X(x) f_Y(y) dx dy \\
&= C_2 \sum_{l=1}^{L} \int_0^{\tau} f_l(y) \mathcal{I}^{\tau\to\infty}_{5,l}(C_1, \frac{P_t X}{\epsilon P_t Y + \sigma^2}) dy \\
&= \log_2(1 + \frac{P_t \tau}{\sigma^2}) + \sum_{l=1}^{L} w_l \left[\mathcal{I}^{0\to\tau}_{5,l}(\frac{\epsilon P_t}{P_t \tau + \sigma^2}) - \mathcal{I}^{0\to\tau}_{5,l}(\frac{\epsilon P_t}{\sigma^2})\right] \\
&\quad + \frac{C_1 C_2}{\ln(2)} \sum_{l_1=1}^{L}\sum_{l_2=1}^{L}\sum_{r=0}^{t_{l_1}-1} w_{l_1} w_{l_2} \sum_{r_1=0}^{r} \frac{\binom{r}{r_1}}{r!} (-1)^{r-r_1} \Bigg(\mathcal{I}^{(T_{l_1}\epsilon, T_{l_1}\frac{\sigma^2}{P_t}, 0, T_{l_1}\tau, r, r_1)}_{9,l_2}(\tau) \\
&\quad - \mathcal{I}^{(T_{l_1}\epsilon, T_{l_1}\frac{\sigma^2}{P_t}, 0, T_{l_1}\tau, r, r_1)}_{9,l_2}(0)\Bigg). \quad (4.21)
\end{aligned}$$

On the other hand, for users which belong to $\tilde{U}_1$, the capacity can be calculated as $R^{PD}_{\tilde{U}_1} = \sum_{l=1}^{L} w_l I_l^{\tau\to\infty}(C_1, \frac{P_t}{\sigma^2})$, and finally we can express the average capacity for PD-NOMA as

$$R^{PD} = \frac{M}{K} R^{PD}_{\hat{U}_1} + \frac{(N-M)}{K} R^{PD}_{\tilde{U}_1} + \frac{M}{K} R^{PD}_{U_2}. \tag{4.22}$$

4.3.2. NOMA-2000

Capacities of users for NOMA-2000 can be defined as

$$R^{WD}_{U_1,k} = \log_2(1 + S_n^{WD}) \quad k \in U_1 \cup U_2. \tag{4.23}$$

Because for both NOMA-2000 and PD-NOMA we assume perfect SIC for users U_2, their average capacities are identical as $R^{PD}_{U_2} = R^{WD}_{U_2}$. On the other hand, by using equations in Table 4.2, the average capacity for U_1 can be described as

$$R^{WD}_{U_1} = \int_{\tau}^{\infty} \log_2(1 + \frac{\epsilon P_t}{\sigma^2} x) f_X(x) dx = \sum_{l=1}^{L} w_l \mathcal{I}_{5,l}^{\tau\to\infty}\left(C_1, \frac{P_t}{\sigma^2 + \epsilon\mu_Z}\right). \tag{4.24}$$

Finally, we can express the average capacity for PD-NOMA as

$$R^{WD} = \frac{N}{K} R^{WD}_{U_1} + \frac{M}{K} R^{WD}_{U_2}. \tag{4.25}$$

4.3.3. No-interference and OMA Bounds

Similar to the previous chapter, we can define the *no-interference* and *OMA* bounds for capacity. Notice that, the SNR definitions for both cases are identical. However, the entire bandwidth is shared for K users in OMA, the relation between capacities of OMA and no-interference bounds is $R^{OMA} = \frac{N}{K} R^{NI}$. Finally, the analytical calculations can be expressed, respectively, as

$$R^{NI}_{U_1} = \int_{\tau}^{\infty} \log_2(1 + \frac{\epsilon P_t}{\sigma^2} x) f_X(x) dx = \sum_{l=1}^{L} w_l I_l^{\tau\to\infty}\left(C_1, \frac{P_t}{\sigma^2}\right), \tag{4.26}$$

$$R_{U_2}^{NI} = \int_0^{\tau} \log_2(1+\frac{\epsilon P_t}{\sigma^2}y) f_Y(y)dy = \sum_{l=1}^{L} w_l I_l^{0\to\tau}\left(C_2, \epsilon\frac{P_t}{\sigma^2}\right), \tag{4.27}$$

$$R^{NI} = \frac{NR_{U_1}^{NI} + MR_{U_2}^{NI}}{N+M}. \tag{4.28}$$

4.4. Capacity under Imperfect SIC

In this section, we repeat the calculations on previous section for generalized fading channels by using the MGD approach.

4.4.1. PD-NOMA

Notice that we have defined capacities under imperfect SIC for users of PD-NOMA, respectively, as

$$R_{U_1,n}^{PD} = \log_2\left(1+\frac{P_t|g_n|^2}{\epsilon P_t|g_{n+N}|^2+\sigma^2}\right), \tag{4.29}$$

$$R_{U_2,n}^{PD} = \begin{cases} \log_2\left(1+\dfrac{\epsilon P_t|g_{n+N}|^2}{\sigma^2}\right), & |g_n|^2 \geq \alpha|g_{n+N}|^2+\beta, \\ \log_2\left(1+\dfrac{\epsilon P_t|g_{n+N}|^2}{P_t|g_n|^2+\sigma^2}\right), & |g_n|^2 < \alpha|g_{n+N}|^2+\beta. \end{cases} \tag{4.30}$$

Because there is only one shot decoding for U_1, capacity definition and average rate of U_1 do not change. However, in this section we calculate the average rate of U_2 by assuming that if a user in outage, BS cannot perform SIC on its signal.

Integral regions on Figure 3.1 also valid for generalized fading models. Integrals in equations (3.59) and (3.60) can be calculated with the same approach discussed in Chapter 4.3.1. as

$$\begin{aligned} R_{U_2}^{PD} &= \int_0^{\tau}\int_{\max(\alpha y+\beta_1,\tau)}^{\infty} \log_2\left(1+\frac{\epsilon P_t Y}{\sigma^2}\right) f_X(x)f_Y(y)dxdy \\ &+ \int_0^{\tau}\int_{\max(\alpha y+\beta_1,\tau)}^{\infty} \log_2\left(1+\frac{\epsilon P_t Y}{\sigma^2+P_t X}\right) f_X(x)f_Y(y)dxdy. \end{aligned} \tag{4.31}$$

Starting from the first integral,

$$\int_0^{\tau}\int_{\max(\alpha y+\beta_1,\tau)}^{\infty}\log_2\left(1+\frac{\epsilon P_t Y}{\sigma^2}\right)f_X(x)f_Y(y)dxdy$$

$$=\frac{C_1C_2}{\ln 2}\sum_{l_1=1}^{L}\sum_{l_2=1}^{L}w_{l_1}w_{l_2}\int_0^{\tau}\ln\left(1+\frac{\epsilon P_t y}{\sigma^2}\right)\left(1-F_{l_1}(\Delta_1)\right)f_{l_2}(y)dy$$

$$=\frac{C_1C_2}{\ln 2}\left(1-F_l(\tau)\right)\sum_{l_2=1}^{L}w_{l_2}\int_0^{\Delta_2}\ln(1+\frac{\epsilon P_t y}{\sigma^2})f_{l_2}(y)dy$$

$$+\frac{C_1C_2}{\ln 2}\sum_{l_1=1}^{L}\sum_{l_2=1}^{L}w_{l_1}w_{l_2}\int_{\Delta_2}^{\tau}\ln(1+\frac{\epsilon P_t y}{\sigma^2})\left(1-F_{l_1}(\alpha y+\beta_1)\right)f_{l_2}(y)dy$$

$$=\frac{C_1C_2}{\ln 2}\left(1-F(\tau)\right)\sum_{l_2=1}^{L}w_{l_2}\left(\mathcal{I}_{7,l_2}^{(\frac{\epsilon P_t}{\sigma^2},1)}(\Delta_2)-\mathcal{I}_{7}^{(\frac{\epsilon P_t}{\sigma^2},1,t_{l_2},T_{l_2})}(0)\right)$$

$$+\frac{C_1C_2}{\ln 2}\sum_{l_1=1}^{L}\sum_{l_2=1}^{L}w_{l_1}w_{l_2}\left(\mathcal{I}_{8,l_1,l_2}^{(\alpha+\epsilon,\beta_1+\frac{\sigma^2}{P_t},\alpha,\beta_1)}(\tau)-\mathcal{I}_{8,l_1,l_2}^{(\alpha+\epsilon,\beta_1+\frac{\sigma^2}{P_t},\alpha,\beta_1)}(\Delta_2)\right), \quad (4.32)$$

where $\Delta_1=\max(\alpha y+\beta_1,\tau)$ and $\Delta_2=\min(\tau,\max(0,\frac{\tau-\beta_1}{\alpha}))$. The second integral is a much more complex one as it was also the case in Rayleigh fading, and its calculations can be given by

$$\int_{\Delta_2}^{\tau}\int_{\tau}^{\alpha y+\beta_1}\ln\left(1+\frac{\epsilon P_t y}{\sigma^2+P_t x}\right)f_X(x)f_Y(y)dxdy$$

$$=\frac{C_1C_2}{\ln 2}\sum_{l_1=1}^{L}\sum_{l_2=1}^{L}w_{l_1}w_{l_2}\int_{\Delta_2}^{\tau}\left(F_{l_1}(\alpha y+\beta_1)-1\right)\ln\left(\frac{\alpha y+\beta_1+\epsilon y+\frac{\sigma^2}{P_t}}{\alpha y+\beta_1+\frac{\sigma^2}{P_t}}\right)f_{l_2}(y)dy$$

$$-\left(F(\tau)-1\right)\sum_{l_2=1}^{L}w_{l_2}\int_{\Delta_2}^{\tau}\ln\left(\frac{\tau+\epsilon y+\frac{\sigma^2}{P_t}}{\tau+\frac{\sigma^2}{P_t}}\right)f_{l_2}(y)dy$$

$$+\sum_{l_1=1}^{L}\sum_{l_2=1}^{L}w_{l_1}w_{l_2}\left[\sum_{r=0}^{t_{l_1}-1}\sum_{r_1=0}^{r}\frac{\binom{r}{r_1}}{r!}\int_{\Delta_2}^{\tau}\left(e^{T_{l_1}\epsilon y+T_{l_1}\frac{\sigma^2}{P_t}}(-T_{l_1}\epsilon y-T_{l_1}\frac{\sigma^2}{P_t})^{r-r_1}\right.\right.$$

$$\left.\left(\Gamma\left(r_1,T_{l_1}\tau+T_{l_1}\epsilon y+T_{l_1}\frac{\sigma^2}{P_t}\right)-\Gamma\left(r_1,T_{l_1}(\alpha y+\beta_1)+T_{l_1}\epsilon y+T_{l_1}\frac{\sigma^2}{P_t}\right)\right)\right.$$

$$-e^{T_{l_1}\frac{\sigma^2}{P_t}}(-T_{l_1}\frac{\sigma^2}{P_t})^{r-r_1}\left(\Gamma\left(r_1, T_{l_1}\tau + T_{l_1}\frac{\sigma^2}{P_t}\right)\right.$$

$$\left.-\Gamma\left(r_1, T_{l_1}(\alpha y+\beta_1) + T_{l_1}\frac{\sigma^2}{P_t}\right)\right)\Bigg] f_{l_2}(y)dy$$

$$= \frac{C_1C_2}{\ln 2}\sum_{l_1=1}^{L}\sum_{l_2=1}^{L} w_{l_1}w_{l_2}\left(\mathcal{I}_{8,l_1,l_2}^{(\alpha+\epsilon,\beta_1+\frac{\sigma^2}{P_t},\alpha,\beta_1)}(\tau) - \mathcal{I}_{8,l_1,l_2}^{(\alpha+\epsilon,\beta_1+\frac{\sigma^2}{P_t},\alpha,\beta_1)}(\Delta_2)\right.$$

$$\left.-\mathcal{I}_{8,l_1,l_2}^{(\alpha,\beta_1+\frac{\sigma^2}{P_t},\alpha,\beta_1)}(\tau) + \mathcal{I}_{8,l_1,l_2}^{(\alpha,\beta_1+\frac{\sigma^2}{P_t},\alpha,\beta_1)}(\Delta_2) - \mathcal{I}_{8,l_1,l_2}^{\left(\frac{\epsilon}{\tau+\frac{\sigma^2}{P_t}},1,0,\tau\right)}(\tau) + \mathcal{I}_{8,l_1,l_2}^{\left(\frac{\epsilon}{\tau+\frac{\sigma^2}{P_t}},1,0,\tau\right)}(\Delta_2)\right)$$

$$+\frac{C_1C_2}{\ln 2}\sum_{l_1=1}^{L}\sum_{l_2=1}^{L} w_{l_1}w_{l_2}\sum_{r=0}^{t_{l_1}-1}\sum_{r_1=0}^{r}\frac{\binom{r}{r_1}}{r!}\left(\mathcal{I}_{10,l}^{(r,r_1,T_l\epsilon,T_l\frac{\sigma^2}{P_t},0,T_l\tau)}(\tau) - \mathcal{I}_{10,l}^{(r,r_1,T_l\epsilon,T_l\frac{\sigma^2}{P_t},0,T_l\tau)}(\Delta_2)\right.$$

$$+\mathcal{I}_{10,l_2}^{(r,r_1,T_l\epsilon,T_l\frac{\sigma^2}{P_t},T_l\alpha,T_l\beta_1)}(\tau) - \mathcal{I}_{10,l_2}^{(r,r_1,T_l\epsilon,T_l\frac{\sigma^2}{P_t},T_l\alpha,T_l\beta_1)}(\Delta_2) + \mathcal{I}_{10,l_2}^{(r,r_1,0,T_l\frac{\sigma^2}{P_t},0,T_l\tau)}(\tau)$$

$$\left.-\mathcal{I}_{10,l_2}^{(r,r_1,0,T_l\frac{\sigma^2}{P_t},0,T_l\tau)}(\Delta_2) + \mathcal{I}_{10,l_2}^{(r,r_1,0,T_l\frac{\sigma^2}{P_t},T_l\alpha,T_l\beta_1)}(\tau) - \mathcal{I}_{10,l_2}^{(r,r_1,0,T_l\frac{\sigma^2}{P_t},T_l\alpha,T_l\beta_1)}(\Delta_2)\right). \quad (4.33)$$

4.4.2. NOMA-2000

In Section 4.2, interference powers caused by users in outage have been calculated as equations (4.14) and (4.15). By using the integral definitions in Table 4.2, the average capacity for NOMA-2000 and user groups can be calculated, respectively, as

$$R_{U_1}^{WD} = \int_{\tau}^{\infty}\log_2\left(1+\frac{\epsilon P_t}{\sigma^2}x\right)f_X(x)dx$$

$$= \sum_{l=1}^{L} w_l\mathcal{I}_{5,l}^{\tau\to\infty}\left(C_1, \frac{P_t}{\sigma^2+\epsilon\mu_Z^{(last)}}\right), \quad (4.34)$$

$$R_{U_2}^{WD} = \int_{0}^{\tau}\log_2(1+\frac{\epsilon P_t}{\sigma^2+\mu_W^{(last)}}y)f_Y(y)dy = \sum_{l=1}^{L} w_l\mathcal{I}_{5,l}^{0\to\tau}\left(C_2, \epsilon\frac{P_t}{\sigma^2}\right), \quad (4.35)$$

$$R^{WD} = \frac{NR_{U_1}^{WD}+MR_{U_1}^{WD}}{M+N}. \quad (4.36)$$

4.4.3. No-interference and OMA Bounds

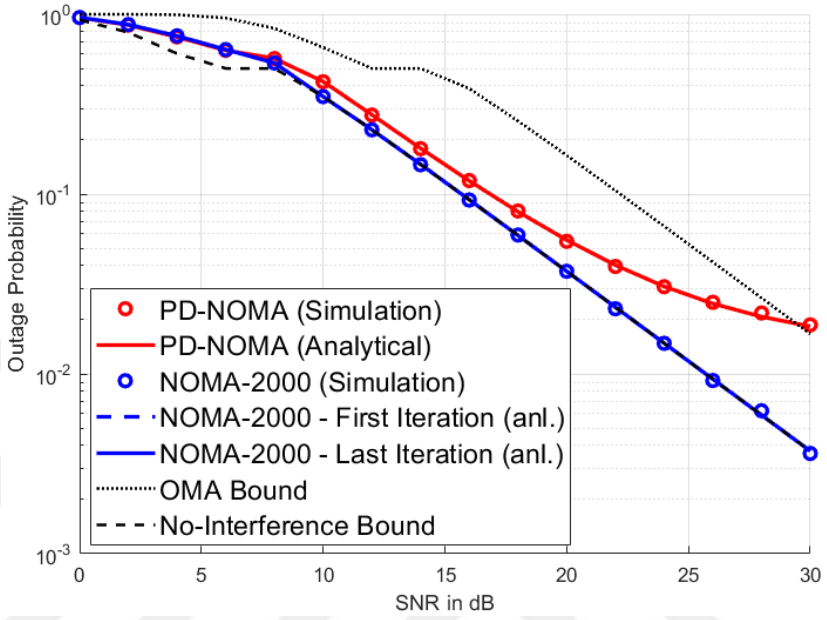
When there exists no interference, we cannot talk about perfect or imperfect SIC. Therefore, calculations in Section 4.3.3 are also valid for this section.

4.5. Numerical Results

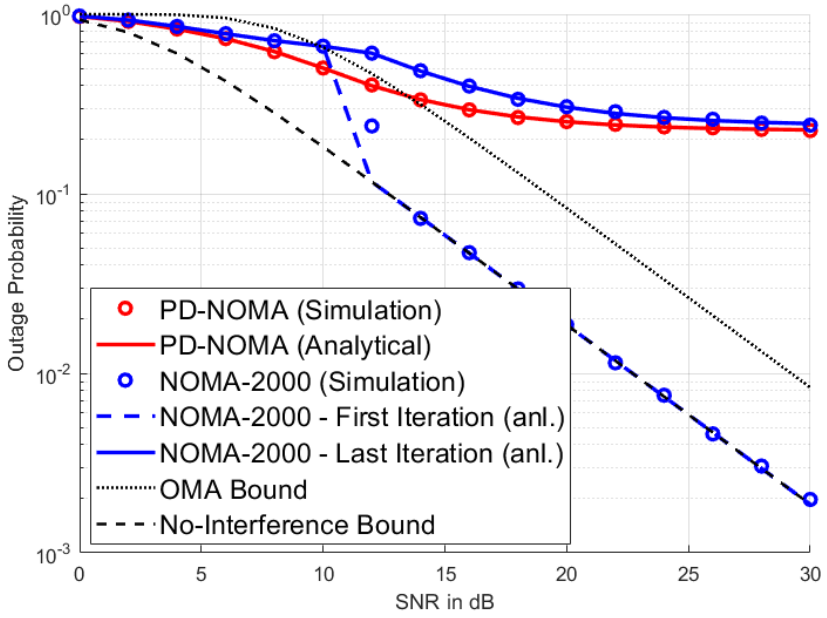
In this section, we provide computer simulations in order to compare NOMA schemes and validate our derivations. As in Chapter 3, overload factor and number of subcarriers (N) are selected as 100% and 1024, respectively, unless otherwise was mentioned. During simulations, 10^6 realizations were performed and average values are illustrated. In the outage probability simulations for NOMA-2000, maximum number of iteration was chosen as 6. In addition, for all simulations, normalized channel gains are used.

4.5.1. Outage Probability

In Figures 4.2 and 4.3 we compare PD-NOMA and NOMA-2000 in terms of outage probability for different fading models and ϵ values. Besides, in Figures 4.4 and 4.5, we also compare fading models with each other. Because each fading model has different OMA and No-interference bounds, these curves are not shown in that curve for the sake of readability. Our first observation is that while NOMA-2000 experiences an outage floor only in two cases (Nakagami-m ($m = 3$),$\epsilon = 1.0$ and $\kappa - \mu$ shadowed ($\kappa = 3, \mu = 2, m = 2), \epsilon = 1.0$), PD-NOMA experience same floor in almost all cases except two of them (Rayleigh,$\epsilon = 0.5$, Rician shadowed ($K = 3, m = 2$),$\epsilon = 0.5$). Furthermore, it can be observed from Figures 4.4.a-4.5.a and the PDFs of fading models in Figure 4.1 that while channel models become more deterministic, the outage performances of PD-NOMA decrease. The reason behind this is that in channels there is less difference between channel gains of U_2 and channel gains of U_1 which causes inevitable interference and performance degradation. However, thanks to iterative SIC and spreading on NOMA-2000, it is not affected in most cases.

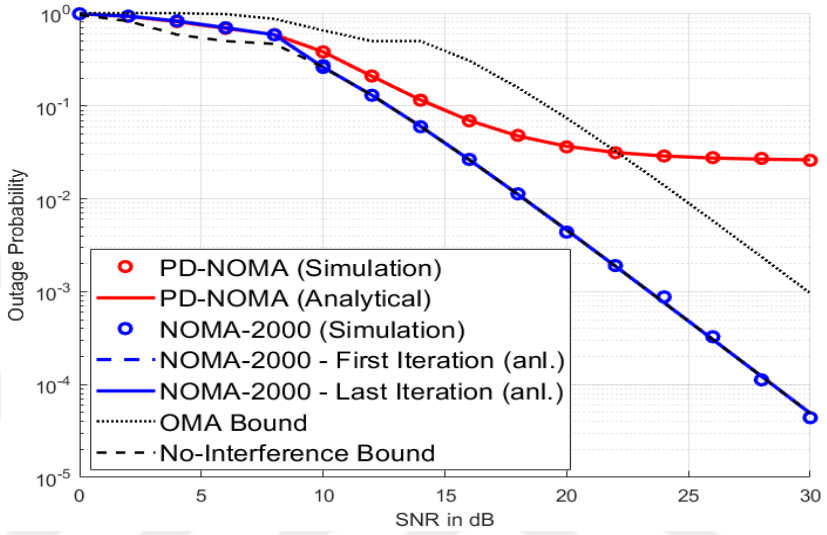


(a)

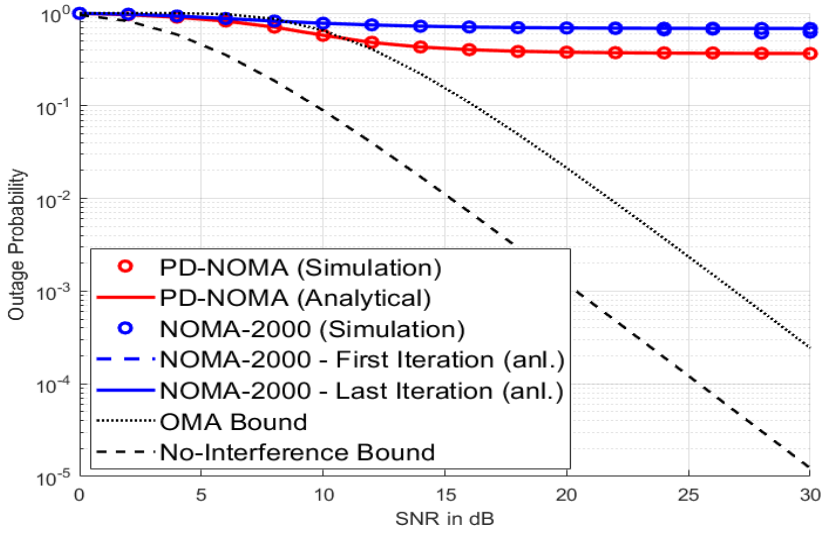


(b)

Figure 4.2. The outage probability of Rician shadowed fading ($K = 2, m = 2$) when target rate= 1.8 bits/s/Hz, a) $\epsilon = 0.5$ and b) $\epsilon = 1.0$.

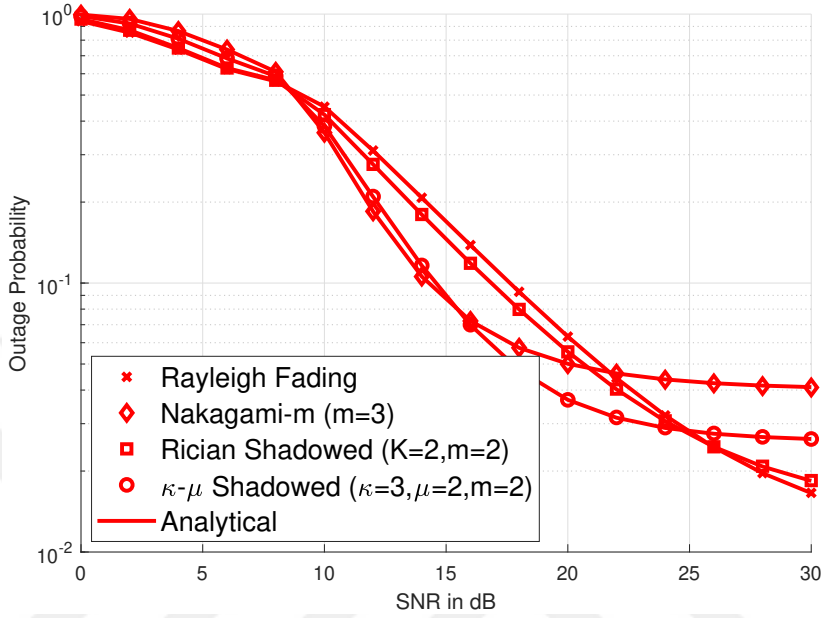


(a)

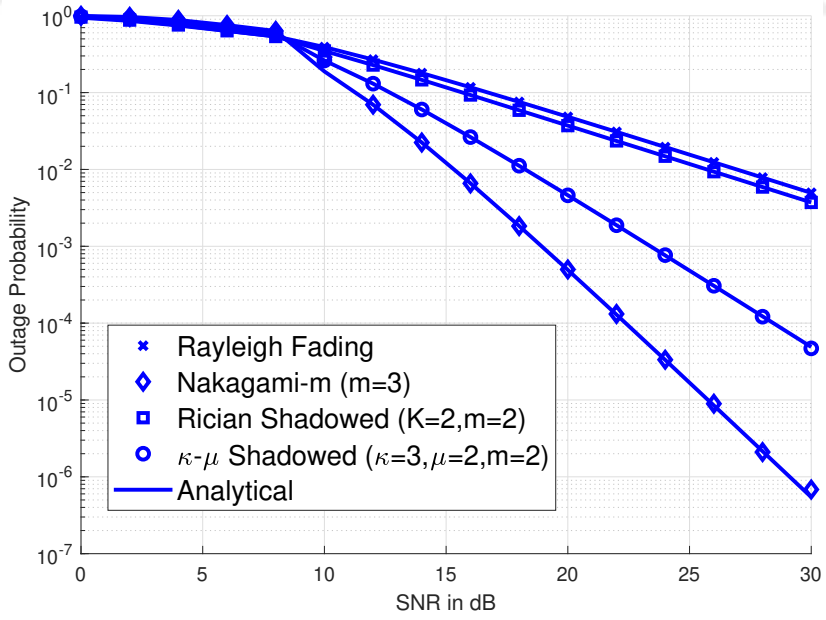


(b)

Figure 4.3. The outage probability of $\kappa - \mu$ shadowed fading ($\kappa = 3, \mu = 2, m = 2$) when target rate= 1.8 bits/s/Hz, a) $\epsilon = 0.5$ and b) $\epsilon = 1.0$.

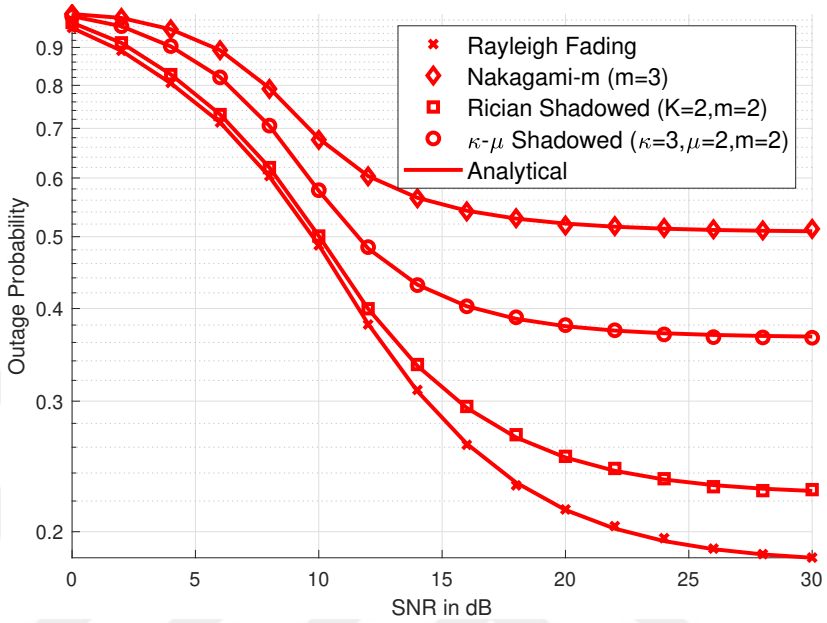


(a)

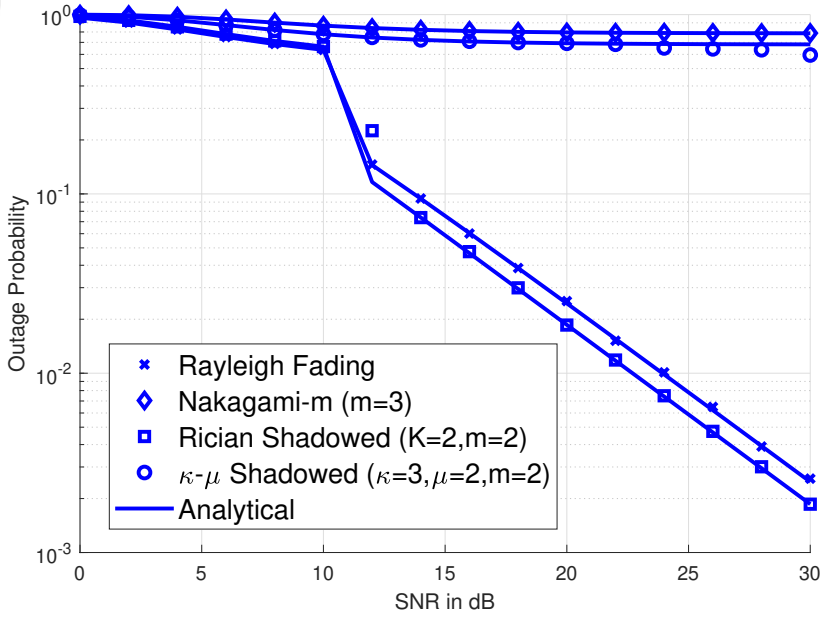


(b)

Figure 4.4. The outage probability of generalized fading channel models when target rate= 1.8 bits/s/Hz and $\epsilon = 0.5$ for a) PD-NOMA and b) for NOMA-2000.



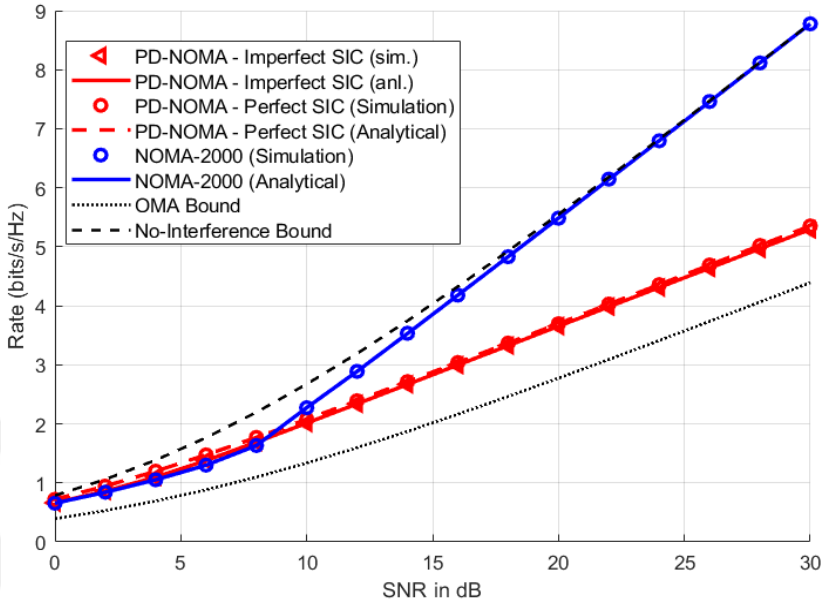
(a)



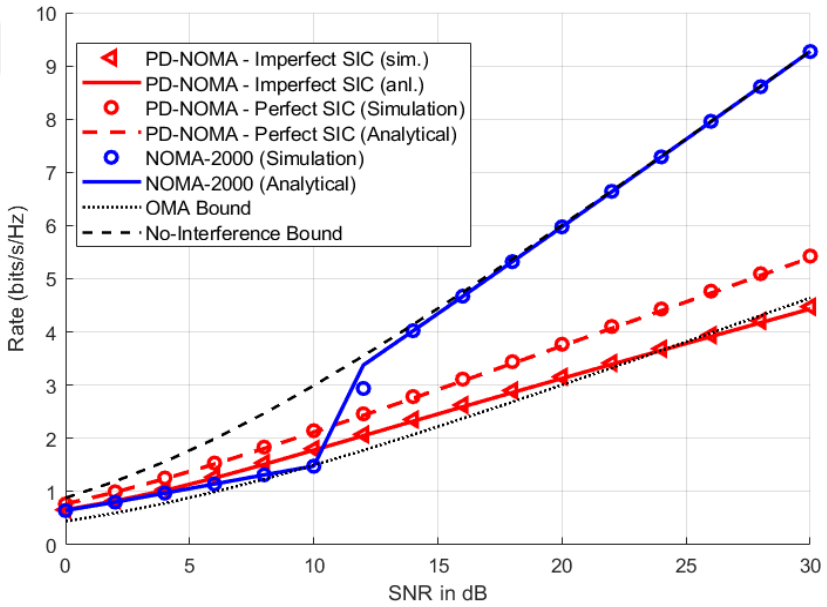
(b)

Figure 4.5. The outage probability of generalized fading channel models when target rate= 1.8 bits/s/Hz and there is no power imbalance ($\epsilon = 1.0$) for a) PD-NOMA and b) for NOMA-2000.

4.5.2. Capacity



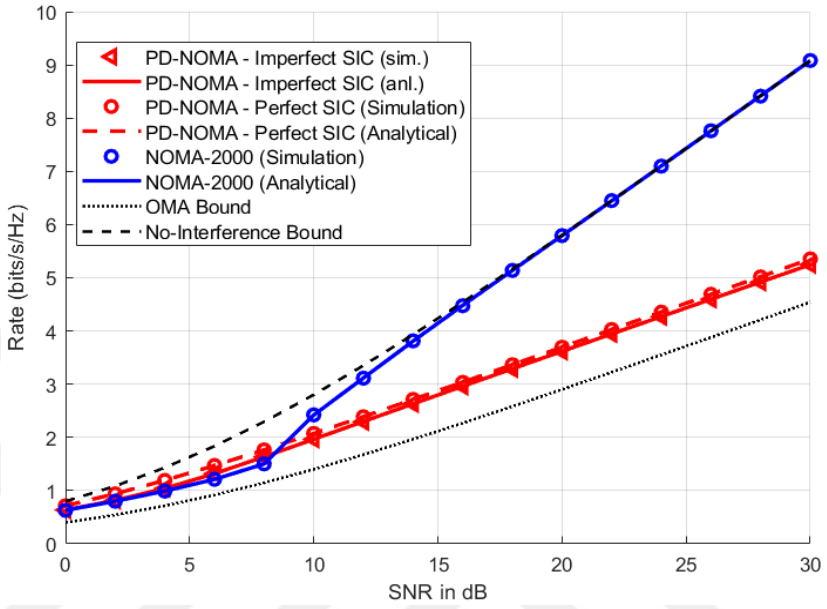
(a)



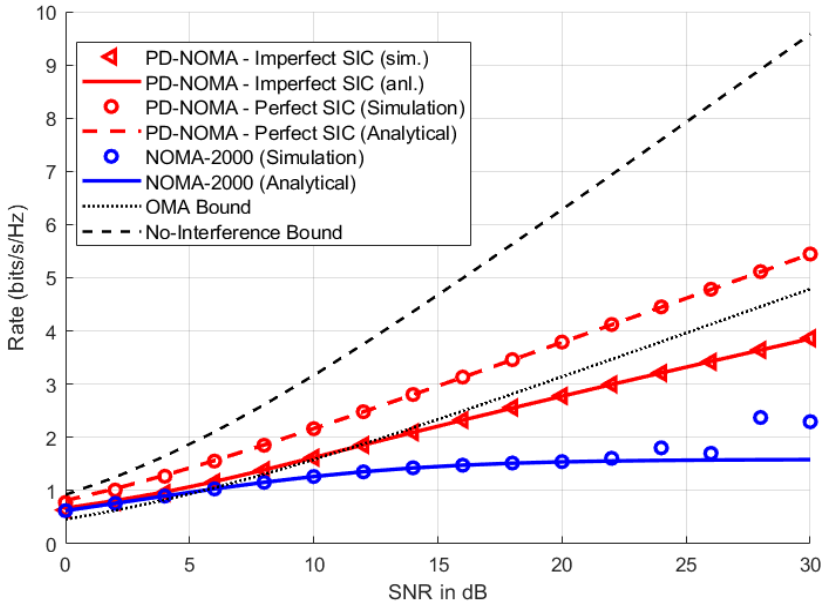
(b)

Figure 4.6. Capacity of Rician shadowed fading ($K = 2, m = 2$) when target rate= 1.8 bits/s/Hz, a) $\epsilon = 0.5$ and b) $\epsilon = 1.0$.

In Figures 4.6 and 4.7 we compare PD-NOMA and NOMA-2000 in terms of outage probability for different fading models and ϵ values. Besides, in Figures 4.9 and 4.8, we also compare fading models with each other. With the SNR/SINR definitions in Chapter 2, PD-NOMA slightly outperforms in terms of capacity.

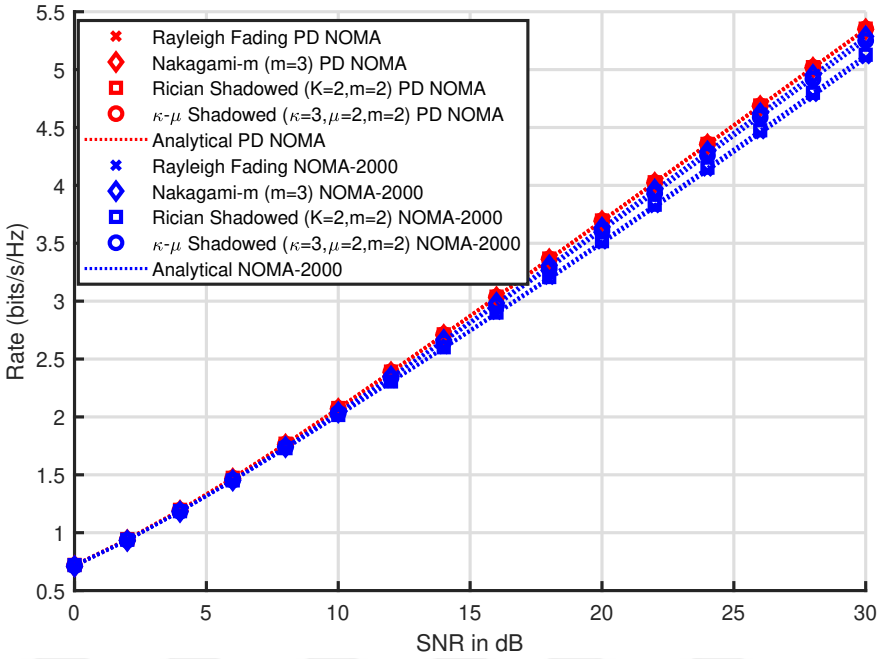


(a)

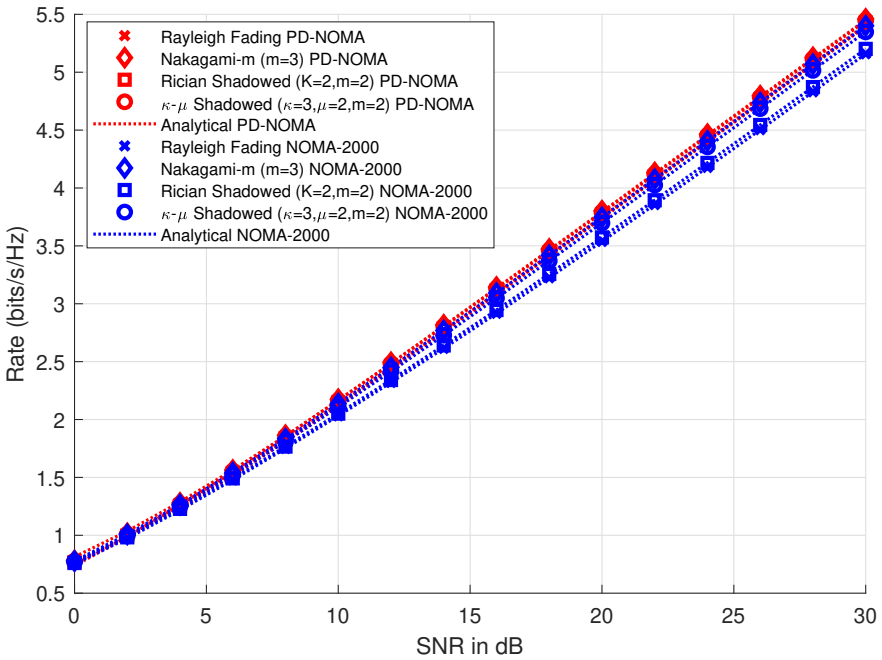


(b)

Figure 4.7. Capacity of $\kappa - \mu$ shadowed fading ($\kappa = 3, \mu = 2, m = 2$) when target rate= 1.8 bits/s/Hz, a) $\epsilon = 0.5$ and b) $\epsilon = 1.0$.

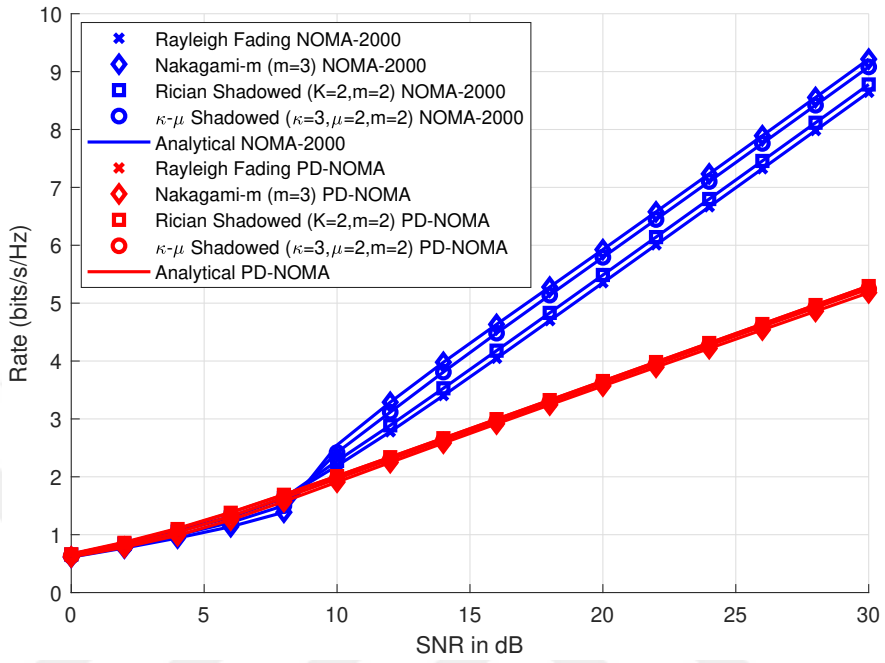


(a)

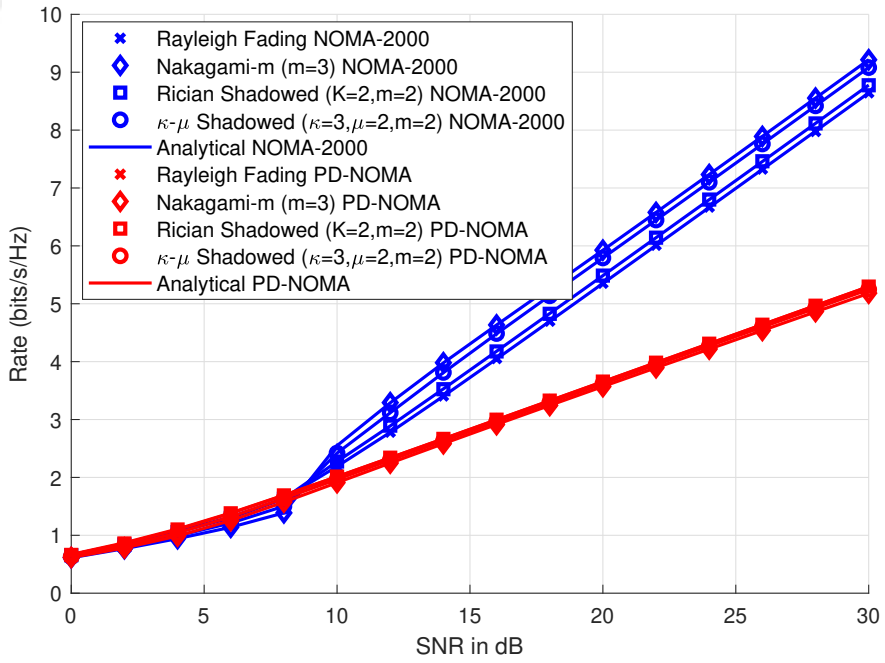


(b)

Figure 4.8. Capacity under perfect SIC assumption comparisons between PD-NOMA and NOMA-2000 when a)$\epsilon = 0.5$, b) $\epsilon = 1.0$.



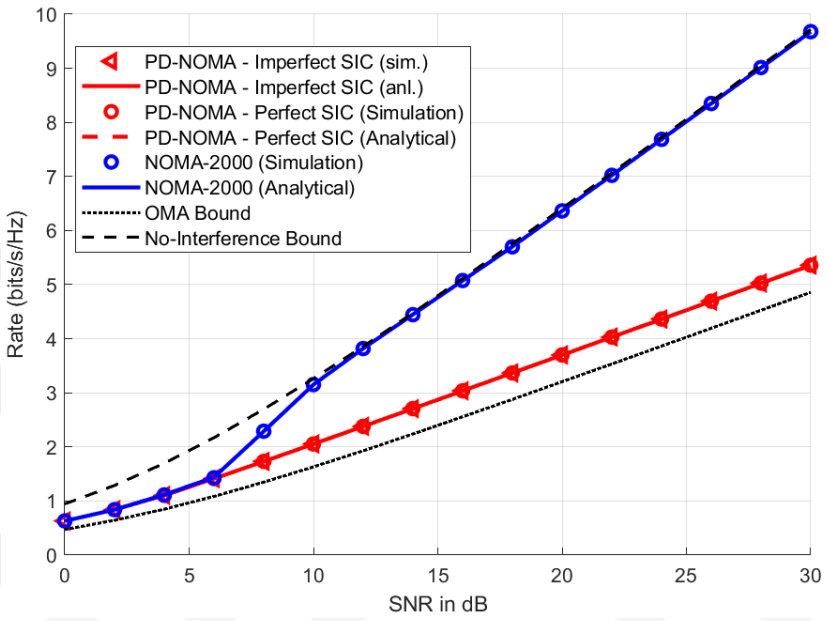
(a)



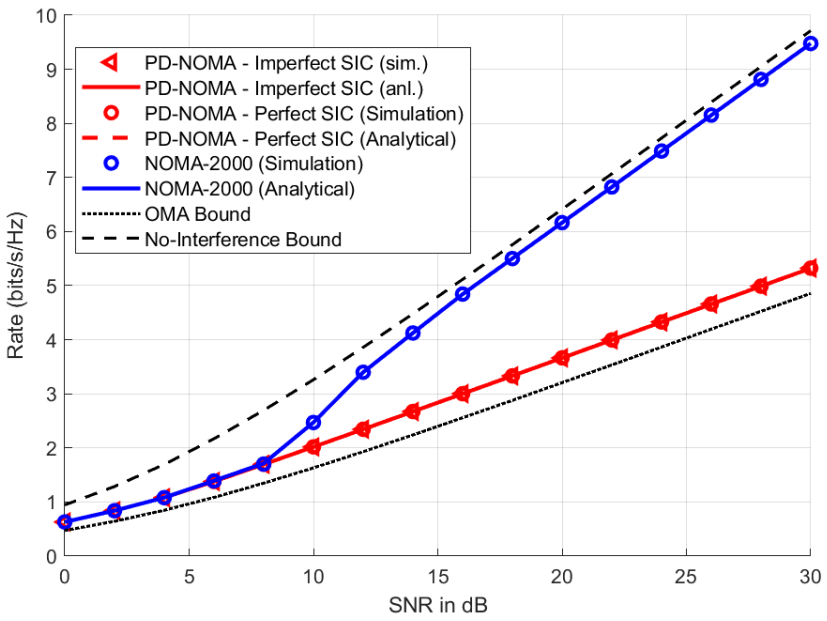
(b)

Figure 4.9. Capacity comparisons under imperfect SIC between PD-NOMA and NOMA-2000 when target rate is 1.8 bits/s/Hz and a)$\epsilon = 0.5$, b) $\epsilon = 1.0$.

However, in Figure 4.9 we compare both NOMA schemes under the imperfect SIC assumption, different power imbalance factors and different channel models. As we have shown in Figure 4.4 and Figure 4.5, NOMA-2000 reaches low outage probabilities which makes its capacity higher.

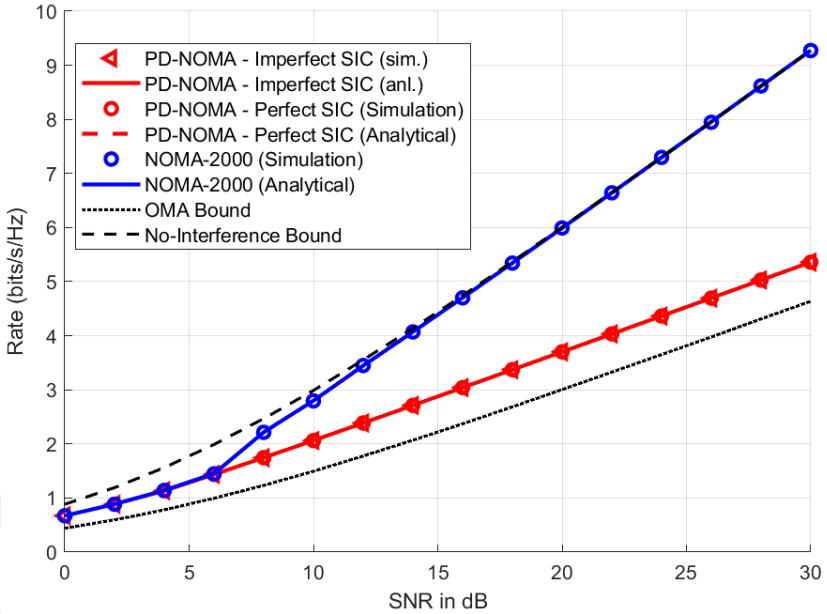


(a)

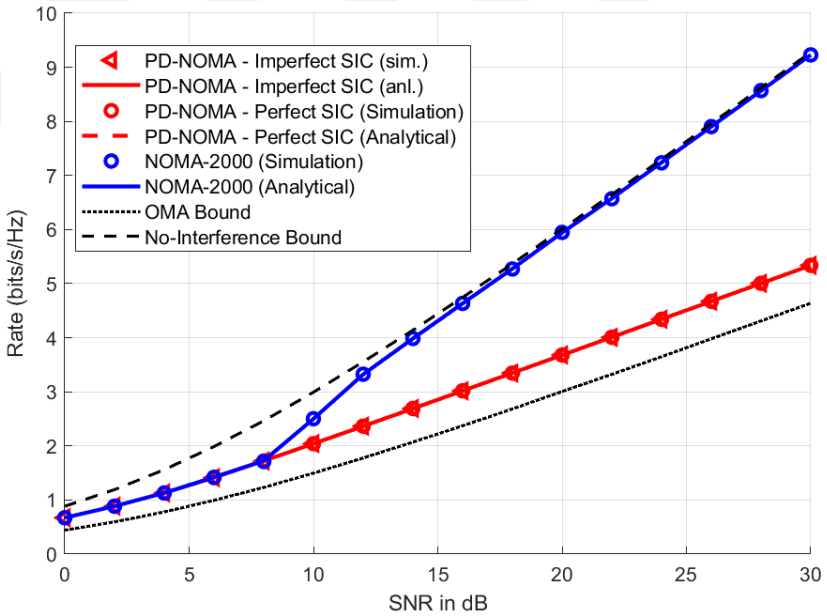


(b)

Figure 4.10. Capacity comparisons between PD-NOMA and NOMA-2000 for Nakagami-m fading ($m = 3$) when ϵ values are selected to maximize capacity and target rates are a) $\hat{R} = 1.5$ bits/s/Hz, and b) $\hat{R} = 1.8$ bits/s/Hz.



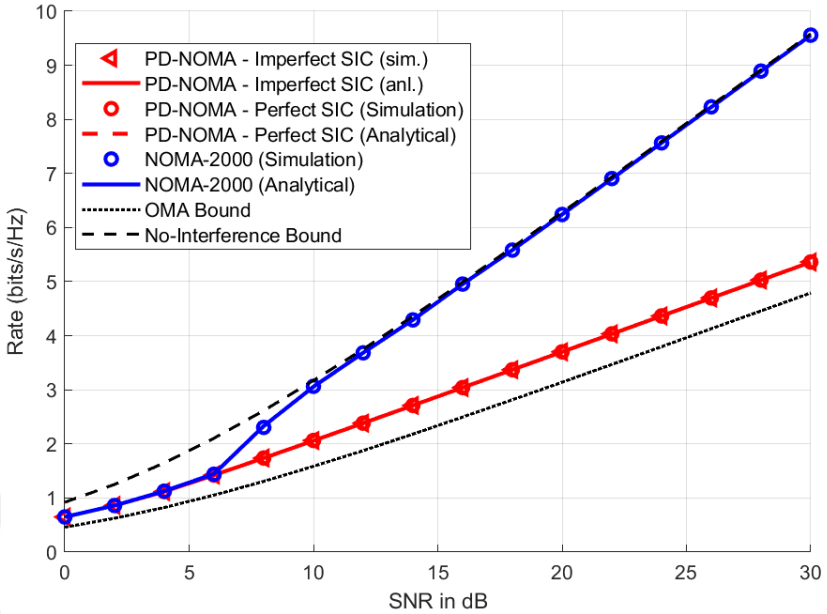
(a)



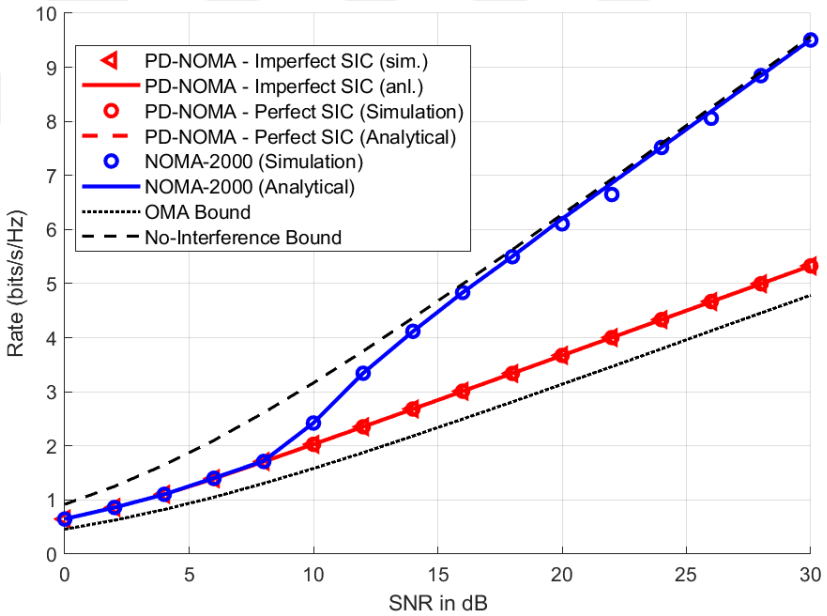
(b)

Figure 4.11. Capacity comparisons between PD-NOMA and NOMA-2000 for Rician shadowed fading($K = 2, m = 2$) when ϵ values are selected to maximize capacity and target rates are a) $\hat{R} = 1.5$ bits/s/Hz, and b) $\hat{R} = 1.8$ bits/s/Hz.

In Figures 4.10, 4.11, 4.12 and 4.13 the power imbalance factors are chosen to maximize their capacities under the imperfect SIC assumption for different target rates and fading models.



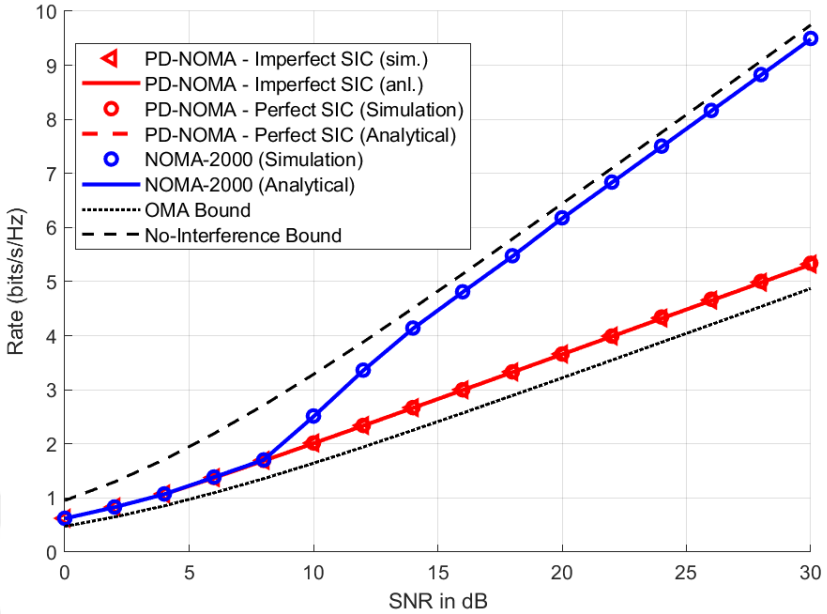
(a)



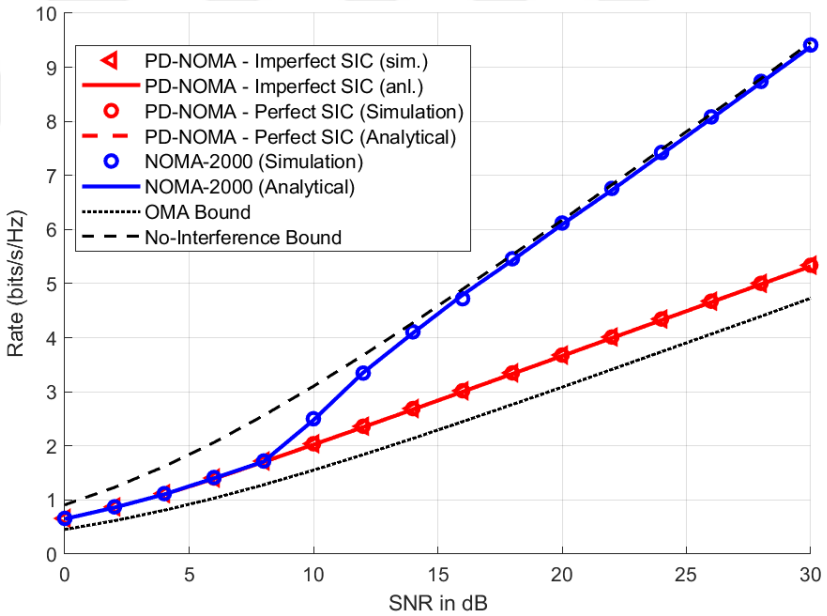
(b)

Figure 4.12. Capacity comparisons between PD-NOMA and NOMA-2000 for $\kappa - \mu$ shadowed fading($\kappa = 3, \mu = 2, m = 2$) when ϵ values are selected to maximize capacity and target rates are a) $\hat{R} = 1.5$ bits/s/Hz, and b) $\hat{R} = 1.8$ bits/s/Hz.

It can be seen that the channel capacity of PD-NOMA is limited with the capacity with perfect SIC assumption. It reaches this bound with an ϵ value such that does not cause an error floor.



(a)



(b)

Figure 4.13. Capacity comparisons between PD-NOMA and NOMA-2000 when ϵ values are selected to maximize capacity and target rates is $\hat{R} = 1.8$ bits/s/Hz for a) $\kappa - \mu$ fading($\kappa = 2, \mu = 2$) and b) Rician fading ($K = 2$).

On the other hand, NOMA-2000 can reach the no-interference bound with an ϵ value in most cases. When the target rate is large enough and the channel model is deterministic, it may not reaches the no-interference bound, however, it still manages to

reach values close to this bound.

4.5.3. Analysis

In this chapter, the analytical calculations of PD-NOMA and NOMA-2000 were repeated for more generalized fading channels. In order to calculate more generic derivations for these fading models, we have used the MGD approximations of them instead of their original PDFs.

Notice that the analytical calculations of PD-NOMA require double integrals since they depend on both channel gains. Since each PDF is expressed as an MGD, double integrals are required to compute the cross terms. It makes analytical calculations for PD-NOMA for generalized fading channel models more complex than NOMA-2000 and Rayleigh fading.

In the last section of the chapter, we have shown numerical results for different cases. We have observed that as the channel models become more deterministic, the interference power becomes stronger which makes a performance degradation for PD-NOMA. On the other hand, NOMA-2000 shows a more robust performance for eliminating the interference power. While the outage probability can reach the no-interference bound in almost all cases in NOMA-2000, PD-NOMA most likely experiences an outage floor. The superiority of PD-NOMA for the channel capacity under perfect SIC assumption continues. However, when we adopt the new capacity definition which takes into account the imperfect SIC, PD-NOMA loses its advantages. On the other hand, when the optimal ϵ values are chosen, the capacity under imperfect SIC performances becomes very close to no-interference upper/lower bounds for NOMA-2000. Our numerical results have shown that NOMA-2000 can reach theoretical bounds with a simple and random pairing scheme but PD-NOMA may need more sophisticated pairing and power allocation.

5. Conclusion

NOMA is a promising technology because it enables the use of the same resources by multiple users. In literature, it is generally referred to as PD-NOMA which a single subcarrier can be used more than one user with different power levels. Another alternative is NOMA-2000 where two waveforms (OFDMA and CDMA in this thesis) are used by two user groups. The main advantage of NOMA-2000 is that the signals for each user group are spreaded and thus they do not experience a high level of interference. Furthermore, in NOMA-2000 each user group also uses SIC which makes it possible to reach the analytical bounds when there is no interference.

In this thesis, the uplink performance of NOMA-2000 and PD-NOMA has been investigated with different performance metrics. Notice that, during all analyses, only a basic user grouping has been assumed in order to satisfy the power imbalance between user groups. While it has been observed that NOMA-2000 can reach the analytical upper/lower bounds with this grouping strategy, PD-NOMA may need more sophisticated user pairing. First, the outage probability has been investigated and it has been concluded that while NOMA-2000 can reach no-interference bound in high SNR, PD-NOMA suffers an outage floor because of the high interference in some subcarriers. Then, an analysis of the average rate has been presented. In this part, it is assumed that the BS can perform perfect SIC to decode signals of U_2 and cannot perform any SIC to decode signals of U_1 for both NOMA schemes. However, they are not realistic approaches thus we define new rates which consider imperfect SIC when decoding signals of U_2 and iterative SIC on NOMA-2000. The main assumption is that if a user is in outage, its signal cannot be decoded and the BS cannot perform SIC on it. With this definition, it can be seen that while the rate of PD-NOMA decreases, NOMA-2000 can reach no interference bounds. Lastly, this analysis has been extended to generalized fading channels. It can be conclude that as the channel gets closer to a deterministic one, PD-NOMA performance is much worse than that of NOMA-2000 because of the improvement of the channel gains of U_2. NOMA-2000, on the other hand, shows more

robust performance thanks to the spreading and iterative SIC. Notice that all these analyses have been performed under the assumption of a simple and random pairing scheme in order to satisfy the basic principle of NOMA for multi-carrier.

The accuracy of the developed analytic results and approximations were confirmed by computer simulations. Extensive comparisons between NOMA-2000, PD-NOMA, and OMA using these metrics confirm the superiority of NOMA-2000 in terms of outage probability and capacity. Together with the fact that NOMA-2000 avoids the error floor encountered with PD-NOMA and can reach theoretical bounds in most cases, this technique turns out to be a very attractive alternative for use in future wireless networks.

As future work, similar derivations can be done with other performance metrics like the BER, fairness or the age of information. Specially, a novel fairness has been defined recently for NOMA in [43] which can be also adapted for NOMA-2000. In this thesis, we show the optimum power imbalance parameters with exhaustively search, but a closed form solution can be derived with optimization. Moreover, the literature is not as rich in works on NOMA-2000 as it is on PD-NOMA. Considering its superior performance compared to PD-NOMA, we believe that NOMA-2000 may deserve more attention. For this reason, MIMO-NOMA-2000, NOMA-2000 with the Internet of Things or NOMA-2000 in Backscatter channels are among interesting applications and possible research areas for this attractive NOMA technique.

REFERENCES

1. Dai, L., B. Wang, Y. Yuan, S. Han, I. Chih-Lin and Z. Wang, "Non-orthogonal Multiple Access for 5G: Solutions, Challenges, Opportunities, and Future Research Trends", *IEEE Communications Magazine*, Vol. 53, No. 9, pp. 74–81, 2015.

2. Ding, Z., X. Lei, G. K. Karagiannidis, R. Schober, J. Yuan and V. K. Bhargava, "A Survey on Non-orthogonal Multiple Access for 5G Networks: Research Challenges and Future Trends", *IEEE Journal on Selected Areas in Communications*, Vol. 35, No. 10, pp. 2181–2195, 2017.

3. Yang, Z., W. Xu, C. Pan, Y. Pan and M. Chen, "On the Optimality of Power Allocation for NOMA Downlinks with Individual QoS Constraints", *IEEE Communications Letters*, Vol. 21, No. 7, pp. 1649–1652, 2017.

4. Şahin, M. M. and H. Arslan, "Application-Based Coexistence of Different Waveforms on Non-Orthogonal Multiple Access", *IEEE Open Journal of the Communications Society*, 2020.

5. Sari, H., A. Maatouk, E. Çalışkan, M. Assaad, M. Koca and G. Gui, "On the foundation of NOMA and Its Application to 5G Cellular Networks", *2018 IEEE Wireless Communications and Networking Conference (WCNC)*, pp. 1–6, 2018.

6. Maatouk, A., E. Çalışkan, M. Koca, M. Assaad, G. Gui and H. Sari, "Frequency-domain NOMA with Two Sets of Orthogonal Signal Waveforms", *IEEE Communications Letters*, Vol. 22, No. 5, pp. 906–909, 2018.

7. Çalışkan, E., M. Koca, G. Gui and H. Sari, "Uplink Performance of NOMA-2000 with Dynamic User Grouping", *2019 IEEE 30th Annual International Symposium on Personal, Indoor and Mobile Radio Communications (PIMRC)*, pp. 1–6, 2019.

8. Sari, H., F. Vanhaverbeke and M. Moeneclaey, "Multiple Access Using Two Sets

of Orthogonal Signal Waveforms", *IEEE Communications Letters*, Vol. 4, No. 1, pp. 4–6, 2000.

9. Sari, H., F. Vanhaverbeke and M. Moeneclaey, "Extending the Capacity of Multiple Access Channels", *IEEE Communications Magazine*, Vol. 38, No. 1, pp. 74–82, 2000.

10. Al Khansa, A., X. Chen, Y. Yin, G. Gui and H. Sari, "Performance Analysis of Power-Domain NOMA and NOMA-2000 on AWGN and Rayleigh Fading Channels", *Physical Communication*, Vol. 43, p. 101185, 2020.

11. Coşandal, I., M. Koca, E. Biglieri and H. Sari, "NOMA-2000 versus PD-NOMA: An Outage Probability Comparison", *IEEE Communications Letters*, Vol. 25, No. 2, pp. 427–431, 2021.

12. Vaezi, M. and H. Vincent Poor, "NOMA: An Information-Theoretic Perspective", M. Vaezi, Z. Ding and H. V. Poor (Editors), *Multiple Access Techniques for 5G Wireless Networks and Beyond*, pp. 167–193, Springer International Publishing, Cham, 2019.

13. Huang, Y., J. Wang and J. Zhu, "Optimal Power Allocation for Downlink NOMA Systems", M. Vaezi, Z. Ding and H. V. Poor (Editors), *Multiple Access Techniques for 5G Wireless Networks and Beyond*, pp. 195–227, Springer International Publishing, Cham, 2019.

14. Parida, P. and S. S. Das, "Power Allocation in OFDM Based NOMA Systems: A DC Programming Approach", *2014 IEEE Globecom Workshops (GC Wkshps)*, pp. 1026–1031, 2014.

15. Gemici, Ö. F., F. Kara, I. Hokelek, G. K. Kurt and H. A. Çırpan, "Resource Allocation for NOMA Downlink Systems: Genetic Algorithm Approach", *2017 40th International Conference on Telecommunications and Signal Processing (TSP)*, pp.

114–118, 2017.

16. Do, D.-T., T.-L. Nguyen, S. Ekin, Z. Kaleem and M. Voznak, "Joint User Grouping and Decoding Order in Uplink/Downlink MISO/SIMO-NOMA", *IEEE Access*, Vol. 8, pp. 143632–143643, 2020.

17. Zhang, J., L. Zhu, Z. Xiao, X. Cao, D. O. Wu and X.-G. Xia, "Optimal and Sub-Optimal Uplink NOMA: Joint User Grouping, Decoding Order, and Power Control", *IEEE Wireless Communications Letters*, Vol. 9, No. 2, pp. 254–257, 2019.

18. Mouni, N. S., A. Kumar and P. K. Upadhyay, "Adaptive User Pairing for NOMA Systems with Imperfect SIC", *IEEE Wireless Communications Letters*, 2021.

19. Im, G. and J. H. Lee, "Outage Probability for Cooperative NOMA Systems with Imperfect SIC in Cognitive Radio Networks", *IEEE Communications Letters*, Vol. 23, No. 4, pp. 692–695, 2019.

20. Mahady, I. A., E. Bedeer, S. Ikki and H. Yanikomeroglu, "Sum-rate Maximization of NOMA Systems under Imperfect Successive Interference Cancellation", *IEEE Communications Letters*, Vol. 23, No. 3, pp. 474–477, 2019.

21. Zeng, M., W. Hao, O. A. Dobre, Z. Ding and H. V. Poor, "Power Minimization for Multi-cell Uplink NOMA with Imperfect SIC", *IEEE Wireless Communications Letters*, Vol. 9, No. 12, pp. 2030–2034, 2020.

22. Liu, M., T. Song and G. Gui, "Deep Cognitive Perspective: Resource Allocation for NOMA-based Heterogeneous IoT with Imperfect SIC", *IEEE Internet of Things Journal*, Vol. 6, No. 2, pp. 2885–2894, 2018.

23. Saetan, W. and S. Thipchaksurat, "Power Allocation for Sum Rate Maximization in 5G NOMA System with Imperfect SIC: A Deep Learning Approach", *2019 4th International Conference on Information Technology (InCIT)*, pp. 195–198, 2019.

24. Zhang, N., J. Wang, G. Kang and Y. Liu, "Uplink Nonorthogonal Multiple Access in 5G Systems", *IEEE Communications Letters*, Vol. 20, No. 3, pp. 458–461, 2016.

25. Liu, Y., M. Derakhshani and S. Lambotharan, "Outage Analysis and Power Allocation in Uuplink Non-orthogonal Multiple Access Systems", *IEEE Communications Letters*, Vol. 22, No. 2, pp. 336–339, 2017.

26. Gao, Y., B. Xia, K. Xiao, Z. Chen, X. Li and S. Zhang, "Theoretical Analysis of the Dynamic Decode Ordering SIC Receiver for Uplink NOMA Systems", *IEEE Communications Letters*, Vol. 21, No. 10, pp. 2246–2249, 2017.

27. Wang, J., B. Xia, K. Xiao, Y. Gao and S. Ma, "Outage Performance Analysis for Wireless Non-orthogonal Multiple Access Systems", *IEEE Access*, Vol. 6, pp. 3611–3618, 2018.

28. Xia, B., J. Wang, K. Xiao, Y. Gao, Y. Yao and S. Ma, "Outage Performance Analysis for the Advanced SIC Receiver in Wireless NOMA Systems", *IEEE Transactions on Vehicular Technology*, Vol. 67, No. 7, pp. 6711–6715, 2018.

29. Yacoub, M. D., "The κ-μ Distribution and the η-μ Distribution", *IEEE Antennas and Propagation Magazine*, Vol. 49, No. 1, pp. 68–81, 2007.

30. Paris, J. F., "Statistical Characterization of κ-μ Shadowed Fading", *IEEE Transactions on Vehicular Technology*, Vol. 63, No. 2, pp. 518–526, 2013.

31. Ramirez-Espinosa, P., F. J. Lopez-Martinez, J. F. Paris, M. D. Yacoub and E. Martos-Naya, "An Extension of the κ-μ Shadowed Fading Model: Statistical Characterization and Applications", *IEEE Transactions on Vehicular Technology*, Vol. 67, No. 5, pp. 3826–3837, 2017.

32. Agarwal, A., R. Chaurasiya, S. Rai and A. K. Jagannatham, "Outage Probability Analysis for NOMA Downlink and Uplink Communication Systems With Generalized Fading Channels", *IEEE Access*, Vol. 8, pp. 220461–220481, 2020.

33. Atapattu, S., C. Tellambura and H. Jiang, "A Mixture Gamma Distribution to Model the SNR of Wireless Channels", *IEEE Transactions on Wireless Communications*, Vol. 10, No. 12, pp. 4193–4203, 2011.

34. Lopez-Martinez, F. J., J. F. Paris and J. M. Romero-Jerez, "The κ-μ Shadowed Fading Model With Integer Fading Parameters", *IEEE Transactions on Vehicular Technology*, Vol. 66, No. 9, pp. 7653–7662, 2017.

35. Zhang, J., X. Chen, K. P. Peppas, X. Li and Y. Liu, "On High-Order Capacity Statistics of Spectrum Aggregation Systems Over κ-μ and κ-μ Shadowed Fading Channels", *IEEE Transactions on Communications*, Vol. 65, No. 2, pp. 935–944, 2016.

36. Chun, Y. J., S. L. Cotton, H. S. Dhillon, F. J. Lopez-Martinez, J. F. Paris and S. K. Yoo, "A Comprehensive Analysis of 5G Heterogeneous Cellular Systems Operating Over κ-μ Shadowed Fading Channels", *IEEE Transactions on Wireless Communications*, Vol. 16, No. 11, pp. 6995–7010, 2017.

37. Sadhwani, D., "Simple and Tightly Approximated Integrals Over κ-μ Shadowed Fading Channel With Applications", *IEEE Transactions on Vehicular Technology*, Vol. 67, No. 10, pp. 10092–10096, 2018.

38. 3GPP TR 36.213, V., *Physical Layer Procedures*, September, 2015.

39. Pliatsios, D. and P. Sarigiannidis, "Resource Allocation Combining Heuristic Matching and Particle Swarm Optimization Approaches: The Case of Downlink Non-orthogonal Multiple Access", *Information*, Vol. 10, No. 11, p. 336, 2019.

40. Çalışkan, E., A. Maatouk, M. Koca, M. Assaad, G. Gui and H. Sari, "A Simple NOMA Scheme with Optimum Detection", *2018 IEEE Global Communications Conference (GLOBECOM)*, pp. 1–6, 2018.

41. Hara, S., T.-H. Lee and R. Prasad, "BER Comparison of DS-CDMA and MC-

CDMAC for Frequency Selective Fading Channels", E. Biglieri and M. Luise (Editors), *Signal Processing in Telecommunications*, pp. 3–14, Springer London, London, 1996.

42. Shanmugan, K. S. and A. M. Breipohl, *Random Signals: Detection, Estimation and Data Analysis*, Wiley, 1988.

43. Gui, G., H. Sari and E. Biglieri, "A New Definition of Fairness for Non-orthogonal Multiple Access", *IEEE Communications Letters*, Vol. 23, No. 7, pp. 1267–1271, 2019.